STAT

PROGRESS REPORT
AND
TECHNICAL SUMMARY

10 September - 30 October 1959

ENGINEERING REPORT NO. 5530

30 October 1959

PROJECT ENGINEER

STAT

VICE PRESIDENT *Roderic M. Scott*

Roderic M. Scott

STAT

REPORT PREPARED BY:

STAT

ASSISTED BY:

TABLE OF CONTENTS

INTRODUCTION

This report is submitted in fulfillment of the requirement of paragraph H, Part I of Contract OM-5400. It is essentially two reports within one cover: A progress report covering the period 10 September to 30 October 1959; and a summary technical report on general work undertaken in the period 14 April to 30 October 1959.

During this last half-year, this Corporation has been charged with the responsibility of determining the general principles for a high performance system to meet the following general specifications:

1. Very high performance;

2. Extensive coverage (4,000 nautical miles, 60% overlap with about 20° convergence, and 60° total transverse coverage);

3. Ease of intelligence extraction (maximum scale and frame type information);

4. Minimum weight (an initial target figure of 500 pounds);

5. Reliability approaching 100%;

6. Volume limitation dependent on specific vehicles;

7. Minimum radio frequency interference; and

8. Unattended operation.

The general system specifications contain many conflicting requirements. For instance, maximum scale implies a larger system and hence is not compatible with either minimum weight or small size. Similarly, extensive coverage is not compatible with minimum weight nor small size since large amounts of film must be carried to permit extensive coverage.

Engineering Report No. 5530   Page 1

The high reliability requirement dictates that this inherently complex system be operationally simple: Generally this can be best accomplished by fewness of operational parts -- that is, what you don't take along can't fail; and it also implies an absence of reciprocating motions and non-uniform motions of moving parts.

Within these specifications and limitations, our primary efforts have been to obtain the high performance, coverage, and reliability desired. Only when a potential system met these standards has it been considered from other points of view. As a consequence, some systems are estimated to exceed the initial weight target or to be incompatible with the specific volume, which has now been selected.

As a consequence of customer scheduling requirements it has been requested that the opportunity provided by the evaluation of vehicle characteristics be used to consider general problems rather than specific details of specific systems. This has permitted rather extensive study, resulting in assurance that there are not obvious fundamental physical limitations to the successful completion of this project, and, further, has pointed the way to specific subsystem breadboarding which would be fruitful to undertake as soon as practical.

Several sub-systems required of any system (e.g. window, v/h sensor, film transport, etc.) have been extensively analyzed and tested. A continuation of this thorough examination will do a great deal to increase the ultimate reliability.

In an effort to avoid bulk and unnecessary duplication in this document, previously reported progress and conclusions are not being repeated in this report. By referring to the list of pertinent documents (Appendix P), other reports containing additional data and conclusions may be located.

PROGRESS

GENERAL:

The progress report contained in this section covers work done during the period 10 September to 30 October. Reference should be made to previous reports (see Appendix ?) for other progress statements covering the period 14 April to 9 September.

LIAISON:

STAT

11 September - [   ] and R.M. Scott visited the Customer to present a progress review and discuss forthcoming work and Customer requirements.

STAT

17 September - [   ] accompanied by the Customer visited the vehicle contractor for technical discussions.

13 October - The Customer and representatives of the vehicle contractor visited this contractor for technical discussions.

STAT

21 October - [   ] and R.M. Scott visited the Customer's office for technical discussions, and also met with the Program Director for a program review and project planning discussion.

V/H SENSOR:

The experimental breadboard grid sensor has been extensively tested, using aerial scenes on an accurate motion (microdensitometer) stage as a simulation of moving ground. The resulting outputs have been analyzed.

Concurrently, the correlation type sensor manufactured by Avion has been proposed to us. Chicago Aerial is reported to have an automatic driftsight type sensor, but we have been unable to obtain any data.

The possibility of programming V/H has been considered. Meteorological

data for the operational altitudes is required before this method can be fully analyzed, and this data has been requested.

AERIAL SPECTRA:

Both methods of obtaining spectra have been put into operation. The photo-optical analyzer has been calibrated, and the scenes analyzed so far show a directional characteristic for scene frequency content. Additional scenes should be analyzed.

The electronic analyzer generally corroborates the photo-optical analyzer, but merits further utilization to properly account for some differences.

WINDOW:

The analysis of temperature profile through the window configuration continued. The analog computer was modified to include the capability of introducing a programmed temperature profile which would simulate thermal conditions through the entire mission. The capability of evaluating the effect of cyclic cooling was also added. An analysis of computer accuracy was completed and indicated improvements were made.

More specific data, of consequence to the window design, was obtained by consultation with the vehicle manufacturer and by further engineering analysis. Temperature profiles were obtained for some specific window configurations.

The philosophy of cyclic cooling was formulated and evaluated. Necessary cooling rates were obtained.

Quantitative data was obtained, by calculation and experiment, of the effect, on the optical wavefront, of index gradients caused by material inhomogeneties or by thermal fluctuations.

Engineering Report No. 5530   Page 4

Further experimental work was done on the development of a suitable low emissivity coating. Ability to manufacture consistently the desired coating thickness, as well as the tendency of the coating to breakdown, was examined. The emissivity of a specific coating at elevated temperatures was determined by test.

The effect of thermal shock was investigated, and quantitative results were obtained. Material quality was examined in an effort to finalize a glazing type. Window size was determined for a specific system, and glazing thicknesses for this size window, for fused silica, were calculated.

Q-BAY ENVIRONMENT:

Calculations were made in an effort to obtain an understanding of the effect of thermal and pressure fluctuations upon the index of refraction of air, and to establish tolerances upon these changes which would enable desired image quality to be obtained.

Experimental investigations were carried out to confirm the critical nature of the index gradient or turbulence problem.

The seemingly necessary isothermal bay concept was discussed with the vehicle manufacturer.

STABILIZATION:

A preliminary analysis of rate gyro stabilization has been made. Some preliminary thinking about inertia-torque stabilization has been done.

IMAGE MOTION COMPENSATION:

Methods of IMC have been worked out for the various comtemplated systems.

FILM TRANSPORT:

A segmented roller (in which the individual segments have freedom of axial movement) has been designed, fabricated and tested. It is worthy of refinement, and should be compared with air-flotation "rollers".

Since several systems may require a spherical focal surface, a breadboard film transport device to move film over the curved focal surface has been designed and fabricated, and some tests have been conducted. Substantial problems remain, and further work must be undertaken.

FILM EVALUATION:

The evaluation of several films was initiated. The emulsions presently being analyzed are: Eastman SO-243, Eastman SO-221, and Fuji Negative Microfilm (Fuji Photo Film Co., Ltd., Tokyo). Basic sensitometric data and resolution capabilities of these films were determined. Recent availability of a sensitometer and completion of special film testing equipment has resulted in initial efforts toward more basic and detailed analysis of pertinent emulsion characteristics.

CEMENTED-JOINTS:

Preliminary experimental work on cementing of mechanical joints has been undertaken. Eastman Adhesive 910 is the only bonding agent presently being tested. At the present time it appears to be thoroughly suitable, providing the surfaces to be joined have been properly prepared. Further work should be undertaken, especially in regard to bond lifetime under service conditions.

PROPOSAL:

The proposal and project plan for forthcoming work was submitted on 21 October in Document 68.

SYSTEM DESIGN:

Specifications of systems under consideration and recommended for construction have been submitted in Documents 59, 62, and 69.

TECHNICAL CONCLUSIONS

V/H SENSOR:

Each of the three possible automatic V/H systems has its own advantages and disadvantages. The automatic drift sight type of sensor must change targets quite frequently at high V/H rates. Since its field of view is narrow it can lock onto some target not of interest, such as a cloud, and yield erroneous information. Such a system could also fail to detect discontinuities such as cliffs. Its sensitivity should be good.

The correlation sensor can also have a difficult time rejecting clouds and responding rapidly to cliffs, mountain peaks, or other such discontinuities in the scene. The response time of this type of system is basically slow and its sensitivity would be good. It is a narrow field device.

The grid type sensor is a wide field device. Its output would consist of a number of frequencies if a number of different objects at different altitudes are in its field of view. The device's response time can be made rapid. The major drawback is that it depends upon the presence of one particular spatial frequency in the image of the terrain. If this frequency is not present there will be no output from the sensor. The correlation sensor depends upon a band of frequencies rather than a single frequency but this is offset by the small field of view which limits its energy acceptance. Our analysis of aerial spectra scenes indicate wide variations in spectra.

Zero crossing measuring techniques, i.e., period measurements, offer a distinct advantage both in spread of response and accuracy in the presence of noise. The experimental recordings made of the V/H sensor

output indicate the need for electronic sophistication in the actual circuitry.

Actual flight testing of the sensing heads will be necessary to evaluate accurately the magnitude of these problems. On the basis of simulated tests either method (correlation or grid) appears to be practical.

It is improbable that programmed V/H could be made accurate to better than ± 1%. However, vernier corrections from a sensor could be applied to such a programmed system to bring it within the desired accuracy. Although a programmed V/H may not have the short term accuracy capabilities of the sensors, it may give better overall performance, and is worthy of much more consideration.

STABILIZATION:

Rate stabilization of the platform appears practical, and its accuracy is largely dependent on the vibrational environment. Preliminary calculations indicate that if vibration isolation is not provided, the applicability of the system is limited to vibrational environments in which the maximum vibration does not exceed an angular rate of two degrees per second.

IMAGE MOTION COMPENSATION:

Preliminary calculation indicate that good IMC correction can be obtained. The Schmidt configurations present a more attractive mechanization solution than does the Flugge system.

WINDOW AND Q-BAY:

The construction of a window configuration to maintain the desired thermal environment appears feasible, and effects upon imagery should be more fully assessed.

The equipment bay should be isothermal to maintain image quality,

and the pressure should be no greater than about 75 mm Hg.

For the window, it is desirable to maintain minimum temperature drop through the glazing materials themselves. In order to limit radiation, a low emissivity coating should be applied to one surface bordering the gaps. It is of no consequence to which side of the gap the coating is applied. A low emissivity coating is most effective in the outermost gap, and two coatings are more effective than one. If only one coating is used, it should be located in the outer gap.

Cooling or heat removal from the window glazings must be present, and the use of cool air for heat removal is recommended. Photographically, it is desirable to eliminate the cooling air from the gaps during an exposure. A cycle of regulated cooling air is recommended. As a maximum tolerance, the net deviation from a linear thermal gradient across the pupil cannot exceed $0.6^{\circ}F$ per inch. Depending on allowable temperature fluctuations of the inner surface, heating may be required in the inner gap.

Further investigation is recommended to finalize material choice.

The approximate window size for the 24 inch Schmidt-System is 10.5 x 18.5 inches with slightly rounded corners and edges. Calculated thicknesses are 0.6, 0.75, and 0.6 inches from outer to inner glazings for a maximum of 5 psia differential across the outer glazing.

SEEING:

As previously reported (Document 57), the turbulence introduces a random deviation of the optical ray, and the estimated standard deviation is 0.2 second in the boundary layer and 0.5 -1.0 seconds in the tropopause.

FILM TRANSPORT:

"Skidding" turns can almost surely be handled without deleterious

friction, either with a refinement of the segmented roller or with an air flotation "roller".

The deformation of film onto a curved focal surface requires additional study, but is not impossible, based on tests conducted on the breadboard transport mechanism.

THERMOELECTRIC COOLING:

Progress within recent years has been rapid in the application of semiconductor materials to thermoelectric devices. Thermoelectric heating and cooling is quite feasible today. These devices are unique in that they can heat or cool by reversing the direction of current flow through the device. This means that a critical device or circuit can be thermostated below, at, or above ambient temperature. Present methods only allow temperature control at some elevated temperature with respect to the ambient. The basic semiconductor material and actual devices can readily be purchased from several sources (e.g. Philco, Admiral, Westinghouse, Texas Instruments, Ohio Semiconductor, American Standard, R.C.A.)

CEMENTED JOINTS:

The work to date has clearly established the possibility of bonding materials together with cements. It is concluded that further work should be undertaken, since the ability to utilize magnesium and beryllium, which are desirable to attenuate vibration, may depend on the practicality of bonding materials together.

SYSTEM DESIGNS:

Maximum effort has been expended in the general examination of nearly two dozen system design concepts. Four of these generally meet the requirements of performance, coverage and reliability, and have been described in detail in Document 69.

APPENDIX A

OPTIMUM DESIGNS FOR FIXED-GRID V/H SENSORS

INTRODUCTION

With modern reconnaissance systems there is a very urgent need for a simple automatic, passive device which will measure the ratio

$$\frac{V}{H} = \frac{\text{Vehicle velocity with respect to ground}}{\text{Vehicle altitude above ground}} \qquad (1)$$

At the present time there are three basic ways of determining this ratio:

1. By tracking individual objects and measuring their apparent angular velocities.

2. By measuring the cross correlation between the light intensity received from two directions and computing V/H from the delay time between signals.

3. By measuring the frequency of signals generated by passing an optical image of the ground through a spatial filter which transmits only the desired image components.

The first method--although it is the one usually used by human beings--requires a great degree of sophistication and complexity for mechanized systems and, therefore, has not yet received much use.

The second method is simple and easily mechanized but has the disadvantage that a high capacity delay device is needed. This device usually takes the form of a tape recorder and, accordingly, has many of the problems associated with moving parts.

The third method is slightly more complex than the second, but can be built without moving parts, and can easily be designed for very high accuracy and very fast response time.

This appendix is concerned with the third type of system, and in particular with a system in which the spatial filter assumes the form of a grid fixed in the image plane of an optical ground viewing system.

Expressions are derived which show how the system response depends on various system parameters, and from these expressions one can choose the optimum parameters.

BASIC PRINCIPLE OF OPERATION

Consider a system consisting of a lens, a grid fixed in the image plane of the lens, and a photocell behind the grid. Let this system move with velocity V at a fixed altitude H above a point source of light located on the ground. As the system moves past the light, the image of the point will move across the grid. The effect of the grid is to periodically attenuate the light so that the electrical signal from the photocell is a periodically pulsed current. If the grid spacing is 2a and the lens focal length, F, then the frequency of the pulsed photocell current is

$$\frac{V}{H}\frac{F}{2a} = \text{frequency.} \tag{2}$$

Where f = focal length of optical system which projects an image of the ground on the grid

$$2a = \text{grid spacing (lines/unit length).}$$

The only restrictions on the operation of this type of system is that the imaging system resolution be somewhat better than $\frac{1}{2a}$ lines/mm and that there is sufficient signal strength from the ground to give a workable signal to noise ratio in the photocell. Since even for high performance systems, a typical value for $\frac{1}{2a}$ would be 5 lines/mm for an f/3, 12-inch focal length system, there is no problem with resolution.

ESTIMATE OF AVAILABLE SIGNAL

Since at the present time very little is known about the character-
istics of various types of ground terrain, as a crude estimate, we will
assume that the ground appears to be uniform except for a dense random
array of areas of diameter b and contrast c. Table I shows estimates of
b and c for various types of terrain.

TABLE I	b	c	bc
Choppy water	2 feet	.05	.1 feet
Sagebrush	2 feet	.2	.4 feet
Wooded area	20 feet	.5	10 feet
Residential housing	50 feet	.5	25 feet
City	100 feet	.5	50 feet

If one compares the total light flux received from two randomly selected
areas, each of area A^2, the average absolute fractional flux difference will be

$$\left\langle \frac{|\Delta B|}{B} \right\rangle \simeq \frac{bc}{A}$$

The area, A^2, is related to the sensor field of view by the relation

$$A^2 = \frac{a^2 nK \ H^2}{f^2}$$

where

$n \ \colon$ the number of grid lines

$ak \ \colon$ the length of the lines

$H \ \colon$ camera altitude.

If the photocell has a sensitivity, N, and the sensor optics an aperture, D,
the sinusoidal output of the photocell will be

$$i_{AC} = N \frac{4 \ D^2 \ a^2 \ nk}{\pi \ f^2} \ \frac{\bar{B} \ bc \ f}{a \ \sqrt{nk} \ H\sqrt{8}} = N \frac{4 \ D^2 \ a \ \sqrt{nk} \ bc \ \bar{B}}{\sqrt{8} \ H \ f \ \pi}$$

where $\bar{B}$ is the average ground brightness.

To see how this looks, consider a 12-inch focal length f/3 system with 1/2 a = 5 lines/mm, $\bar{B}$ = 10 foot candles n = k = 500 lines, N = 1 amp/lumen, bc = .4 ft. (sagebrush desert), H = 100,000 ft.

Under these conditions we find that

$$\frac{i_{AC}}{N} = 2.05 \times 10^{-7} \text{ lumen}$$

or

$$i_{AC} = 0.205 \mu \text{ amp.}$$

which is a quite useable current. If V/H = 0.01 radians/sec the average frequency of this sinusoidal signal would be 30 cycles/sec., while f or V/H = 0.1 rad/sec., this frequency would be 300 cps. By using photomultiplier photodetectors, this current could be increased by a hundred fold to give potential operation over desert in near darkness.

Since V/H is proportional to this frequency, all that remains to be done is to measure this frequency. We proposed to do this by counting the number of times the A.C. component of the signal crosses zero. For a sine wave input of frequency $\frac{V}{H}\frac{F}{2a}$ there are $\frac{V}{H}\frac{F}{a}$ zero crossings per second.

COMPARISON WITH AUTOCORRELATION SYSTEM

The useable signal in an autocorrelation type V/H system has been computed under the same assumptions as the fixed grid system. Here the useable current is

$$i_{rms} = \frac{N \; 4D^2 a \; bc \; \bar{B}}{\pi \; H \; f\sqrt{8}}$$

which differs by a factor $\sqrt{nk}$ from the grid system current. Here, however, the assumptions about the ground characteristics do not apply as much as in
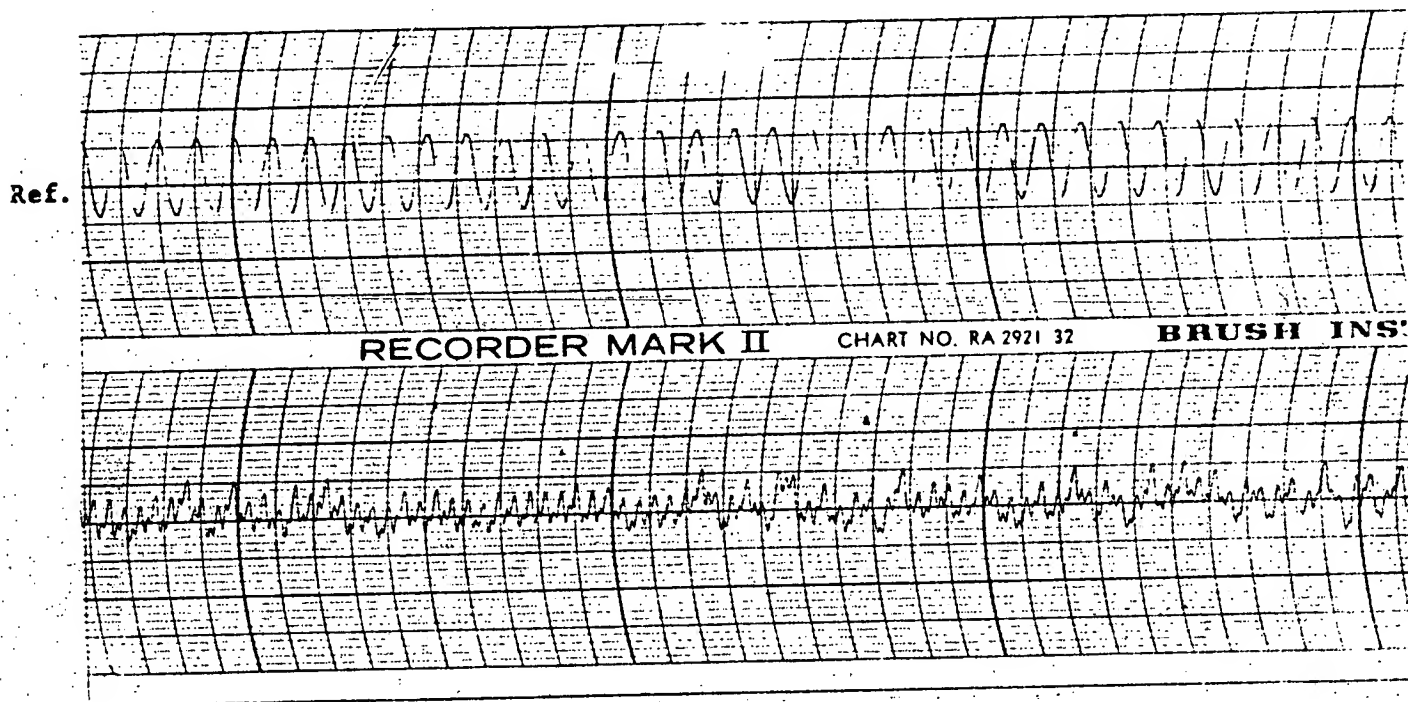
the case of the grid system, so that the two systems will probably have about the same net useable signal strengths.
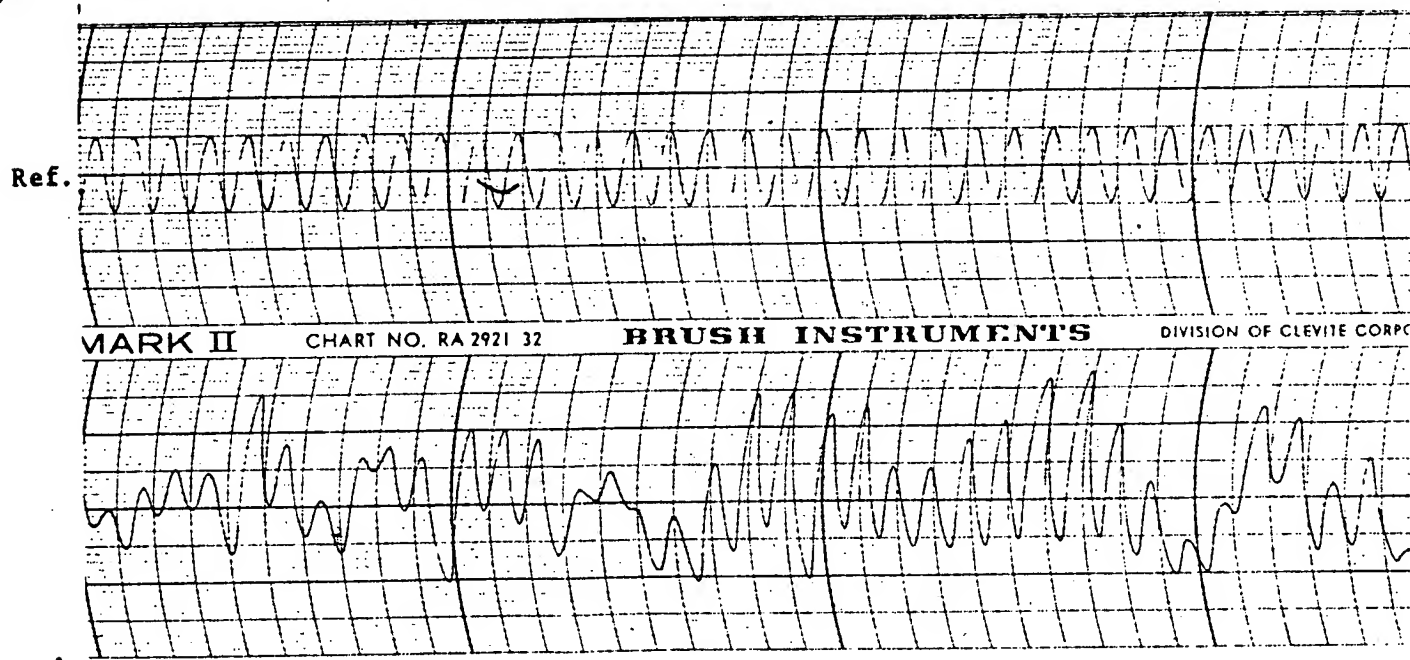
EXPERIMENTAL RESULTS

Recordings of the output of A/fixed grid V/H sensor are given in Figures A-1 to A-6.

GRID = 6 lines/mm

Reference channel = 24 cps at 0.2 volts/line
Recorder speed = 125 mm/sec

No Filter
Negative = HR-73B Camera
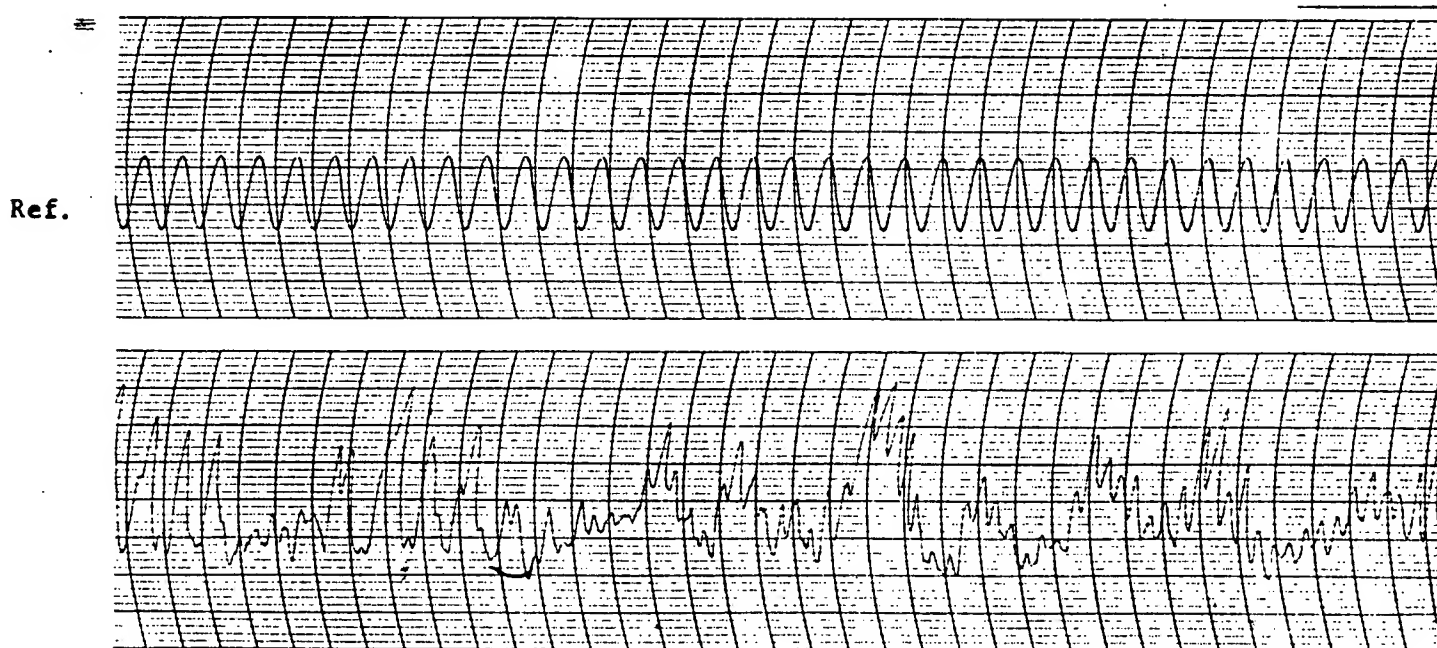X - Axis = .05 volts/line

Low-Pass Filter

Figure A-1
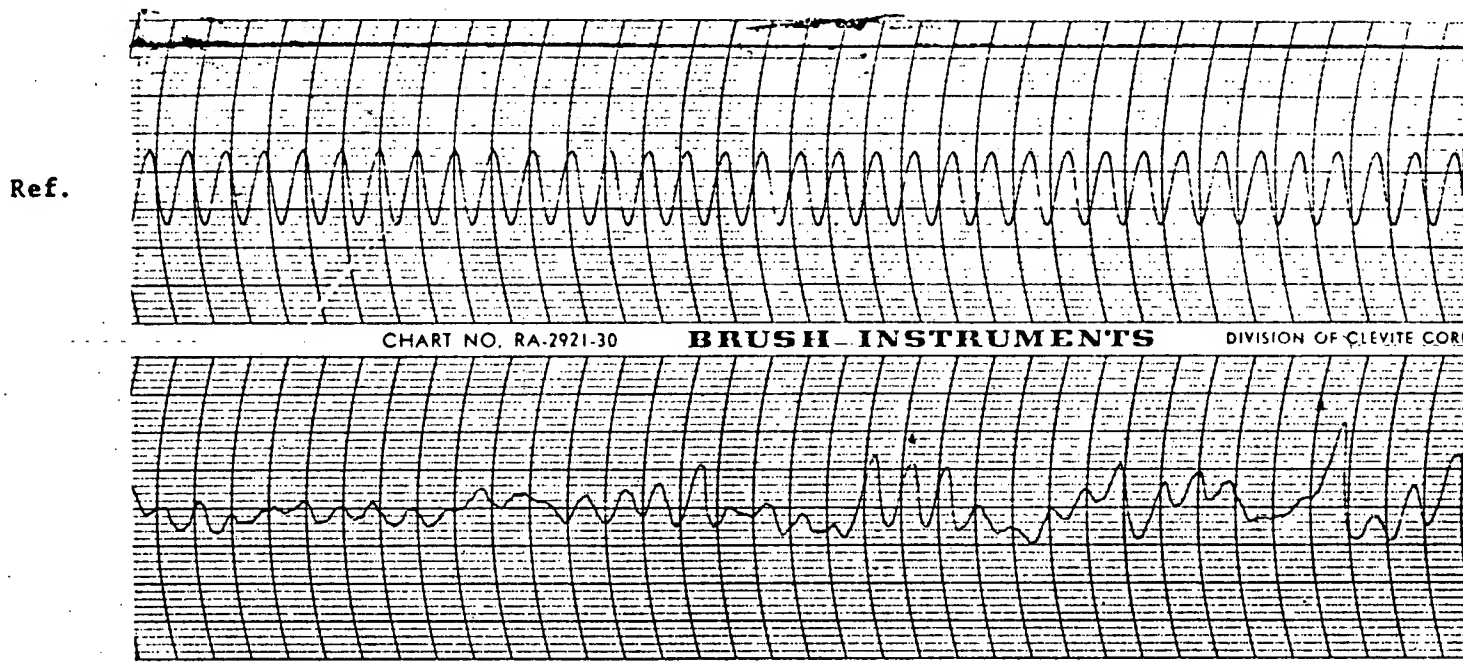
Eng. Report No. 5530

Negative = HR-73B Camera
X - Axis = .05 volts/line (increased sensitivity due to recharged
battery (light source)).

Page 17

GRID = 6 lines/mm

Reference channel = 24 cps at 0.2 volts/line
Recorder speed = 125 mm/sec

Ref.

CHART NO. RA-2921-30   **BRUSH INSTRUMENTS**   DIVISION OF CLEVITE CORP.

Negative = HR-73B Camera
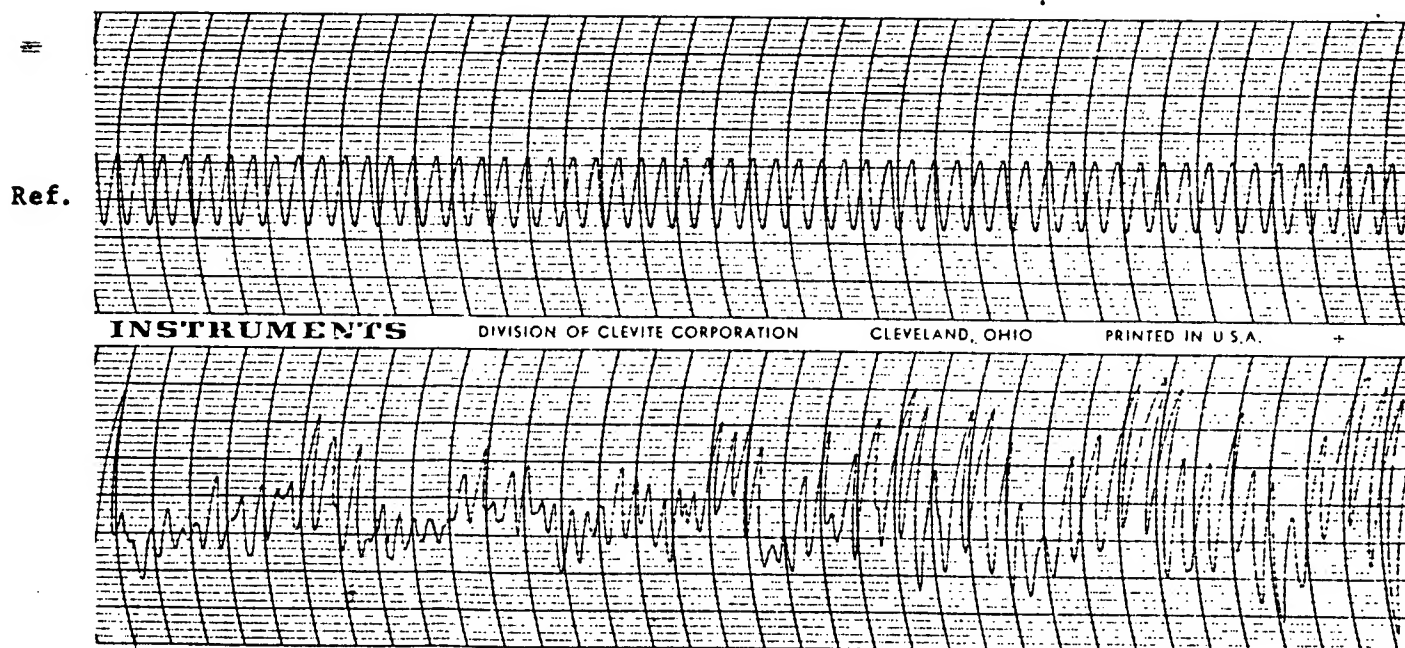X - Axis = 0.2 volts/line

Ref.

Negative = 501 Tracking Camera
X - Axis = 0.2 volts/line

GRID = 10 lines/mm

Reference channel = 40 cps at 0.2 volts/line
Recorder speed   = 125 mm/sec.
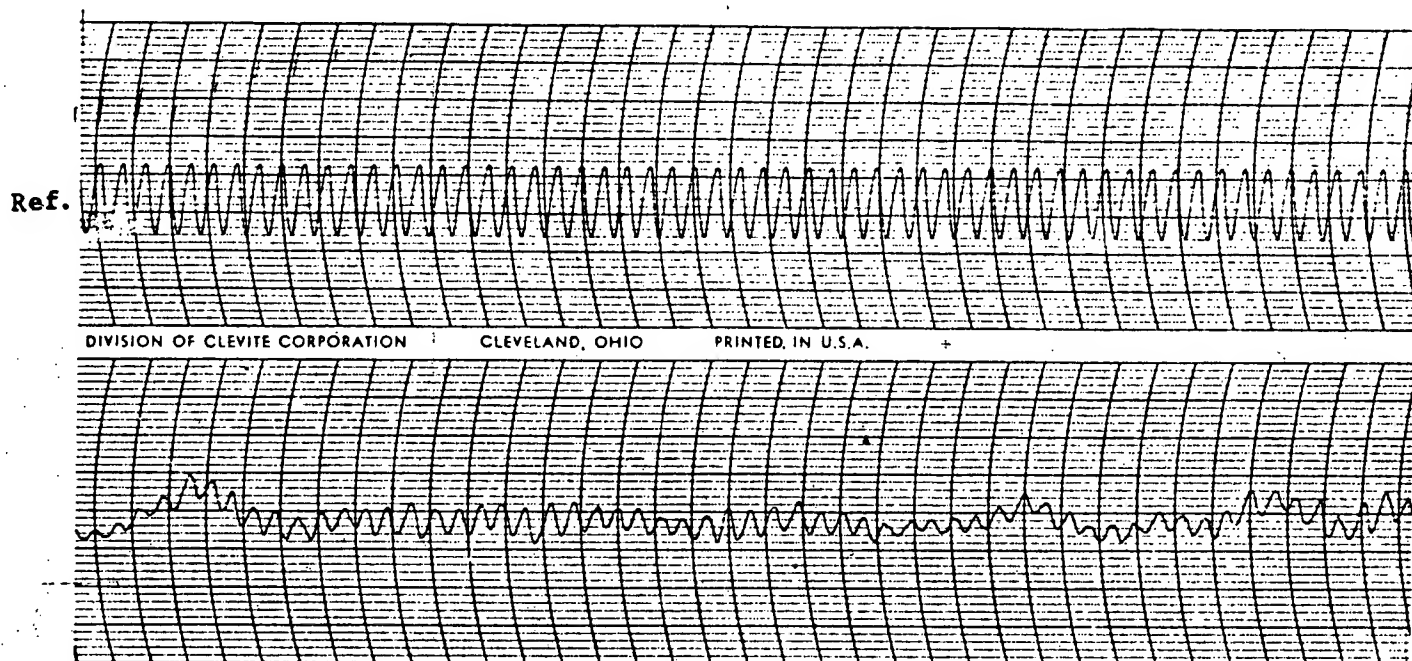
Ref.

DIVISION OF CLEVITE CORPORATION   CLEVELAND, OHIO   PRINTED IN U.S.A.   +

Negative = HR-73B Camera
X - Axis = 0.2 volts/line

Ref.

INSTRUMENTS   DIVISION OF CLEVITE CORPORATION   CLEVELAND, OHIO   PRINTED IN U.S.A.   +

Negative = 501 Tracking Camera
X - Axis = 0.2 volts/line

Figure A-3

GRID = 15 lines/mm

Reference channel =   60cps at 0.2 volts/line
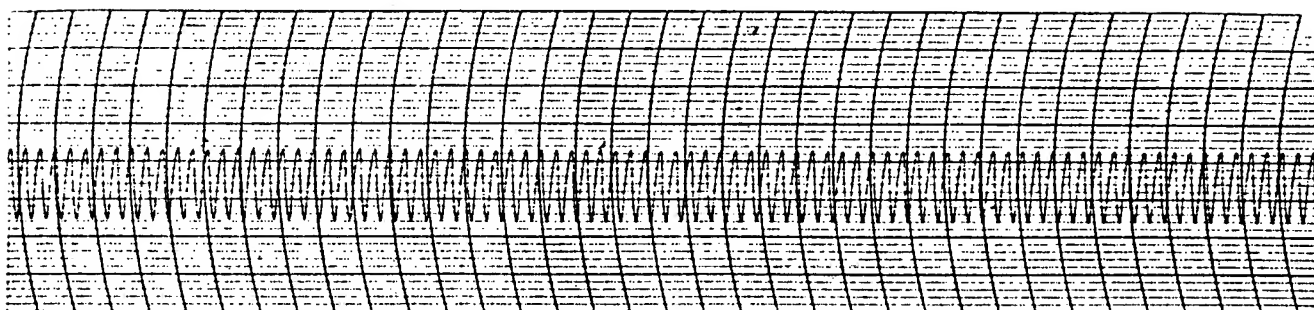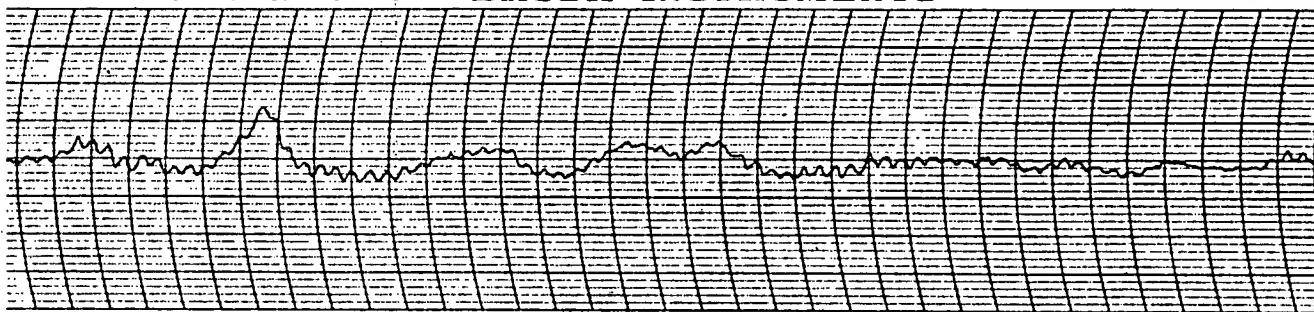Recorder speed   =   125 mm/sec
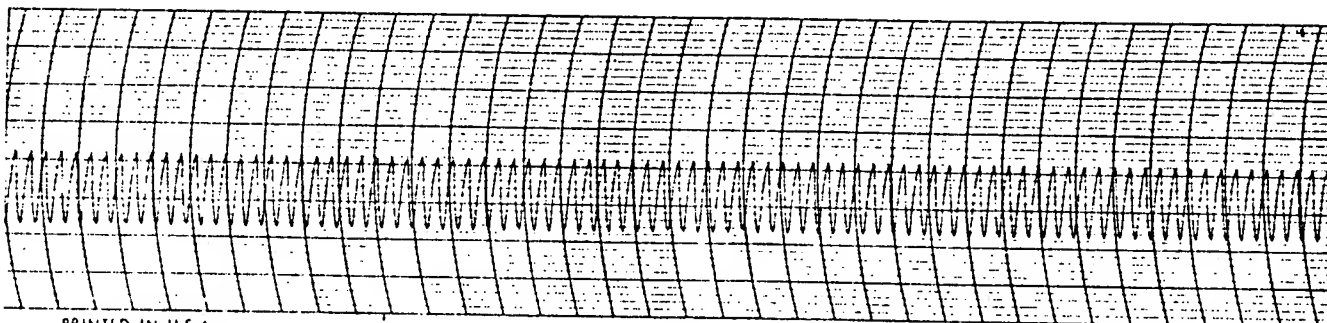

CHART NO. RA-2921-30   **BRUSH INSTRUMENTS**   DIVISION OF CLEVITE CORPORATION

Negative =   HR - 73B   Camera
X - Axis =   0.2 volts/line

PRINTED IN U.S.A.

Negative =   501 Tracking Camera
X - Axis =   0.2 volts/line

Figure A-4

Engineering Report No. 5530   Page 20

GRID = 20 lines/mm

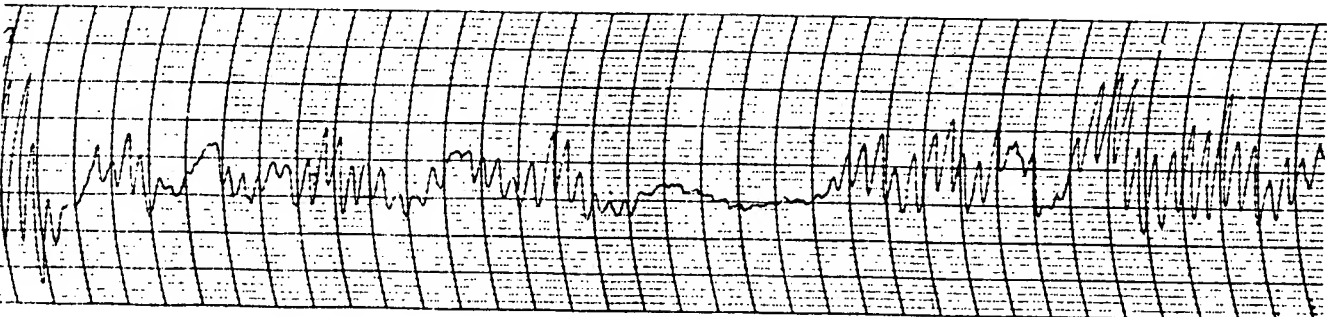Reference channel =   80 cps at 0.2 volts/line
Recorder Speed   = 125 mm/sec
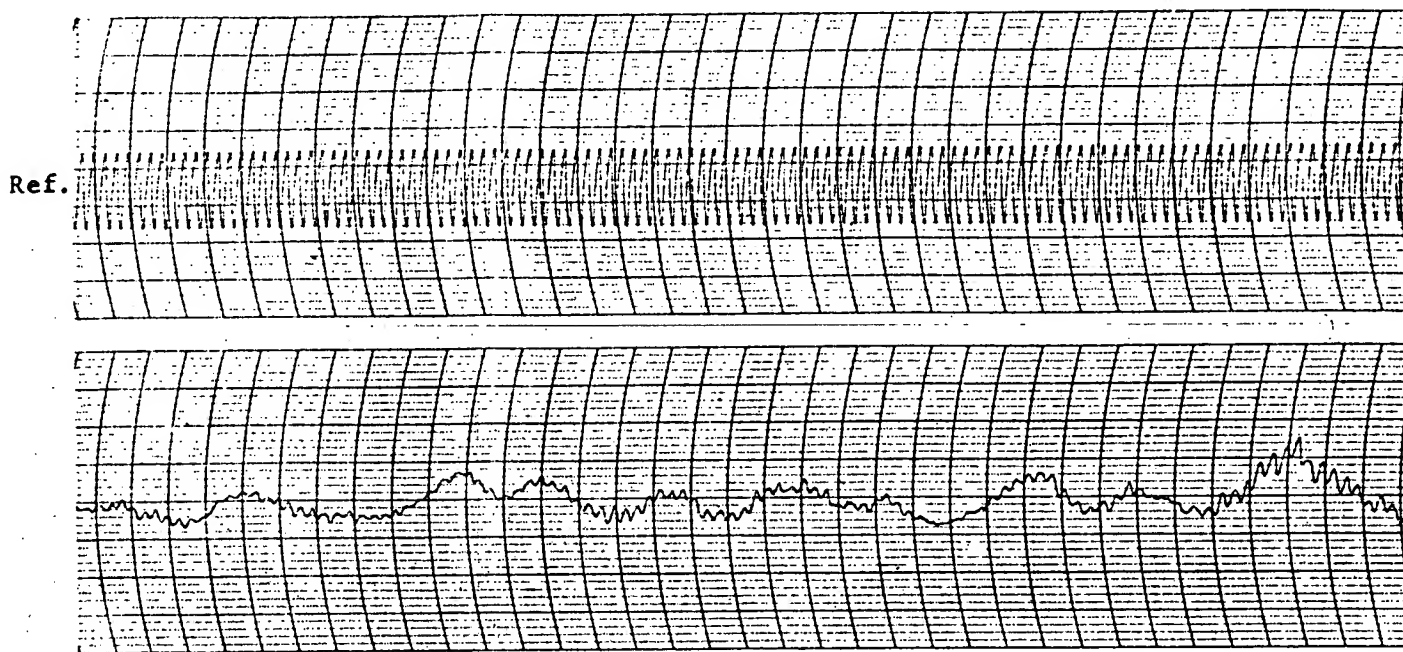
Ref.

Negative =   HR - 73B Camera
X - Axis =   0.2 volts/line

Ref.

Negative = 501 Tracking Camera
X - Axis = 0.2 volts/line

Figure A-5

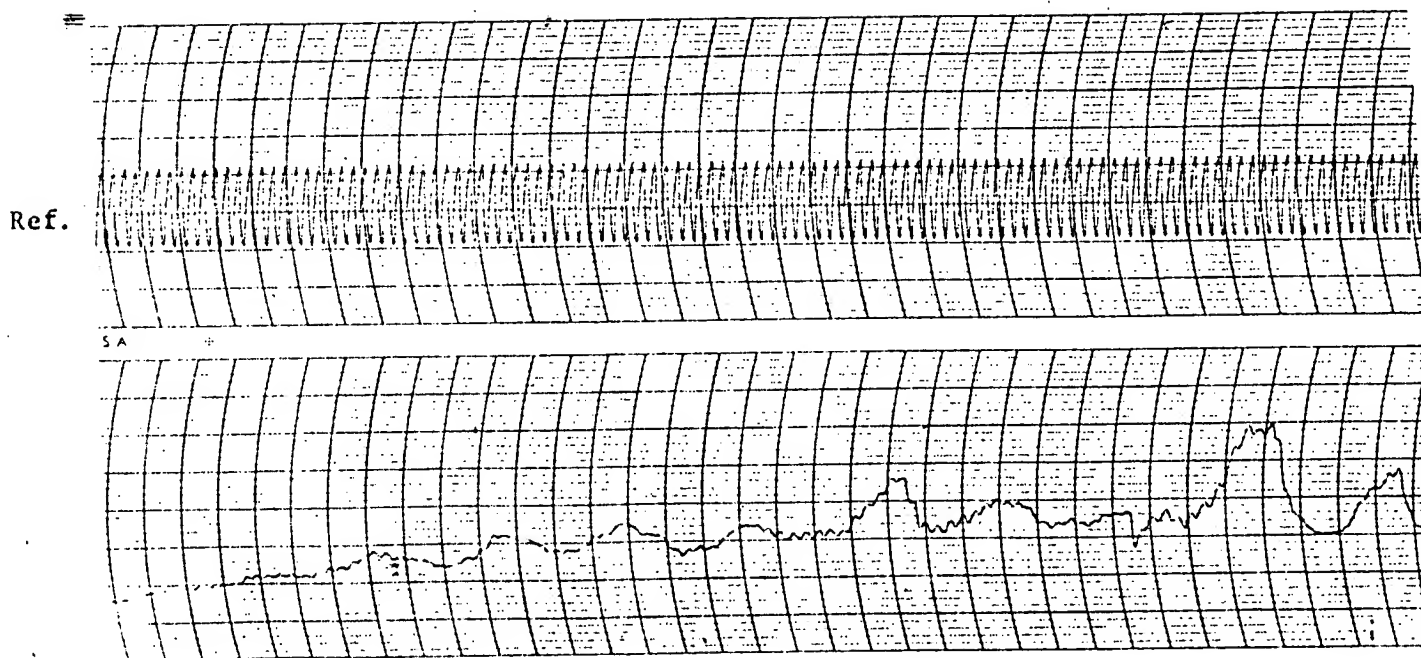Engineering Report No. 5530   Page 21

GRID = 25 lines/mm

Reference channel = 100 cps at 0.2 volts/line

Recorder speed = 125 mm/sec

Ref.

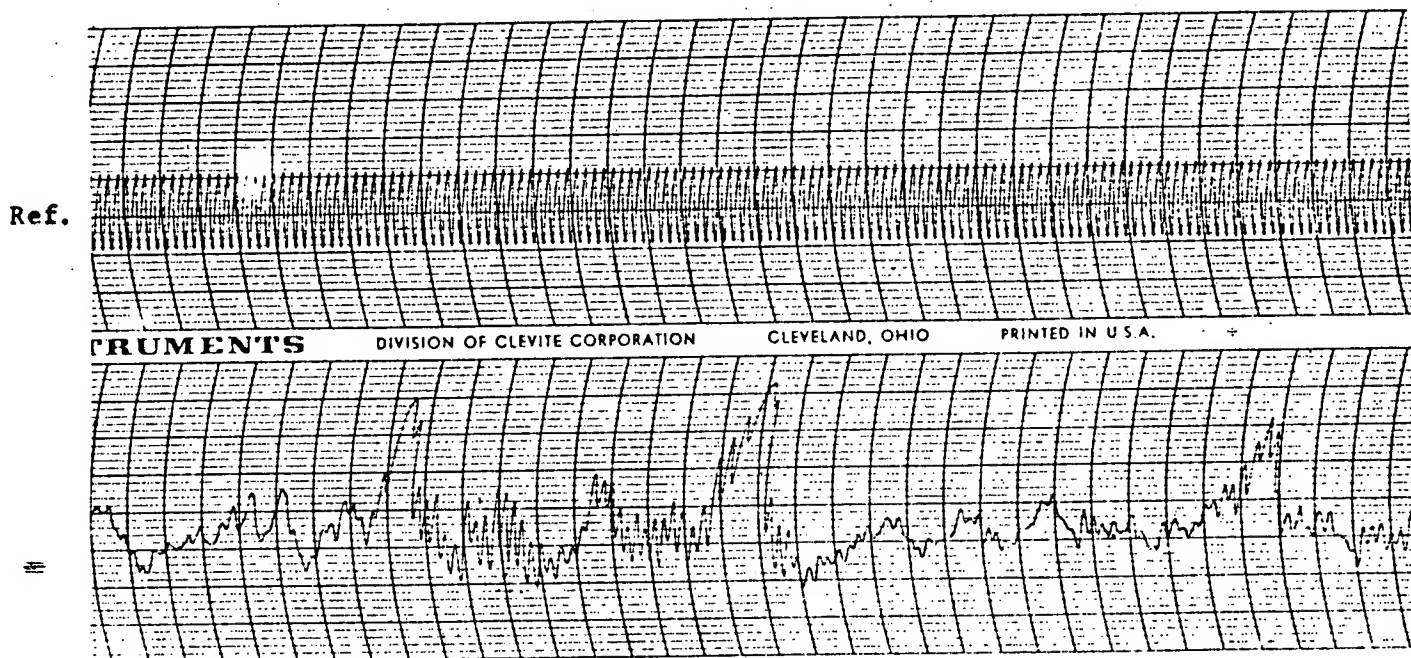Negative = 501 Tracking Camera

X - Axis = 0.2 volts/line

Figure A-6

APPENDIX B

FREQUENCY SPECTRUM OF A FINITE GRATING

The spectrum of an infinite grating is given by the well known Fourier series expression for a square wave. If the grating is not infinite the spectrum is obtained by convolving the spectrum of the window function, or length of the grating, with that of the line spectrum of the grating itself. The effect of this is to widen the lines into a sin x/x function whose width depends upon the length of the window function; the wider the window, the narrower the function becomes. When the window function becomes infinitely long then the sin x/x function becomes a single frequency or line.

Consider the grating below consisting of 200 transmitting and 200 non-transmitting spaces, each one of which is 1/20 mm wide
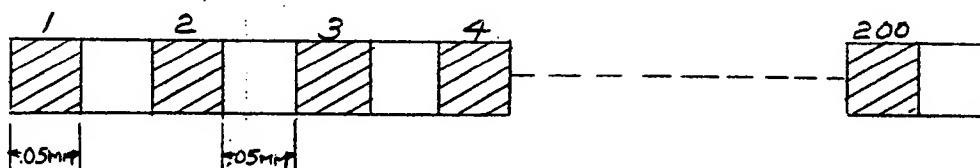
The basic line spectrum is given by the following:

Spatial frequency cycles per mm	Amplitude Coefficient Normalized
0	1
10	2
30	-2/3
50	2/5
70	2/7
90	2/9

as illustrated in Figure B-1. The window function is equal to a spatial pulse 20 mm long. The spectrum of this is a sin x/x function with minima at $\pm$ 1/20 cycles per mm, $\pm$ 1/10 c/mm, $\pm$ 3/20 c/mm, $\pm$ 1/5 c/mm, etc. Its maxima are at 0 cycles per mm, $\pm$ 3/40 c/mm, $\pm$ 5/40 c/mm, etc., as illustrated in Figure B-1.

If each line in the basic spectrum is replaced by the above function by substituting the line frequency for the zero frequency (using the superposition theorem) we now have the spectrum of the grating.
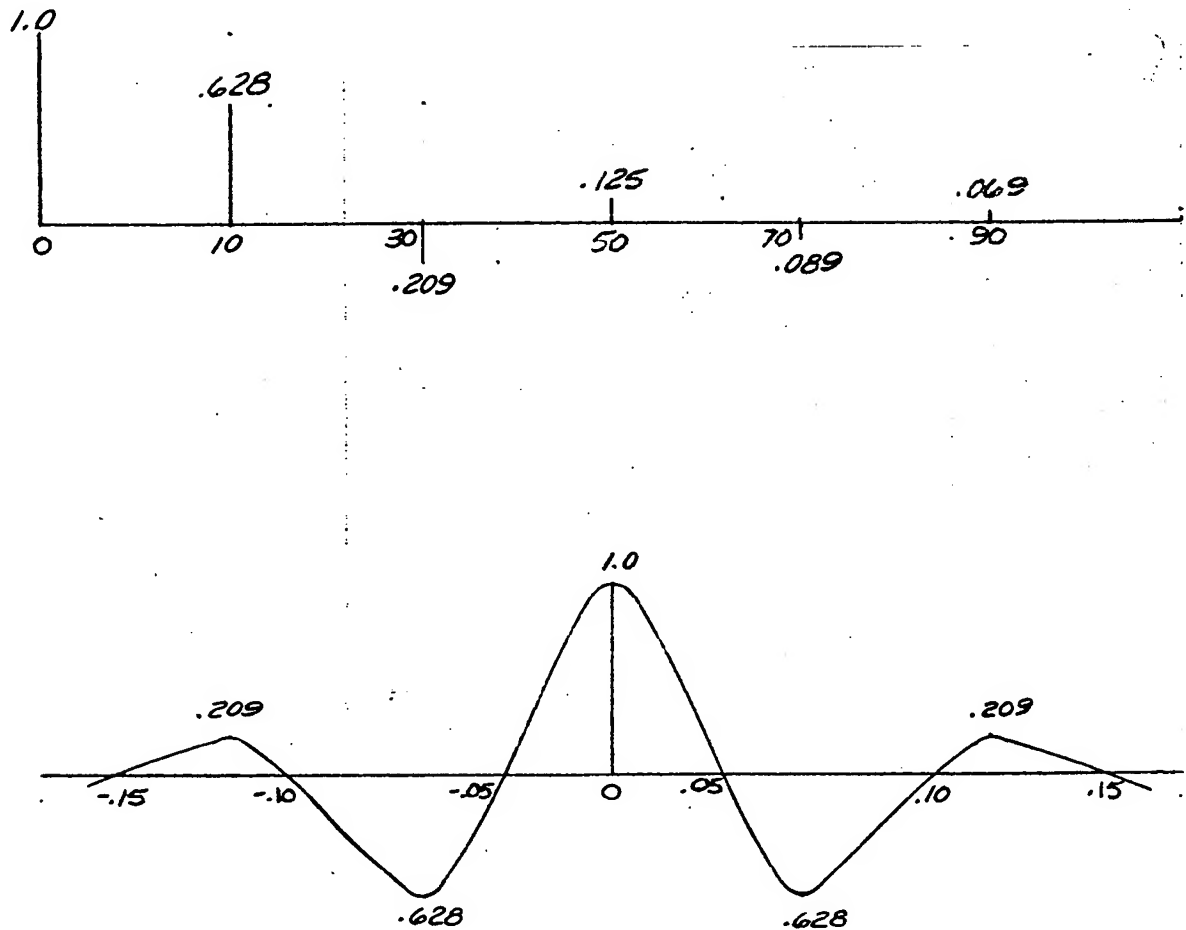
SPECTRUM OF A GRATING

FIG. B-1

It is of interest to note that the basic pass frequency of the grating, 10 cycles per mm, is widened to a band roughly equal to $10 \neq .05$ cycles per mm. Thus an error can exist in the presence of an irregular terrain frequency distribution. To minimize this potential error the number of lines in the grating should be as large as possible. Roughly the possible error is given by the product of 100 times the reciprocal of the number lines in the grating.

APPENDIX C

ELECTRONIC SCENE ANALYSIS

The essential elements of the electronic scene analyzer are shown in the block diagram, Figure C-1. A Leeds & Northrup microdensitometer has been modified to obtain a higher scanning speed than is normally obtained with this instrument. Normally the fastest scan speed is 5/6 mm per second. The temporal frequencies obtained from scanning a negative are given by the product of the scan speed times the spatial frequencies in the negative. For a range of spatial frequencies from 1 cycle per mm to 200 cycles per mm, the temporal range would be 5/6 cycles per second to 167 cycles per second. This is a difficult range for the direct recording process. This is possible to record with the FM process but the stability requirements on the transport mechanism become very stringent, and the mechanism becomes expensive. For example, a $\pm$ 0.2% variation in tape speed at a center frequency of 3000 cycles means a $\pm$ 12 cps variation in playback and recording which means an error of $\pm$ 10 cycles per mm in the measurement of the spectrum. Increasing the scanning speed to 14.6 mm per second increases the temporal frequency range to 14.6 - 2920 cycles per second. It is practical to record to 20 cycles per second and lower. The difficulty in the low frequency range is in reproduction. Hence, by recording at 3 3/4 inches per second and playing back at 7 1/2 inches per second, the temporal range becomes 29.2 to 5840 cycles per second. This is a very feasible range to work with.

A photomultiplier head was made for the L&N to replace the photo-tube pick-up supplied with this instrument. The signal from this photomultiplier is then amplified in the recording amplifier, Figure C-2, and recorded on standard 1/4 inch wide magnetic tape on a Viking series 85 Transport. A
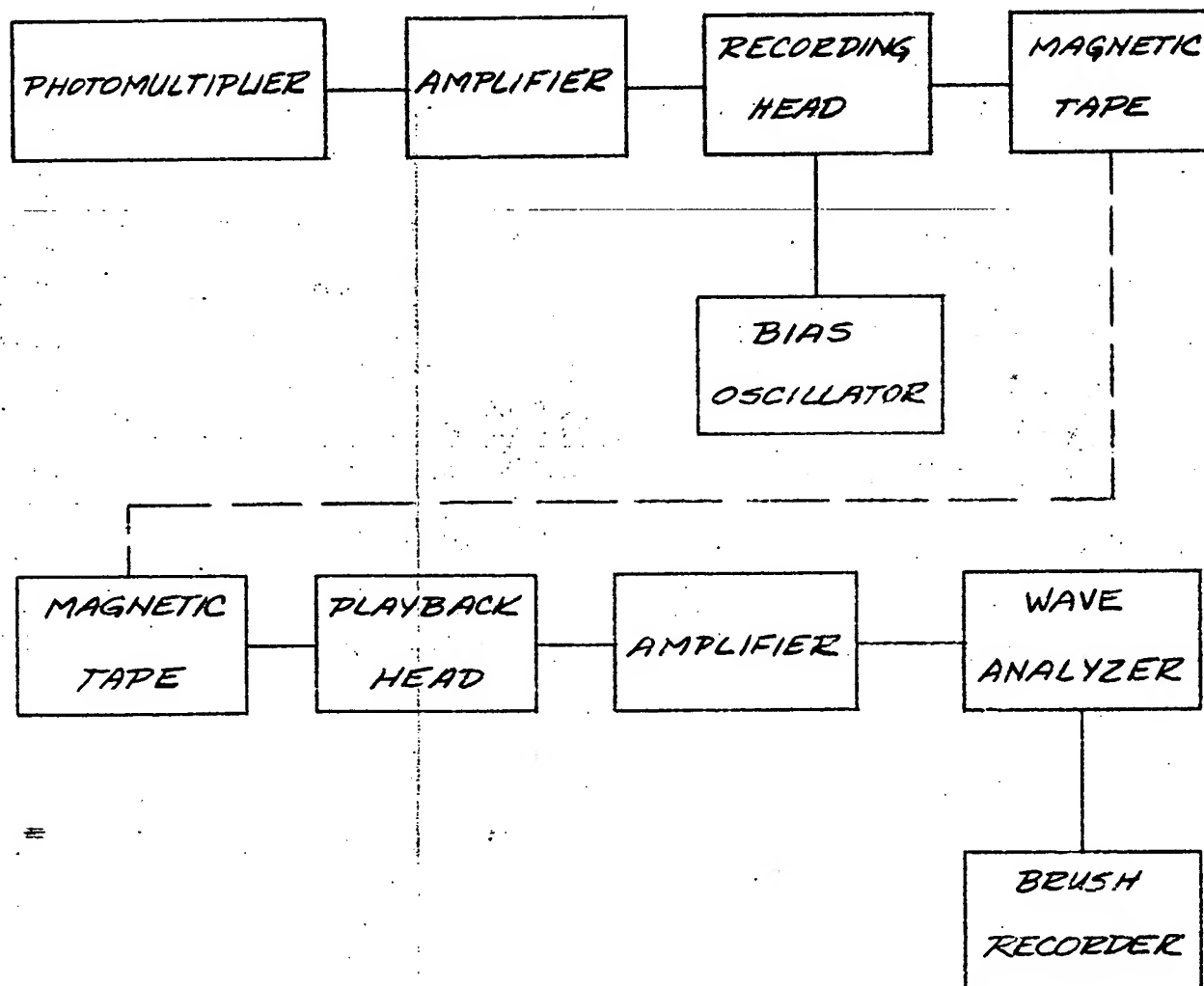
ELECTRONIC SCENE ANALYZER

FIG. C-1
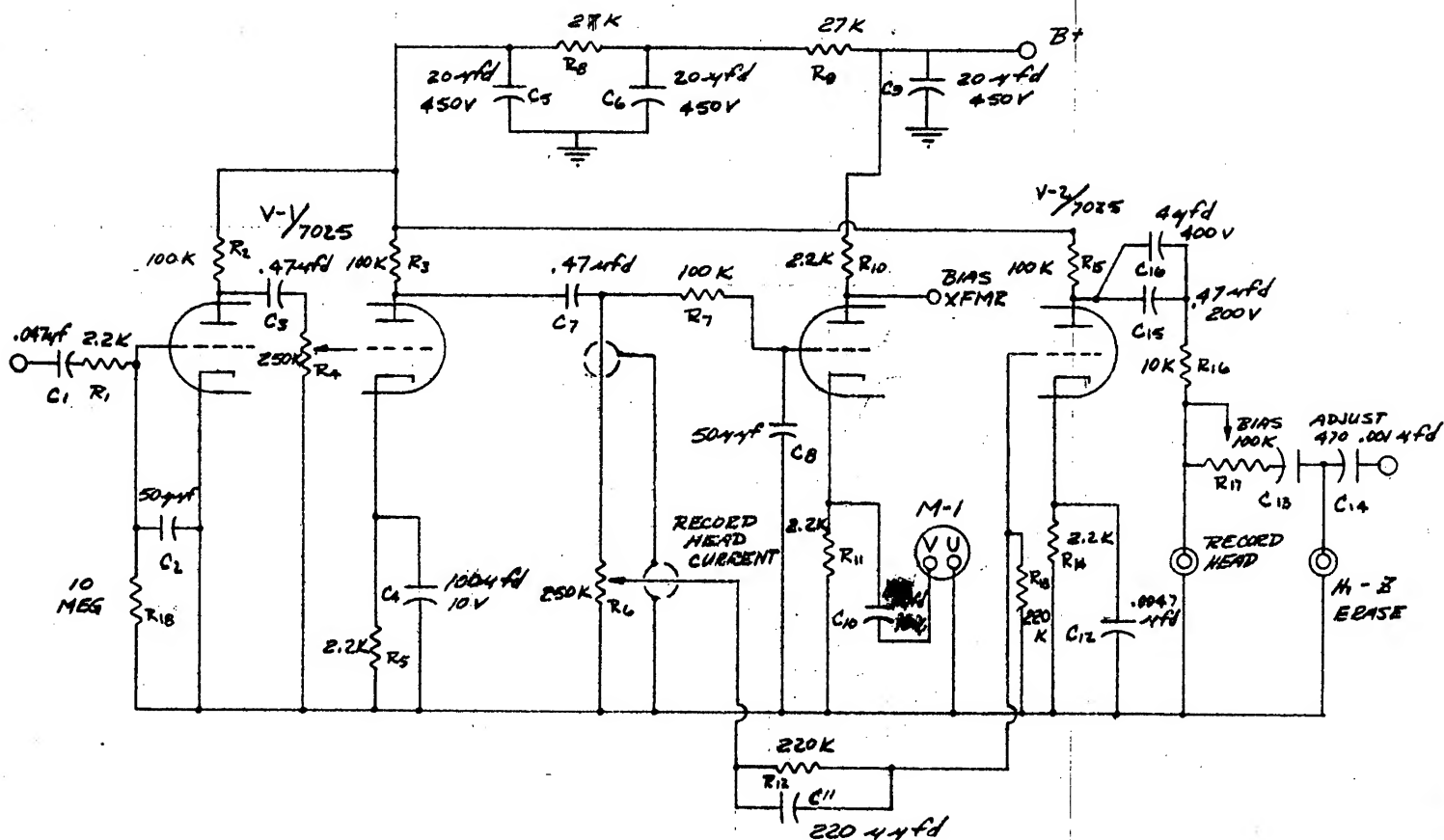
RECORD AMP.

FIG C-2

second playback head is used to simultaneously monitor the recording. The
tape, which is used in the form of a 55-inch continuous loop, is then played
back through the playback amplifier, Figure C-3. This signal is then put
into the General Radio Wave Analyzer. The frequency selector dial of the
wave analyzer is driven by a constant speed motor and the output of the
analyzer is recorded on a Brush Mark II Recorder. The General Radio Wave
Analyzer is not ideal for this work because the calibration of its frequency
selector dial is not a linear function of angle of rotation. Thus, the
frequency scale of the recordings is not linear and the recordings are cumber-
some to interpret. This difficulty will be resolved by the use of the Hewlett
Packard Wave Analyzer, which is being procured for this program. The frequency
calibration of this instrument is a linear function of shaft rotation, so
the frequency scale on the final recording is linear.
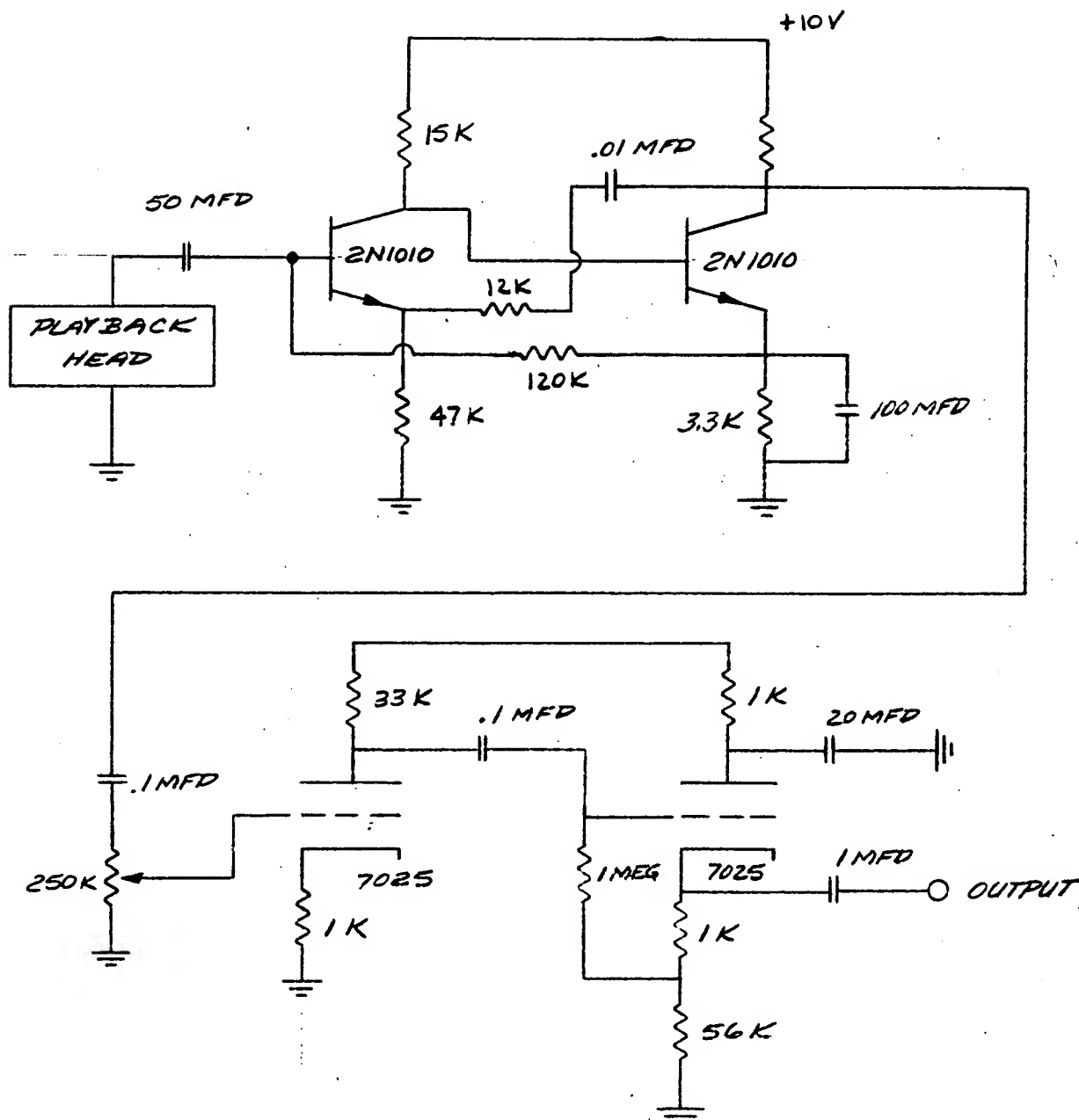
PLAYBACK AMPLIFIER SCHEMATIC

FIG. C-3

APPENDIX D

STABILIZATION BY RATE GYRO FEEDBACK

The purpose of this analysis is to determine, within first order accuracy, the feasibility of utilizing a rate feedback closed loop control system for stabilizing a platform with respect to its inertial axis. The performance characteristics of a commercially available subminiature precision rate gyro and a low inertia servo motor have been utilized in making this analysis (see references below).

The following assumptions have been made:

1. The vibrational environment and mechanical vibration isolation described in Reference 1 is assumed.

2. Non-linearities in all components are assumed negligible.

3. An ideal gear reduction unit is assumed (gear inertia, friction and backlash are negligible) or a direct drive motor is used.

4. Time delay of the servo motor's winding is negligible.

5. Time delay of the rate gyro's torque windings (if one is used in place of spring loading) is negligible.

6. Time delay of the amplifier is negligible.

---

1. The Exploratory Analysis of Isolation Philosophies for the Protection of an Ultra-Sensitive "R" System (Project 2570).

2. John Oster Manufacturing Company Catalog -- Low Inertia Servo-Motor, Type 15-5153.

3. The U.S. Time Corporation, Gyro Division Catalog -- "Subminiature Rate Gyro" Model No. 40.

7. The only source of noise within the closed loop system is assumed to be that of the rate gyro as specified by the manufacturer, i.e., amplifier and servo motor noise (due to hysteresis and harmonics) are assumed negligible.

8. The effect of linear acceleration of the airframe on gyro performance is negligible.

9. The effects of temperature variations on component performance is negligible.

10. The angular rate of deviation of the stabilized platform from its inertial axis must not exceed 1/10 of 1° per second.

11. The moment of inertia of the fully equipped platform is estimated not to exceed 4000 lbs.-in-sec.^{2}.

The approach used in analyzing the performance of the proposed rate feedback stabilization system was to assume a theoretical rate feedback system in the form of a system block diagram where each component in the system is represented by a block with its input and output signal sonnections to other blocks indicated by arrows which indicate the direction of the transmitted signal (see Figure D-1).

The component dynamic is now examined. In order to reduce the complexity of the problem, simplifying assumptions have been made regarding the dynamic characteristics of each of the components (see Assumptions). We believe these assumptions to be justified since a first order approximation of the performance of the proposed system is acceptable at this stage in the development and the results will indicate the optimum performance that can be expected from physically realizable equipment.

DESCRIPTIVE BLOCK DIAGRAM
- BROKEN LINES INDICATE MECHANICAL COUPLING
- SOLID LINES INDICATE ELECTRICAL CONNECTIONS

Θ_i = AIRFRAME VIBRATION DISPLACEMENT

Θ_L = STABLE PLATFORM DISPLACEMENT

E_s = OUTPUT SIGNAL OF RATE GYRO

E_M = OUTPUT SIGNAL OF AMPLIFIER

VEHICLE

Θ_i

SERVO-MOTOR
DIRECT DRIVE
OR
REDUCTION GEAR

Θ_L STABILIZED PLATFORM

E_M AMPLIFIER

E_s

RATE GYRO
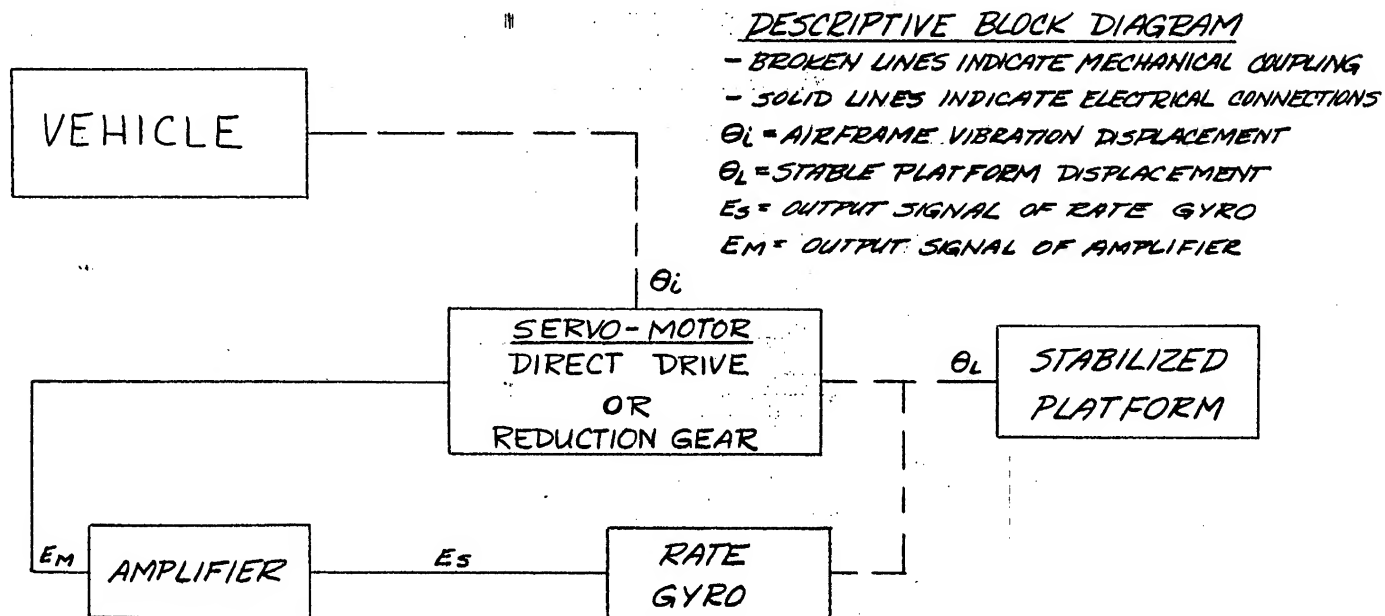
RATE FEEDBACK STABILIZATION SYSTEM

FIG. D-1

Differential equations which determine the dynamic performance of each of the idealized components are now derived and, by means of the Fourier transformation, transformed into an operational transfer function of frequency which will provide the gain (or attenuation) and phase shift which the component causes on a sinusoidal input signal of a given frequency. The transfer function is now associated with its corresponding blocks in the system block diagram and, by means of conventional-feedback-control theory, operational transfer functions for both open and closed loop response of the system are derived. The parameters of these transfer functions are related to the inertia, drag, spring constant and other physical parameters of the components.

The next step in the analysis is to select a servo motor capable of supplying the peak power and torque requirements of the stabilized platform. By neglecting bearing friction and viscous drag, the platform may be assumed to present a purely inertial load to the motor. Using the estimated maximum moment of inertia, the maximum allowable angular velocity of the stabilized platform, and the expected vibration environment, the peak torque, peak power and average power requirements of the load were determined. Using these calculated values, a suitable servo motor was selected (see Reference 2) and the required gear ratio determined. Referring to torque-speed curve and torque-versus control voltage (at stall) curve, the motor parameters were determined and supplied to the open and closed loop transfer functions.

The following procedure was used to estimate the performance characteristics and dynamic parameters that a suitable rate gyro would require. A good compromise between speed of response and overshoot for many practical feedback control systems is obtained when the system parameters are adjusted so that the gain margin of the open loop transfer function is (-10 db) and its

phase margin is (30 deg.). Solving the open loop transfer function for the above gain margin yields an expression which shows that the required open loop gain constant is directly proportional to the product of the rate gyro's damping factor and resonant frequency.

The solution of the open loop transfer function for a phase margin of 30 deg. indicates that the rate gyro damping factor should be three tenths. Substituting the derived relations and values into the closed loop transfer function gives us an expression for this function in which the only unknown parameter is the resonant frequency of the rate gyro. The absolute magnitude, i.e., gain of the closed loop transfer function, defines the "transmissibility" of the proposed rate feedback stabilization system, shown in Figure D-2.

The selection of the rate gyro was made on the basis of required full scale range, resolution, zero errors and residual noise. All of these factors were found to fall well below the maximum tolerable values required by the stability performance requirements for the rate gyro which was selected (see Reference 3). The nominal damping factor of this rate gyro is 1/2 of critical damping and, thereby exceeds the optimum damping factor (3/10 of critical). Therefore, response of this rate gyro is somewhat more sluggish than that which is desired and may require a higher open loop gain and, consequently, more amplification than that which is required by the optimum rate gyro.

Resonant frequency of the selected gyro is 26 cps. This frequency is permissible if the transmissibility characteristics of the vibration isolators approximate system "A" (described on page 26 of Reference 1), but is somewhat closer to the resonant frequency of system "B" (same reference).

Engineering Report No. 5530   Page 35
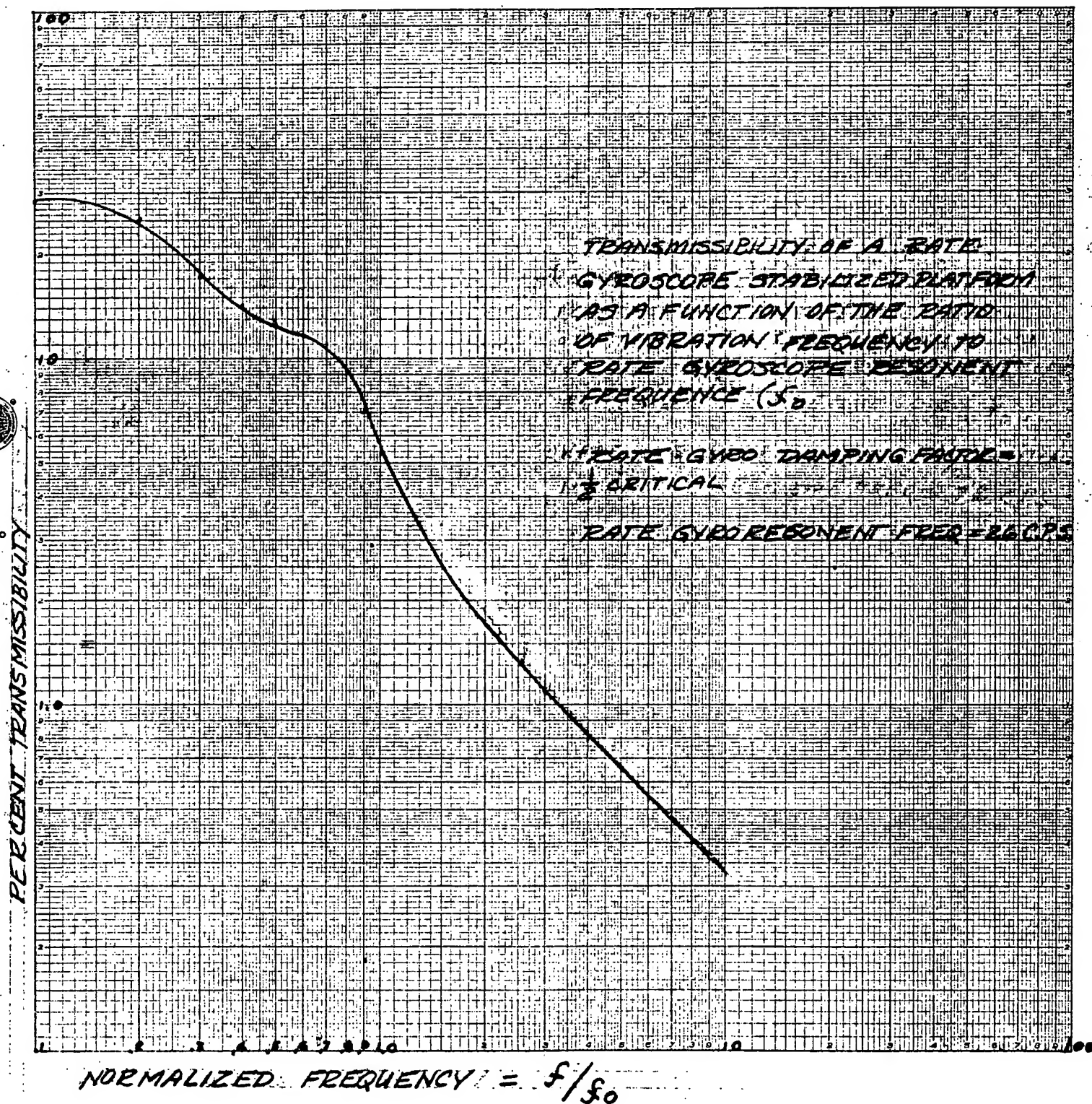
FIG. D-2

However, if the anticipated vibrational environment approximates that provided in Reference 1 (page 11 of 26), the coincidence of the vibration isolation and stabilization systems resonance should not result in excessive vibrations at 26 cps. The maximum transmissibility at 26 cps for the rate stabilization system "B" vibration isolators is three percent, giving a system transmissibility at resonance of 0.15% while the transmissibility when system "A" isolators are used would be less than 0.04%. Class B system would allow a maximum vibrational environment of 67 deg/sec. at 26 cps which is far in excess of what is to be expected from the vehicle at this frequency.

The effect of residual gyro noise on the noise level of the closed loop stabilization system output was next evaluated. All other possible sources of noise were considered negligible in this analysis. The expected maximum noise level of the closed loop stabilization system due to the presence of rate gyro noise should not be greater than twelve percent of the gyro's redisual noise. This residual noise is given by the manufacturer as not exceeding 0.08 deg/sec maximum. The system noise should, therefore, not exceed 0.09 deg/sec. a tolerable value.

The results of the analysis, described above, leads to the following conclusions concerning the practicality of a rate feedback stabilization.

1. Rate stabilization of the stabilized platform is practical if a precision rate gyroscope of the type described in Reference 3 is used to generate the angular rate signal and the vibrational environment and isolation approximates that described in Reference 3.

2. If vibration isolation is not provided, the applicability of the system is limited to vibrational environments in which the maximum vibration does not exceed an angular rate of two degrees per second.

3. Damping factor for the selected rate gyro is somewhat higher than the calculated optimum value indicating some sluggishness in the gyro's response to input angular rate deviations. However, rate gyros with lower damping factors than that of the selected unit are commercially available if required.

4. Gyro noise effect should not prove to be a problem in the rate feedback stabilization system.

APPENDIX E

THERMAL EVALUATION OF WINDOW PROBLEM

The solution of transient heat flow equations is necessary for the proper analysis of the thermal aspect by the window problem. An initial solution was attempted by mathematical methods, but was found to be too complex for convenient theoretical analysis. An electrical analog method was derived for the solution of these equations. Not only did the analog method afford a means of obtaining the basic heat data, but it also enabled a convenient and efficient means for evaluation of various proposed window design parameters and configurations.

The initial analog design was based upon a simulation of the existing experimental window configuration; two eight inch diameter, 0.878 inch thick fused silica glazings and one eight inch diameter, 0.480 inch BK-7 inner glazing, Figure 1. This was done to enable a comparison of analog data with that of actual experiment.
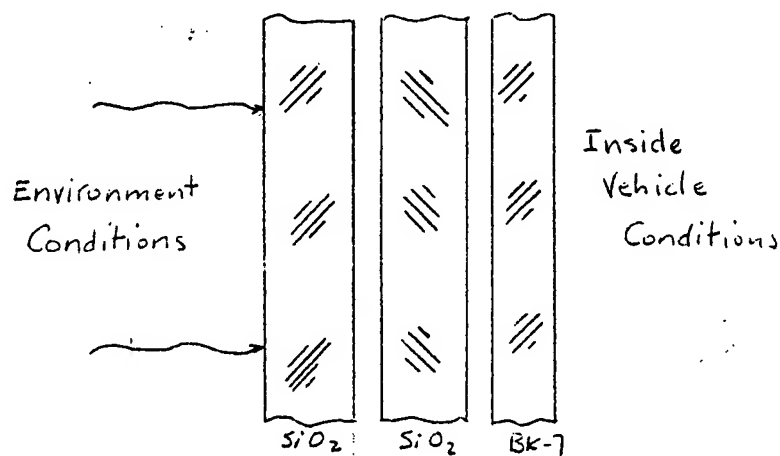

Figure 1

The design of the analog computer is based on the following:

The properties of Corning 7940 fused silica are:

* Specific heat = Cp = 0.2008 $\frac{cal}{gm^oC}$ = 0.2008 $\frac{Btu}{lb^oF}$

* Density = ρ = 2.2 gm/cc = 0.0793 $\frac{lb}{in^3}$

* Thermal Conductivity = K = 0.0037 $\frac{cal\ cm}{cm^2\ sec^oC}$ = 0.075 $\frac{Btu\ in}{in^2\ hr^oF}$

* (Taken from data compiled by Corning Glass Works)

Average values in the range between -20°F to 550°F were used since the quantities do not change appreciably with temperature.

$$Cp\rho = (0.2008) \frac{Btu}{lb^oF} (0.0793) \frac{lb}{in^3} = 0.0159 \frac{Btu}{in^3\ ^oF}$$

$$\frac{Cp\rho}{K} = \frac{0.0159 \frac{Btu}{in^3\ ^oF}}{0.075 \frac{Btu\ in}{in^2\ hr^oF}} = 0.213 \frac{hr}{in^2} = 767 \frac{sec}{in^2}$$

CONDUCTION:

For convenience, each fused silica glass glazing is divided into seven equal sections of width, d.
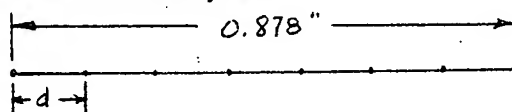
$$\therefore d = \frac{0.878}{7} = 0.1252 \text{ in.}$$

Electrically, the thermal properties of these sections are represented by tee sections as in Figure 2.
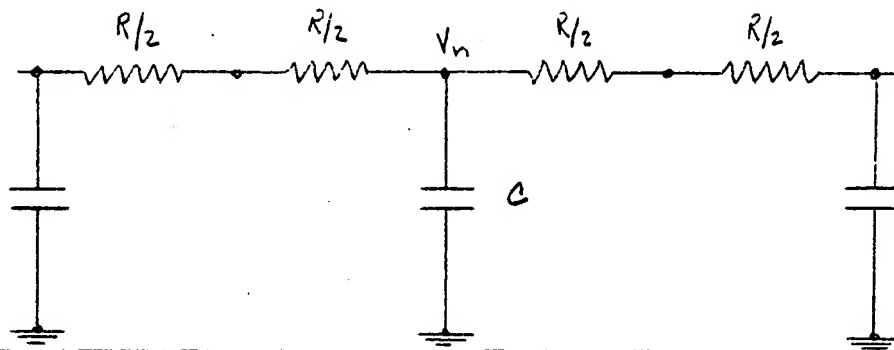
Figure 2 - Tee Sections

Where the resistors are analogous to the resistance of the material to conduct heat across its section, the capacitor is an analogy of the ability of the material to retain heat, and the voltage drop across the tee is analogous to the temperature drop across the section.

$$V_n^{(t)} = \frac{1}{C} \int_0^t \left[\frac{(V_{n+1} - V_n)}{R} + \frac{(V_{n-1} - V_n)}{R} \right] dt + V_n^{(0)}$$

$$= \frac{1}{RC} \int_0^t (V_{n-1} - 2V_n + V_{n+1}) \, dt + V_n^{(0)} \qquad \text{Eq. (1)}$$

From transient heat conduction relations,

$$\frac{d^2\theta}{dx^2}(x,t) = \frac{C\rho}{k} \quad \frac{d\theta}{dt_\omega}(x,t) \qquad \text{Eq. (2)}$$

Where θ = temperature, and is a function of x and t.

d = thickness of the section

t = time

x = distance to window section

Since,

$$\frac{d^2 \theta_n}{dx^2} \cong \frac{\theta_{n+1} - 2\theta_n + \theta_{n-1}}{d^2}$$

Eq. (3)

where $\theta_n = \theta\left(nd + \frac{d}{2}, t\right)$

Then from equations (2) and (3),

$$\frac{d^2 \theta_n}{dx^2} \cong \frac{\theta_{n+1} - 2\theta_n + \theta_{n-1}}{d^2} = \frac{C_p \rho}{K} \frac{d\theta_n}{dt_\omega}$$

or, $\theta_{n+1} - 2\theta_n + \theta_{n-1} = \frac{d^2 C_p \rho}{K} \frac{d\theta_n}{dt}$

Eq. (4)

Differentiating Equation (1),

$$RC \frac{dV_n}{dt_c} = (V_{n+1} - 2V_n + V_{n-1})$$

Eq. (5)

Note that equations (4) and (5) are of the same form.

A time scale factor, S, is now introduced that relates computer time, t_c, with the actual window time, t_ω.

$$\therefore t_\omega = S t_c$$

Eq. (6)

Introducing Eq. (6) to Eq. (5)

$$SRC \frac{dV_n}{dt_\omega} = (V_{n+1} - 2V_n + V_{n-1})$$

Eq. (7)

Since voltage is the analog of temperature, then from eqns. (4) and (7)

$$SRC = \frac{d^2 C_p \rho}{K} = (.1252)^2 \, in^2 \, (767) \frac{sec}{in^2}$$

$$= 12.05 \, sec$$

Let R = 39 KΩ

C = 1 μf

Then RC = 0.039 sec.

And $\delta = \dfrac{12.05}{.039}$ = 309

Time Scale Factor = δ = 309

At equilibrium, the flow of heat through each section is

$$h = -K \frac{d\theta}{dx}$$

but $\dfrac{d\theta_n}{dx} \simeq \dfrac{\theta_{n+\frac{1}{2}} - \theta_{n-\frac{1}{2}}}{d}$

$\therefore h = -\dfrac{K}{d} \left(\theta_{n+\frac{1}{2}} - \theta_{n-\frac{1}{2}} \right)$ Eq. (8)

Electrically, this is analogous to the current through n

or $i_n = - \dfrac{V_{n+\frac{1}{2}} - V_{n-\frac{1}{2}}}{R}$ Eq. (9)

and $\dfrac{K}{d}$ is analogous to $\dfrac{1}{R}$

Now, let the relationship between voltage and temperature be

     T = aV + b   Eq. (10)

where a and b are constants

Introducing the relationship of eqn. (10) to eqn. (8),

$$h = -\frac{K}{d} \left[\left(a V_{n+\frac{1}{2}} + b \right) - \left(a V_{n-\frac{1}{2}} + b \right) \right]$$

$$h = -\frac{aK}{d} \left(V_{n+\frac{1}{2}} - V_{n-\frac{1}{2}} \right)$$

And from eqn. (9)

$$h = +\frac{aK}{d} R\, i_n$$

     Eq. (11)

$$\frac{KR}{d} = \frac{0.075 \frac{Btu}{in \, hr \, {}^{\circ}F} \left(\frac{1.8 {}^{\circ}F}{{}^{\circ}K}\right)}{.1252 \, in.} \times \frac{1 \, hr}{3600 \, sec} \times 39,000 \, ohms$$

$$= 12.0 \frac{Btu}{in^2 \, sec \, {}^{\circ}K} \times \frac{Volts}{amp}$$

$$\therefore \; h = + 12.0 \, a \, i_n \frac{Btu}{in^2 \, sec \, {}^{\circ}K} \times \frac{Volts}{amp} \times \frac{{}^{\circ}K}{Volts} \times amp = \frac{Btu}{in^2 \, sec}$$

Eq. (12)

RADIATION:

The radiation of heat across the gap between the windows is
represented thermally by

$$h_{rad} = \sigma \frac{\epsilon_1 \epsilon_2}{\epsilon_1 + \epsilon_2 - \epsilon_1 \epsilon_2} \left[\Theta_{n+\frac{1}{2}}{}^4 - \Theta_{m-\frac{1}{2}}{}^4 \right]$$

Eq. (13)

where σ is the Stefan-Boltzmann constant $= 0.1713 \times 10^{-8} \frac{Btu}{ft^2 \, hr \, {}^{\circ}R^4}$

ϵ_1 = emissivity at surface of first window

ϵ_2 = emissivity at surface of second window

$\Theta_{n+\frac{1}{2}}$ = temperature at surface of first window

$\Theta_{m-\frac{1}{2}}$ = temperature at surface of second window

If the ratio of $\Theta_{n+\frac{1}{2}}$ to $\Theta_{m-\frac{1}{2}}$ (in absolute measurement) is up to 2, then

$$\Theta_{n+\frac{1}{2}}{}^4 - \Theta_{m-\frac{1}{2}}{}^4 \cong \left(\Theta_{n+\frac{1}{2}} - \Theta_{m-\frac{1}{2}} \right) \left(\Theta_{ave}{}^3 \right) \times 4$$

And from eq. (13)

$$h_{rad} = \sigma \frac{\epsilon_1 \epsilon_2}{\epsilon_1 + \epsilon_2 - \epsilon_1 \epsilon_2} 4 \left(\Theta_{ave}{}^3 \right) \left(\Theta_{n+\frac{1}{2}} - \Theta_{m-\frac{1}{2}} \right)$$

Eq. (14)

Eq. (14) is of the same form of eq. (9), thus

$$i = \frac{h_{rad}}{4 \, a \, \sigma \frac{\epsilon_1 \epsilon_2}{\epsilon_1 + \epsilon_2 - \epsilon_1 \epsilon_2} \Theta_{ave}{}^3 \, R}$$

Since, from eq. (12)

$$h = 12.0 \, a \, i_n$$

then

$$1 = \frac{12.0 air}{4 a \sigma \frac{\epsilon_1 \epsilon_2}{\epsilon_1 + \epsilon_2 - \epsilon_1 \epsilon_2} \theta_{ave}^3 R}$$

and

$$R = \frac{12.0}{4 \sigma \frac{\epsilon_1 \epsilon_2}{\epsilon_1 + \epsilon_2 - \epsilon_1 \epsilon_2} \theta_{ave}^3} \qquad \text{Eq. (15)}$$

where $= 0.1713 \times 10^{-8} \dfrac{Btu}{ft^2 \, hr \, {}^\circ R^4}$

$= 3.47 \times 10^{-14} \dfrac{Btu}{in^2 \, sec \, {}^\circ k^4}$

substituting into eq. 15 for various θ_{ave}, the following values of R are found:

<u>Case 1 - No coatings on window surfaces</u>

$\theta\,{}^\circ k$	ϵ_1	ϵ_2	$\dfrac{\epsilon_1 \epsilon_2}{\epsilon_1 + \epsilon_2 - \epsilon_1 \epsilon_2}$	$R = \dfrac{12.0}{4 \sigma \frac{\epsilon_1 \epsilon_2}{\epsilon_1 + \epsilon_2 - \epsilon_1 \epsilon_2} \theta_{ave}^3} \times 10^{-6}$ megohms
300	.89	.89	.800	3. 96
400	.87	.87	.770	1.82
500	.84	.84	.724	.99
600	.81	.81	.681	.61
700	.77	.77	.626	.418

<u>Case 2 - One window surface coated, the other not coated</u>

300	.89	.2	.195	17.00
400	.87	.2	.194	7.22
500	.84	.2	.193	3.71
600	.81	.2	.191	2.18
700	.77	.2	.189	1.38

Case 3 - Both window surfaces coated

$\Theta \, ^\circ K$	ϵ_1	ϵ_2	$\dfrac{\epsilon_1 \epsilon_2}{\epsilon_1 + \epsilon_2 - \epsilon_1 \epsilon_2}$	$R = \dfrac{12.0}{46 \dfrac{\epsilon_1 \epsilon_2}{\epsilon_1 + \epsilon_2 - \epsilon_1 \epsilon_2} \Theta_{ave}^3} \times 10^{-6} \, megohms$
300	.2	.2	.111	30.00
400	.2	.2	.111	12.60
500	.2	.2	.111	6.46
600	.2	.2	.111	3.74
700	.2	.2	.111	2.38

Since the emissivities are functions of temperature, an average slope

(taken at the mid-point of the range) must be found that will fit the relationship

between resistance and temperature.

Thus for Case 1:

$$\left(\frac{\Theta_2}{\Theta_1}\right)^k = \frac{R^2}{R^1}$$

$$\left(\frac{760}{300}\right)^k = \frac{.118}{3.96}$$

$$2.33^k = .104$$

$$k = -2.68$$

For Case 2:

$$\left(\frac{\Theta_2}{\Theta_1}\right)^k = \frac{R_2}{R_1}$$

$$\left(\frac{700}{300}\right)^k = \frac{1.38}{17.00}$$

$$2.33^k = .0813$$

$$k = -2.97$$

And for Case 3:

$$\left(\frac{\theta_2}{\theta_1}\right)^k = \frac{R_2}{R_1}$$

$$2.33\, k = \frac{2.38}{30.00} = .0794$$

$$k = -3.00$$

A curve was drawn based on measured values of detector resistance vs. voltage.

Transposing values to correspond with the slopes calculated above,

corresponding voltages are calculated below.

The slope relationship is:

$$\frac{d \log R}{d \log T} = \frac{nT}{T-b}$$

Eq. (16)

For Case 1:

From "Detector Resistance vs. Voltage" curve, n = -3.41

$$\frac{d \log R}{d \log T} = -2.68 \qquad \frac{nT}{T-b} = \frac{-3.41(500)}{500-b}$$

$$\therefore -2.68 = \frac{-3.41(500)}{500-b}$$

$$\text{and} \quad b = -136 \quad (@ 500\,°k)$$

Since T = aV + b

then   500 = 65a - 136

and a = 9.8

Thus, the corresponding voltages for each θ value taken are:

θ	V
300	44.5
400	54.7
500	65.0
600	75.1

θ	V
700	85.4
0	13.7

For Case 2:

$$n = -3.55$$

$$\frac{d \log R}{d \log T} = -2.97 \quad \frac{nT}{T-b} = \frac{-3.55(500)}{(500-b)}$$

$$\therefore -2.97 = \frac{-3.55(500)}{500-b}$$

and b = -97.8

since T = aV + b

then   500 = 45a - 97.8

and   a = 13.25

θ	V
300	30.0
400	37.5
500	45.0
600	52.6
700	60.0

For Case 3:

$$n = -3.62$$

$$\frac{d \log R}{d \log T} = -3.00 \quad \frac{nT}{T-b} = \frac{-3.62(500)}{500-b}$$

$$\therefore -3.00 = \frac{-3.62(500)}{500-b}$$

and b = -103.3

then 500 = 38a - 103.3

and a = 15.9

Engineering Report No. 5530

$\underline{\theta}$	$\underline{V}$
300	25.4
400	31.6
500	38.0
600	44.2
700	50.5

CONVECTION:

The thermal convection of heat caused by an air stream through the gap between the windows is represented as in Figure 3 below
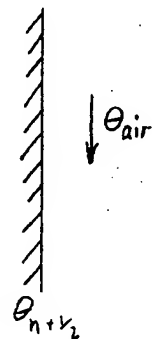
$$h_{conv.} = Q \left[\theta_{n+\frac{1}{2}} - \theta_{air} \right] \qquad \text{Eq. (17)}$$

where Q = Convection Constant

Figure (3) Convection Schematic

Electrically, the heat convection is simulated by Figure 4 below.
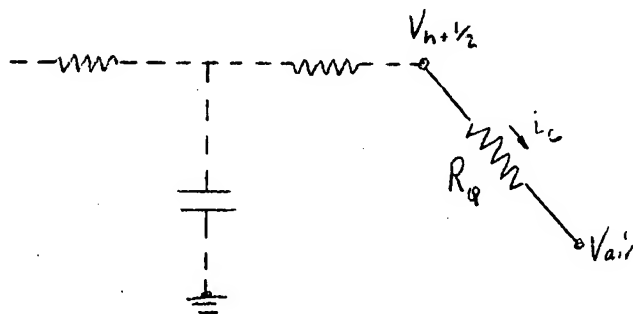
$$i_c = \frac{1}{R_Q} \left[V_{n+\frac{1}{2}} - V_{air} \right] \qquad \text{Eq. (18)}$$

Since $T = aV + b$, and from eqs. (17) and (18)

$$i = \frac{h}{Q a R_Q} = \frac{12.0 \, a \, i}{Q \, a \, R_Q} = \frac{12.0 \, i}{Q \, R_Q} \text{ amps}$$

and $R_Q = \frac{12.0}{Q}$ ohms where Q is in units of $\frac{Btu}{sec \, in^2 \, °K}$ Eq. (18a)

It is intended that the value of R_Q will be chosen to suit various window

parameters.

The last window is of BK-7 rather than fused-silica quartz and is

0.480 in. thick. Because of the differences, it becomes necessary to calculate

the total resistance value required in the analog of the last window.

For BK-7

$$Cp = 0.199 \, \frac{Btu}{lb \, °F}$$

$$\rho = 160 \, \frac{lb}{ft^3} = 0.093 \, \frac{lb}{in^3}$$

$$K = 5.5 \, \frac{Btu \, in}{ft^2 \, hr \, °F} = 0.0382 \, \frac{Btu}{in \, hr \, °F}$$

$$\frac{Cp \, \rho}{K} = 0.482 \, \frac{hr}{in^2} = 1735 \, \frac{sec}{in^2}$$

From eqs. (4) and (7):

$$\mathcal{J} R C = \frac{d^2 \, C_\rho \, \rho}{K}$$

$\mathcal{J}$ has been established as being 309

$C = 1 \, \mu f = 1 \times 10^{-6}$ farad

$d = \frac{.480}{5} = 0.096$ in. (using five sections)

$\therefore R = \frac{(.0092) \, in^2 \, (1735) \, \frac{sec}{in^2}}{309 \, (1 \times 10^{-6}) \, farad} = .051 \times 10^6$ ohms

$R \cong 49,000 \, \Omega$

ANALYSIS OF ANALOG ACCURACY:

The errors inherent in the electrical analogy of the thermal heat transfer across the window system are briefly discussed below.

The mathematical outline of the computer involves differential equations which may be functions of complex form. The differential quantities were approximated by making them equal to finite increment quantities or, in other words, dx was approximated by Δx (eq. (3), eq. (8)). Seven sections were used in the analogy of the quartz thickness.

Using a fused silica glass window divided into seven equal sections of width, d, the heat flow through each section is

$$h = -KA \frac{dT}{dx}$$
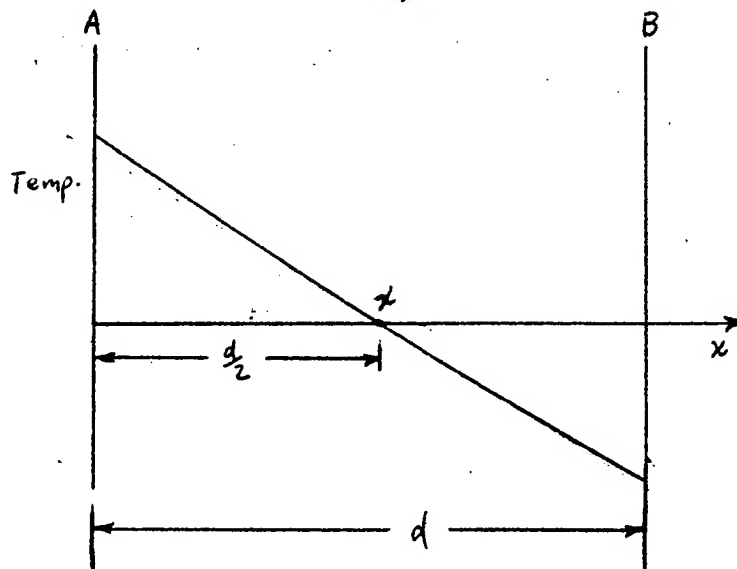
We can approximate over a small interval the temperature function by a taylor expansion about point x.

At edge B the temperature can be written as

$$T_{(x+\frac{d}{2})} = T_{(x)} + T'_{(x)}\frac{d}{2} + \frac{T''_{(x)}}{2}\frac{d^2}{4} + \frac{T'''_{(x)}}{8\cdot6}d^3 + \dots \qquad \text{(Eq. 20)}$$

At edge A the temperature can be written as

$$T_{(x-\frac{d}{2})} = T_{(x)} - T'_{(x)}\frac{d}{2} + \frac{T''_{(x)}}{2\cdot4}d^2 - \frac{T'''_{(x)}}{8\cdot6}d^3 + \dots \qquad \text{(Eq. 21)}$$

$$\therefore \; T_A - T_B = T'_{(x)}d + \frac{T'''(x)d^3}{6\cdot4} + \dots \qquad \text{(Eq. 22)}$$

were T'(x) is the True Temperature gradient at x.

Rewriting eq. (22) we have

$$\frac{T_A - T_B}{d} = T'_{(x)} + \frac{T'''_{(x)}}{6}\cdot\frac{d^2}{4} + \dots$$

However, after the first 5 minutes T(x) in the first plate is sufficiently
linear such that

$$\left| \frac{\frac{T_A - T_B}{d} - T'_{(x)}}{T'_{(x)}} \right| << 1$$

From this result we estimate that the major effect of this approximation
is to give an error in the time scale of 3 minutes or less.

The determining the temperature dependent parameters, namely, thermal
conductivity, specific heat, and emissivity, the mean value of each parameter
was calculated over the temperature range of operation. These approximations
are considered to introduce no greater error than the magnitude of error inherent

in the compilation of the original data for fused silica.

The heat transfer coefficient for forced convection in the second gap is dependent on physical properties of the coolant and the configuration of the apparatus. The physical properties were calculated at the mean of the cooling air. The plate was assumed to be a square configuration. The error due to these assumptions is considered to be almost negligible.

Further sources of error are due to innate inaccuracies in the electrical components (for example, capacitor leakage and tolerance in resistor values). The expected errors due to component inaccuracies were calculated to be about 5.4%.

The errors induced by components can be found as follows:

We denote the N elements of a sample by x_1, x_2, $x_3 + \ldots + x_N$, where the values of each element are distributed independently of the other values and according to the given distribution function x. The variable x has a mean ξ and variance σ^2.

The sum and the mean of the values

$$S_x = x_1 + x_2 + \ldots\ldots + x_N$$

$$\bar{x} = \frac{1}{N} (x_1 + x_2 + \ldots\ldots + x_N)$$

vary from sample to sample.

Now

$$M(S_x) = M(x_1) + M(x_2) + \ldots\ldots + M(x_N) = N\xi$$

$$V(x) = V(x_1) + V(x_2) + \ldots\ldots + V(x_N) = N\sigma^2$$

where M is mean and V is variance.

Consequently

$$M(\overline{X}) = \mathcal{E}$$

$$V(\overline{X}) = \frac{\sigma^2}{N}$$

The standard error is defined as the square root of the variance thus

$$S.E. = \frac{\sigma}{\sqrt{N}}$$

The standard error of 25 resistors and 21 capacitors is

Capacitors

$$x_1 = x_2 = x_3 = x_N = 20\%$$

$$\sigma = \left[\frac{\Sigma fi \ (x_1 - \overline{x})^2}{\Sigma fi} \right]^{1/2} = 20\%$$

$$N = 21 \qquad \sqrt{N} = 4.6$$

$$S.E. = \frac{20\%}{4.6} = 4.4\%$$

Resistors

$$x_1 = x_2 = x_3 = x_N = 5\%$$

$$\sigma = 5\%$$

$$\sqrt{N} = 5$$

$$S.E. = \frac{5\%}{5} = 1.0\%$$

Total error in system $\simeq 4.4\% + 1.0\% = 5.4\%$

The error caused by approximating the $(\theta_1^4 - \theta_2^4)$ term in the radiation relation by $4(\theta_1 - \theta_2)(\theta_{ave}^3)$ eq. (14) can be calculated.

For the radiation equation:

$$\theta_1{}^4 - \theta_2{}^4 = 4 (\theta_1 - \theta_2) \theta_{ave}{}^3 \qquad\text{Eq. (23)}$$

The range of values for θ_1/θ_2 which make the above approximation good to within

(x%) can be found as follows:

$$\text{Percent accuracy} = \chi = \frac{4 \theta_{ave}^3 (\theta_1 - \theta_2)}{\theta_1{}^4 - \theta_2{}^4} \qquad\text{Eq. (24)}$$

but

$$\theta_{ave} = \frac{\theta_1 + \theta_2}{2}$$

Thus eq. (24) become

$$\chi = \frac{50 (\theta_1 + \theta_2)^3 (\theta_1 - \theta_2)}{\theta_1{}^4 - \theta_2{}^4}$$

$$= \frac{50 (\theta_1 + \theta_2)^2 (\theta_1{}^2 - \theta_2^2)}{(\theta_1{}^2 - \theta_2{}^2)(\theta_1{}^2 + \theta_2{}^2)} = \frac{50 (\theta_1 + \theta_2)^2}{\theta_1{}^2 + \theta_2{}^2}$$

$$\chi = 50 \frac{\left(\frac{\theta_1}{\theta_2} + 1\right)^2}{\left(\frac{\theta_1}{\theta_2}\right)^2 + 1} \qquad\text{Eq. (25)}$$

Rewritting eq. (25)

$$\left(\chi - 50\right)\left(\frac{\theta_1}{\theta_2}\right)^2 - 100 \left(\frac{\theta_1}{\theta_2}\right) + \left(\chi - 50\right) = 0 \qquad\text{Eq. (26)}$$

Using equation 26 the following values of θ_1/θ_2 were calculated for various

values of

% Error (χ)	θ_1/θ_2
0	1.00
1	1.22
2	1.33
5	1.59

% Error ($\swarrow$)	θ_1/θ_2
8	1.84
10	2.00
13.9	2.25
15.6	2.50
17.6	2.75
20.0	3.00

The maximum value of θ_1/θ_2 about 2.5, occurs between surface 2 and 3 of the proposed window configuration. The simulation inaccuracies are presumed to be about 5%. The use of empirical relations for heat convection are probably accurate within ±30%.

The analog is designed to be a one dimensional model and does not take into account conduction, convection, or radiation to the side walls or the window supports, although some corrections can be easily made if these effects are small.

The recording instrument can be read accurately to the nearest quarter of a scale division (± 1/8). This can amount to an error of $2.2F^{\circ}$ or a total error of 0.4% over the temperature range.

DETERMINATION OF COOLING AIR TEMPERATURE AND RATE:

The primary objective of the cooling air is to maintain the inner surface of the window at a preselected temperature; 130°F has been used in this analysis. However, the manner in which this is accomplished will ultimately be a determining factor in establishing the thermal profile of the window.

Cooling air will necessarily be introduced from one edge of the inner gap. This will result in a thermal gradient, in the direction of air flow, in both adjacent glazings. The allowable gradient in each glazing is determined by such factors as tolerance to index of refraction changes in the glazing and in the equipment bay environment, and effect of non-uniform thermal expansion of the glazings. These tolerances have been discussed in Appendix F.

Various investigators have analyzed the heat transfer characteristics for laminar flow between parallel plates. Their data indicates that the coefficient of heat transfer increases linearly with cooling air velocity in a particular parameter range. Beyond that range, it varies nonlinearly; the degree of nonlinearity being determined by the window and cooling air parameters.

The inner glazings will develop a thermal gradient which has a close correspondence to the temperature of the cooling air across the window. To minimize the thermal gradient in the inner glazing, it is necessary to introduce a high rate of cooling at a small temperature difference relative to the inner glazing. The limiting case is one which soaks the inner glazing in 130°F air to maintain it uniformly at 130°F.

The gradient in the middle glazing is somewhat different in behavior, since it has a thermal history different than the inner glazing. The magnitude of the gradient can be reduced by tipping one or both of the glazings to form a wedge-shaped gap. Such a configuration will increase velocity

with a decreasing ΔT, between glazing and air. However, since cooling may vary nonlinearly with velocity, such a wedge shaped gap may result in a non-linear gradient. The magnitude of tolerable non-linearity becomes a major consideration, as set by optical considerations (Appendix F).

Therefore, in any case, some gradient will result. Based on these considerations, a cooling rate and cooling air temperature can be established which avoids or minimizes harmful optical degradations caused by thermally induced index changes. Further work is necessary in understanding the optical behavior of the glazings and equipment bay environment, and also in establishing more detailed thermal data before this value can be determined.

The thermal analog is a one dimension model. The analysis of thermal profile obtained by using the analog computer is representative, for any one set of input conditions, of a section through the window, such as the leading edge. The required coefficient of heat transfer to obtain desired cooling of the inner surface along the section analyzed was determined. This coefficient is a function of temperature difference of the air to inner surface temperature and velocity. Thus, although temperature of the cooling air and its subsequent velocity have not yet been finalized, a complete temperature profile through the one dimensional model can be obtained.

Figures E-4 and E-5 show the temperature profile for the six window surfaces, for such a section. The input heat profile into surface 1 is obtained from mission profile data and corresponding temperature.

TEMPERATURE PROFILE
WINDOW CONFIGURATION

I-3 One surface of each gap coated
Vacuum in outer Gap
35°F Cooling Air in Inner Gap

FIG. E-4

Engineering Report No. 5530

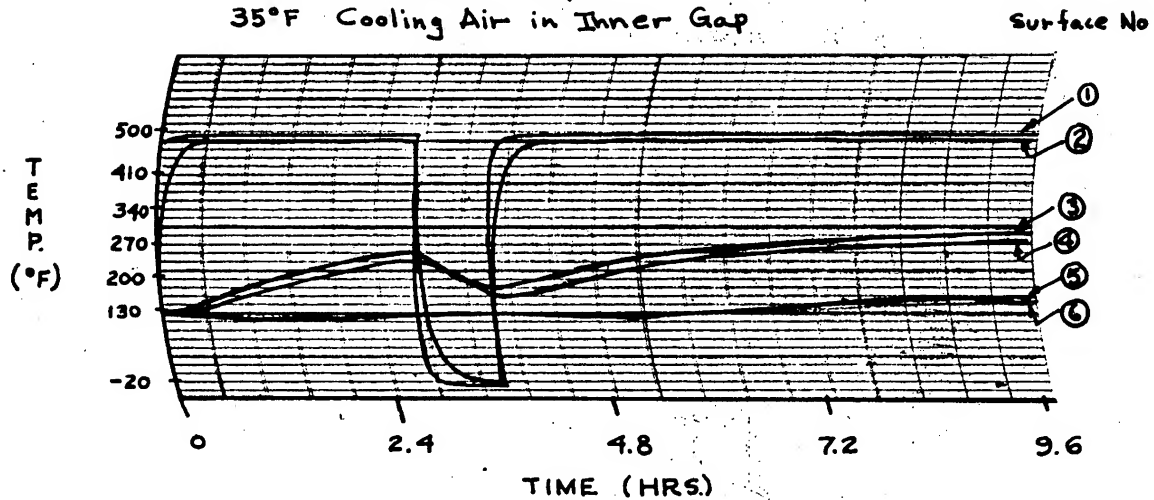## TEMPERATURE PROFILE
WINDOW CONFIGURATION

K-1 One Surface of Outer Gap Coated
Vacuum in Outer Gap
35°F Cooling Air in Inner Gap

Surface No.

TEMP. (°F)

500
410
340
270
200
130
-20

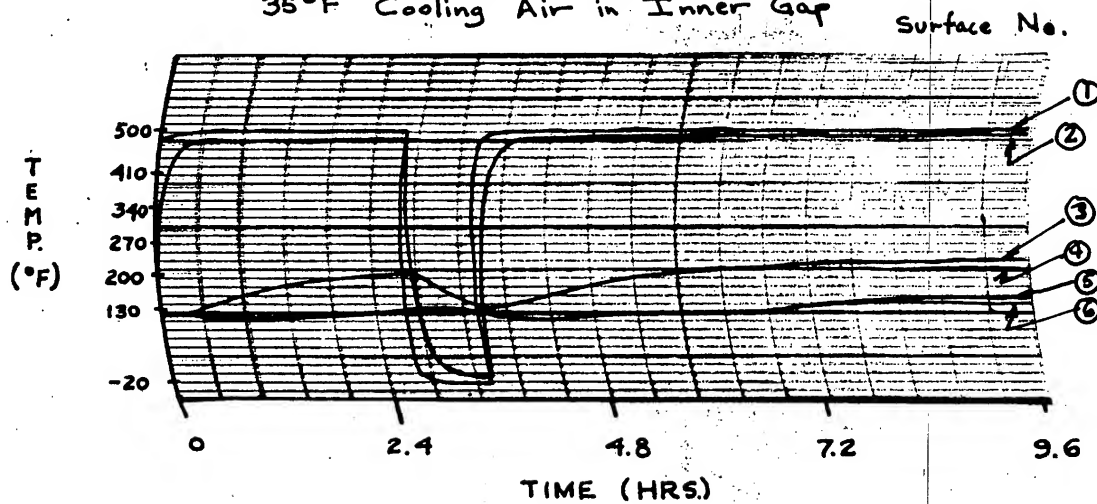0   2.4   4.8   7.2   9.6

TIME (HRS.)

FIG. E-5

Page 61

APPENDIX F

INVESTIGATION OF IMAGE DISTORTION IN WINDOW AND EQUIPMENT BAY

Discarding all influences upon the image forming wavefront prior to the window (which have been discussed in Document 57) the wavefront from an infinite object may be considered plane. The quality of the image which is produced by such wavefronts is determined by such factors as diffraction effects, correction of the image forming optics, and distortion of the incoming plane waves. The required correction and permissible diffraction limits have been established which will result in such image quality as to result in the desired resolution. It is necessary to establish tolerances upon allowable wave deformation resulting from bay environment and window effects in order to maintain the necessary image quality.

The criterion upon which this analysis is based is that deviations of 1/10 wave per inch from a place wavefront are tolerable. This is equivalent to a ray deviation of 1 second of arc or 4.8×10^{-6} radians.

One source of wavefront distortion is index fluctuations or inhomogeneties of the window material. Fluctuations of index as well as index gradients have been determined for suitable window materials. These values are listed in Figure F-1.

It is not a straightforward analysis to ascertain the allowable index fluctuations based on the established deformation tolerances. This is because the nature of the fluctuations themselves have a decided influence upon their relative effect. For example, several sharp index "spikes" which exceed what would normally be excessive limits are actually more tolerable than continuous fluctuations which have wavey shapes whose amplitudes are within

COMPARISON OF OPTICAL PROPERTIES

| Property	Material	1723 Aluminosilicate	7900 Vycox	7940 Fused Silica
Refractive Index (N_d line)		1.546 (1)	1.458 (1)	1.459 (1)
Homogeneity Index gradient/inch/inch thickness		3.8×10^{-5} (2)	3×10^{-6} (1)	8×10^{-6} (1)
Homogeneity (for 20 inch diameter blank) Index gradient/center to edge/inch thickness		----------	1×10^{-5} (1)	2×10^{-5} (1)
$\dfrac{\Delta n}{\Delta T}$ $\dfrac{\text{Change of Index}}{\text{Change of Temperature (}^{\circ}\text{C)}}$ at .6μ				100×10^{-7} (3)
Transmission, percent 1/4" thickness		90 - 92 (1)	91 - 92 (1)	92 (1)
Total Emissivity	300°F	.90 (1)	.87 (1)	.82 (1)
	600°F	.90	.88	.81
	900°F	.89	.87	.79

(1) Data from Corning Glass   (2) Measured value   (3) N.B.S. Vol. 53, p. 188

Figure F-1

tolerable limits. Not enough is known as yet about the statistical nature and shape of index fluctuations in each of the materials to most efficiently minimize the distortions from this cause.

An initial approach to the problem, which considers the allowable index variation across the pupil is as indicated in the following diagram.
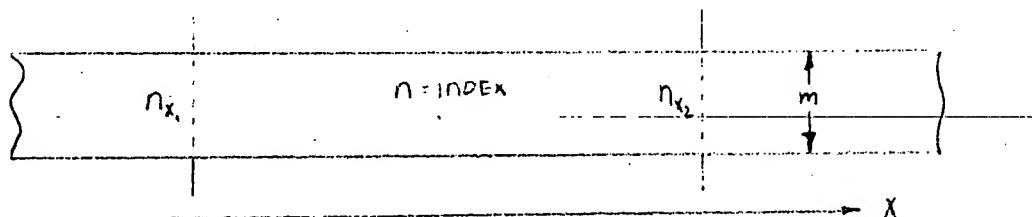
Optical Path Length $= mn$

Optical Path Difference$_{(x_2 - x_1)} = m(n_{x_2} - n_{x_1})$

$$OPD = m \Delta n$$

$$\frac{1}{10} \lambda = 6 \times 10^{-6} \text{ cm for } \lambda = .6\mu$$

Therefore

$$\Delta n = \frac{6 \times 10^{-6}}{m}$$

where Δn is the tolerable index change per inch.

Evaluating Δn for several thicknesses, we obtain

thickness (cm)	Δn
1	6×10^{-6}
2	3×10^{-6}
3	2×10^{-6}
4	1.5×10^{-6}
5	1.2×10^{-6}

According to this analysis, in a 5 cm thick window, a linear gradient which exceeds 1.2×10^{-6} change in index across the pupil is intolerable. The effect of a

linear gradient is only to translate the image laterally with respect to the film plane, with no resulting image deterioration. The allowable image translation is dictated by pointing accuracy requirements and upon tolerable resultant chromatic effects. For a monochromatic system, $\Delta n \leq 10^{-1}$ could be tolerated. Therefore translations resultant from $\Delta n = 1.2 \times 10^{-6}$ are certainly tolerable.

A more realistic analysis is to consider the index fluctuations to have the form of sine-waves. This type of gradient is much less tolerable than the linear one, since it has the effect of spreading the energy of the image. Consider a 1 second energy spread (± 1/2 sec.). The sinusoidal gradient can be represented as a varying linear function as shown in the figure below:
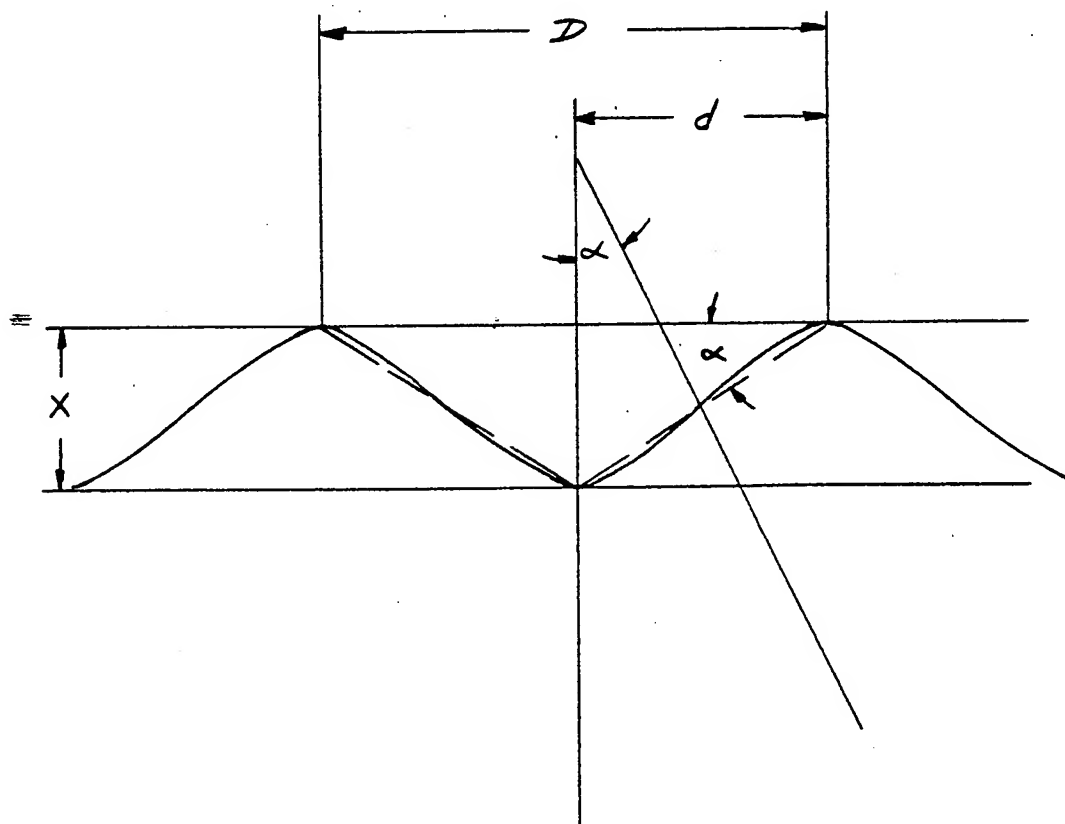
α = tolerable ray deviation

$\qquad = \pm .5$ second

$\qquad = \pm 2.4 \times 10^{-6}$ radians

$$\frac{x}{d} = \alpha$$

$$x = \alpha d$$

for d = 1.2 cm

$$x = \frac{2.4 \times 10^{-6}}{1.2}$$

$$x = 2 \times 10^{-6} \text{ cm}$$

$x = OPD = m \triangle n$ where m = thickness

$$\triangle n = \frac{2 \times 10^{-6}}{m}$$

and since $2d = D \approx 1$ inch

$\triangle n$ represents index gradient per inch across pupil.

Evaluating $\triangle n$ for various thicknesses, we obtain:

thickness (cm)	n
1	2×10^{-6}
2	1×10^{-6}
3	$.66 \times 10^{-6}$
4	$.5 \times 10^{-6}$
5	$.4 \times 10^{-6}$

The validity of this analysis depends largely on whether a linear approximation of the sine-wave is a realistic representation of energy distribution.

The fact remains that it is possible to make acceptable schlieren windows of comparable thickness from such material as fused silica. Corning estimates an index gradient of 8×10^{-6} per inch across the aperture, for a one

inch thick blank (see Figure F-1). This is an order of magnitude
in excess of the tolerance calculated above, eventhough schlieren windows require
similar wave deformation tolerances as are applied here.

Some improvement in minimizing the effects of index fluctuations
can be brought about by local figuring of the polished window. This has the
effect of locally varying the window thickness to compensate for varying index,
maintaining:

$$mn = constant$$

This is more feasible for a schlieren window than for this configuration, since
the schlieren window is one piece of glass, used at normal incidence. Parallax
which is present in a spaced three glazing configuration would diminish the
effectiveness of this technique.

The analysis of index variations within the glazing material indicates
that further investigation is necessary to establish whether available material
is of sufficiently good homogeniety as to not impair optical performance. In
particular, it is desirable to understand more about the shape and statistical
nature of these fluctuations.

The effect of a thermal gradient in the glazing materials on a
plane optical wavefront must be determined to establish the tolerable magnitude
and shape of such a gradient. For the purpose of analysis the gradient can be
divided into two components, one normal to the window surface, and one parallel
to the window surface.

The effect of a thermal gradient normal to the parallel surfaces of
a glazing material on a plane wavefront would be a uniform retardation across
the entire wavefront. The wavefront itself would be undistorted after having
passed through the window, and consequently the image quality would be unaffected.

A method for computing the effects of a lateral thermal gradient on an incident wavefront has been investigated theoretically by G.G. Sliusarev[1]. The investigation is based on the change in shape of an optical component under the influence of non-uniform heating as well as the effect of the gradient on the index of refraction. The results indicate that for an optical element in the shape of a plane parallel plate, the deviation of a light ray is directly proportional to the thermal gradient g, and to the nominal thickness e, of the optical element. For a plate of refractive index n, linear coefficient of thermal expansion α, the coefficient of change of refractive index with temperature β, the deviation ξ, is given by:

$$\xi = eg (n-1) + eg\beta = eg \left[(n-1)\alpha + \beta\right] = Keg \qquad \text{Eq. (1)}$$

A plane parallel plate under the influence of a temperature gradient would expand by different amounts along its length, becoming wedge shaped and displaying the optical properties of a prism. A ray of light incident on the plate would therefore be deviated by an amount ξ_1 given by: $\xi_1 = eg \alpha (n-1)$. In addition, there would be a second deviation due to the change of refractive index with temperature given by:

$$\xi_2 = eg\beta$$

The total deviation is the sum of these two deviations and is given by the Sliusarev equation, (1).

For the particular case of a fused silica plate:

$$\alpha = 3 \times 10^{-7} \text{ per } {}^{\circ}F$$

$$\beta = 55.5 \times 10^{-7} \text{ per } {}^{\circ}F$$

$$n = 1.459$$

$$K = \left[(1.459-1)(3 \times 10^{-7}) + 55.556 \times 10^{-7}\right] = 5.6933 \times 10^{-6}$$

$$\xi = (5.6933 \times 10^{-6}) \text{ eg}$$

1
OPTICS AND SPECTROSCOPY, Vol. VI, No. 2, February 1959 - "Influence of Temperature Gradient of Glass of Optical Systems on the Image Produced by the Latter"

The total deviation of a ray is therefore a linear function of the local value of the thermal gradient. A plot of the deviation against the gradient is shown for various thicknesses in Figure F-2. The shape of the thermal gradient will cause different effects upon an impinging plane wavefront. The simplest case of a linear gradient will result in a wave deviation, but no wave distortion. This will have no effect on the image except a displacement of the image laterally along the focal surface. Such an image displacement, in the magnitudes anticipated, is tolerable. The next simplest case is that of a gradient assuming a quadratic form. The effect of such a gradient would be to introduce cylindrical power, and distort the plane wavefront along one axis. The result would be astigmatism of the image. The tolerance for the amount which a thermal gradient can depart from linear can be determined by establishing a value for the allowable wave deformation.

In general the same approach holds for any variation in the thermal gradient as long as this variation is not too rapid.

The specific configuration under consideration is that of three glazings, separated by gaps. A cooling air flow in the inner gap will cause a thermal gradient along the two inner glazings. For the condition of vacuum in the outer gap, any thermal gradient across the outer glazing caused by the gradient of the inner glazings would be of second order consideration. Inasmuch as the gradient produced in the two inner glazings is in the same direction, they can be considered as one thick glazing, 1.5 inches for this analysis.

If $\mathcal{E}_1$ = Keg$_1$ is the deviation at some arbitrary point along the length of the plate and $\mathcal{E}_2$ = Keg$_2$ the deviation at a second point, the $\Delta\mathcal{E}$ = Ke(g$_2$-g$_1$) = KeΔg or Δg = $\frac{1}{Ke}\Delta\mathcal{E}$. For a plane wavefront striking the plate at normal incidence, the maximum allowable change in g, the thermal gradient, across the entire pupil, is:

$$\Delta g = \frac{1}{(5.6922 \times 10^{-6})\left(\frac{3}{2}\right)} \quad 5 \times 10^{-6}$$

DEVIATION AS A FUNCTION OF THERMAL GRADIENT
WITH THICKNESS t AS A PARAMETER

FIGURE 5-2

$$= \frac{.595^{o}F}{in}$$
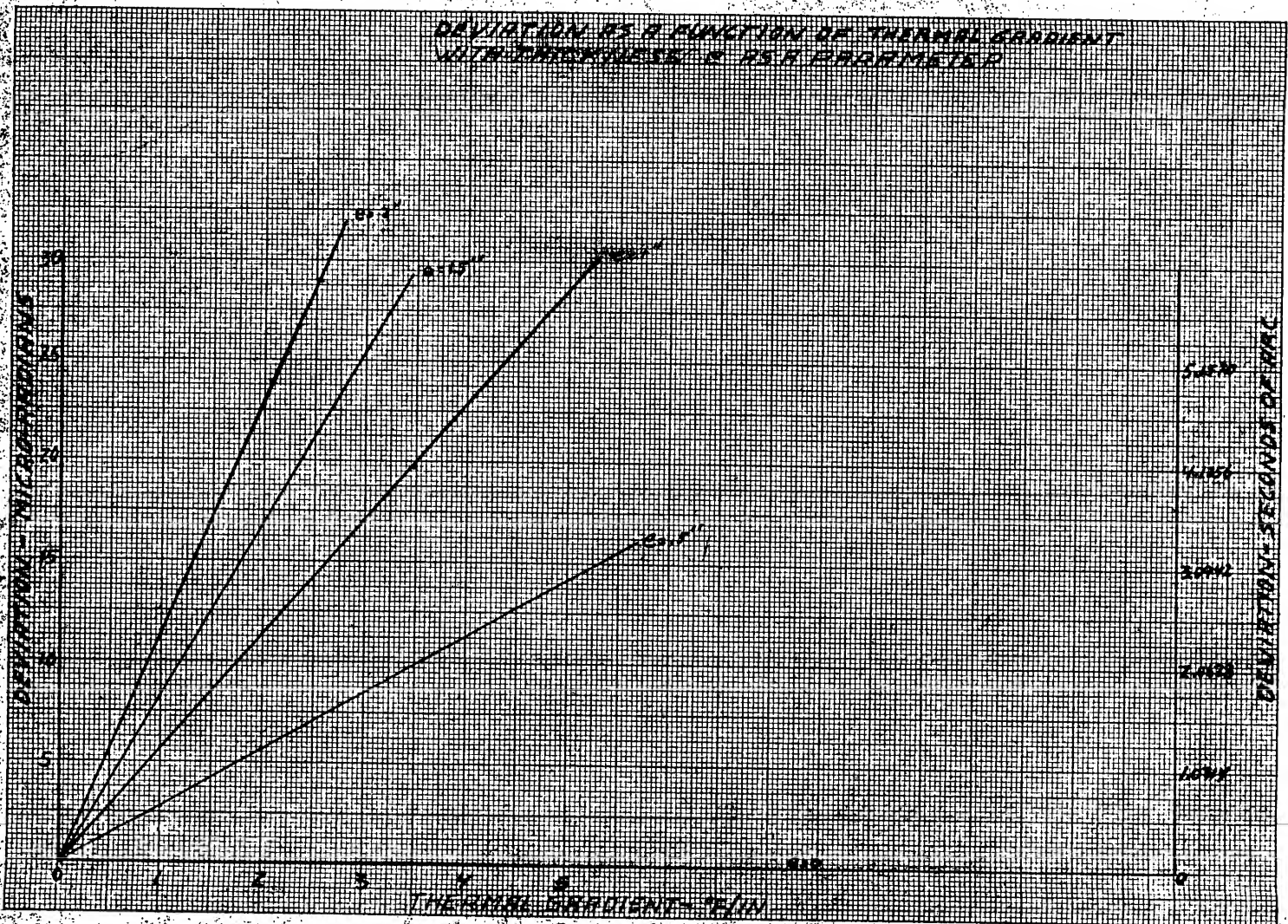
based on $\Delta \mathcal{E} \leq 5 \times 10^{-6}$ radians.

This value, unfortunately, even though imposing a tight limit, considers only the case of normal incidence. For oblique incidence, the allowable gradient variance decreases appreciably. This case has not yet been analyzed.

Finally the nature of index fluctuations in the air present in the optical path must be analyzed.

The dependence of optical index on gas density is given quite accurately[2] by

$$(n-1) = \frac{\rho}{\rho_0} \ (n_0-1)$$

where   n = index of refraction, and

ρ = density.

It is also known[3] that

$$\frac{\rho}{\rho_0} = \left(\frac{P}{760}\right)\left(\frac{273}{T}\right)$$

for a constant volume, where

P = Pressure in mm. of Hg

T = Temperature in ^{o}K.

Consequently, we can express the dependence of index on pressure and temperature by

$$(n-1) = \left(\frac{P}{760}\right)\left(\frac{273}{T}\right)(n_0-1).$$

---

[2] - Jenkins & White, "Fundamentals of Optics" 2nd Ed., Page 251

[3] - American Institute of Physics Handbook, page 3-56

For $\lambda = .6\mu$, $n_0 - 1 = 2.92 \times 10^{-4}$, when $P = 760$ mm., $T = 273^\circ K$.   So,

$$(n-1) = 1.05 \times 10^{-4} \; \frac{P}{T} \; ,$$

and therefore

$$\frac{\partial n}{\partial P} = \frac{1.05 \times 10^{-4}}{T} \quad \text{per mm. Hg}$$

$$\frac{\partial n}{\partial T} = - 1.05 \times 10^{-4} \; \frac{P}{T^2} \quad \text{per } ^\circ K.$$

Thus we arrive at the following table:

Variant \ Condition	P = 1/3 atm = 250 mm		P = 1/10 atm = 75 mm	
	$T = 110^\circ F = 316^\circ K$	$T = 130^\circ F = 328^\circ K$	$T = 110^\circ F = 316^\circ K$	$T = 130^\circ F = 328^\circ K$
$\frac{\partial n}{\partial P}$ (per mm Hg)	3.3×10^{-7}	3.2×10^{-7}	3.3×10^{-7}	3.2×10^{-7}
$- \frac{\partial n}{\partial T}$ (per $^\circ K$)	2.6×10^{-7}	2.4×10^{-7}	7.8×10^{-8}	7.3×10^{-8}

Furthermore

$$\Delta n = \frac{\partial n}{\partial P} \Delta P + \frac{\partial n}{\partial T} \Delta T$$

$$= \left(\frac{\partial n}{\partial P} \frac{\partial P}{\partial T} + \frac{\partial n}{\partial T} \right) \Delta T$$

$$= \left(\frac{\partial n}{\partial P} + \frac{\partial n}{\partial T} \frac{\partial T}{\partial P} \right) \Delta P \; ,$$

and the last two expressions allow calculation of Δn as a function of either ΔT or ΔP alone, providing the functional relation of P and T is known.

Now, consider two light beams passing through a gas layer m meters
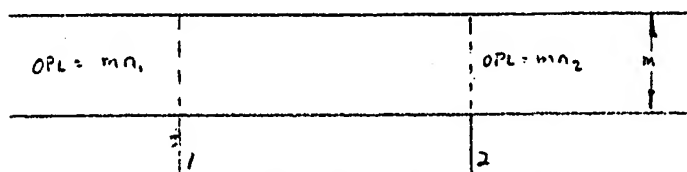
thick.   The optical path difference is $(mn_1 - mn_2)$ or $m \Delta n$.   This difference

must everywhere be less than about $1/10\lambda$ where λ = wavelength of light.

If we assume m = 0.5 meter,

$$\frac{\lambda}{10m} = \frac{.6 \times 10^{-6}}{10 \times .5} = 1.2 \times 10^{-7}$$

Consequently $\Delta h \leq 1.2 \times 10^{-7}$ is required, and this is nearly achieved when

$$\Delta P \leq .38 \text{ mm Hg} \qquad (T = \text{constant})$$

$$\Delta T \leq .5 \text{ }^{\circ}K \qquad (P = 1/3 \text{ atmosphere})$$

$$\Delta T \leq 1.5 \text{ }^{\circ}K \qquad (P = 1/10 \text{ atmosphere})$$

It can also be achieved in wider limits of either ΔP or ΔT provided $\frac{\partial P}{\partial T} > 0$

since $\frac{\partial n}{\partial P} > 0$ and $\frac{\partial n}{\partial T} < 0$. That is, if increasing pressure is accompanied

by increasing temperature (or both decreasing), then Δn is reduced. For a

Boyle's Law gas, at least, $\frac{\partial P}{\partial T} > 0$ always.

However, the nature of turbulence is not well understood. There is some question as to whether it follows the laws of an ideal gas, as indicated above.

Consider the case of adiabatic conditions where:

$$T^{\gamma} P^{1-\gamma} = \text{constant}$$

Evaluating the constant at operating conditions of 130°F and 1/10 atmosphere

$$T^{\gamma} P^{1-\gamma} = (328)^{\gamma} (75)^{1-\gamma}$$

$$= \frac{3300}{5.9}$$

$$= 560$$

Therefore $T = 560 \ P^{\frac{\gamma-1}{\gamma}}$

$$\frac{\partial T}{\partial P} = \frac{\gamma-1}{\gamma} \ 560^{\frac{1}{\gamma}} \ P^{\frac{\gamma-1}{\gamma}-1}$$

$$= \frac{\gamma - 1}{\gamma} \ 560^{\frac{1}{\gamma}} - P^{-\frac{1}{\gamma}}$$

$$= \frac{.41}{1.41} \ (560)^{.71} \ P^{-.71}$$

$$= 25.9 \ P^{-.71}$$

at $P = 75$ mm Hg

$$\frac{\partial T}{\partial P} = 1.20$$

From the previous analysis, we have

$$\frac{\Delta n}{\Delta P} = \left(\frac{\partial n}{\partial P} + \frac{\partial n}{\partial T} \ \frac{\partial T}{\partial P} \right)$$

substituting

$$\frac{\Delta n}{\Delta P} = 3.2 \times 10^{-7} - (7.3 \times 10^{-8} \times 1.24)$$

$$\frac{\Delta n}{\Delta P} = 2.3 \times 10^{-7}$$

for $P = 75$ mm

$T = 130^{\circ}F$

and $\frac{\Delta n}{\Delta T} = \left(\frac{\partial n}{\partial P} \ \frac{\partial P}{\partial T} + \frac{\partial n}{\partial T} \right)$

substituting:

$$\frac{\Delta n}{\Delta T} = (3.2 \times 10^{-7}) \ (.8) - 7.3 \times 10^{-8}$$

$$= 2.56 \times 10^{-7} - 7.3 \times 10^{-8}$$

$$= 1.83 \times 10^{-7}$$

for $P = 75$ mm

$T = 130^{\circ}F$

In order to maintain the established tolerance that

$$\Delta n \leq 1.2 \times 10^{-7}$$

$\Delta P \leq .52$ mm Hg. and

$\Delta T \leq .65^{\circ}K$

assuming adiabatic conditions at 1/10 atmosphere and $130^\circ F$ temperature.

Experimental studies were carried out in an effort to confirm the critical effect of thermally induced index fluctuations. It was found that image quality was decidedly influenced by the pressure environment, and image quality improved with a decrease in pressure.

APPENDIX G

DEVELOPMENT OF A LOW EMISSIVITY COATING
### SUITABLE FOR WINDOW APPLICATIONS

An investigation was carried out to ascertain what material could
be used as a coating on the glazing surface which would provide high transmission
properties in the region .4 to .7μ and high reflectance properties in the near
and far infrared. Preliminary work indicated that a thin layer of gold
might have the desired properties.

Several fused silica samples were coated with different thicknesses
of gold, with a protective undercoat and overcoat. Spectrophotometer results
indicate that transmittance, and electrical conductivity were dependent upon
coating thickness for the thickness range of $5\overset{o}{A}$ to $60\overset{o}{A}$ investigated. Infinite
resistance was exhibited by the thinner coatings. The coating which exhibited
the most desirable optical properties had a resistance of 22 ohms/square,
an integrated transmission of 70% in the visible region, and an integrated
emissivity of 0.2. Figure G-1 shows the transmittance and reflectance values
for a $47\overset{o}{A}$ coating on a fused silica substrate. Emissivity was calculated on
the basis of:

$$\epsilon = 1 - (T_{meas} + R_{meas})$$

The nature of the gold coating is such that it exhibits the
tendency to change its properties under certain thermal conditions. Tests
were carried out to determine whether the coating would breakdown in the
temperature range for which it would be used. Tests so far have produced
the following results:

1. Coatings on fused silica and glass, subjected to temperatures

FUSED SILICA - COATED
TRANSMITTANCE & REFLECTANCE
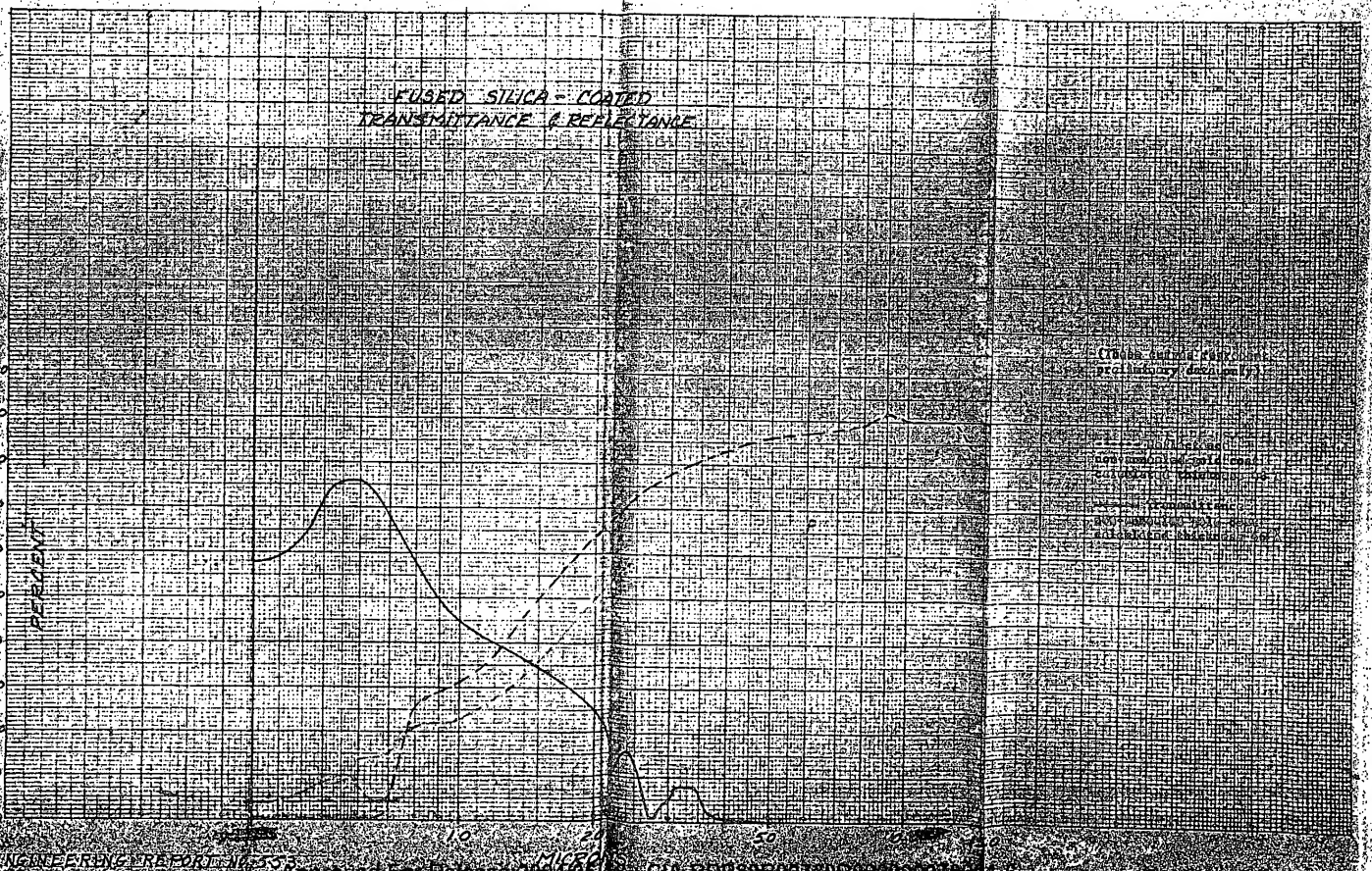
up to 600°F for as long as 24 hours have maintained, to a first order, their original electrical properties.

2. Some samples, on glass substrates, subjected to 900°F environments, have changed properties within 1/2 hour of heating. The resistance has been infinite, indicating that the optical properties, in the infrared region, have become undesirable.

The emissivity of several coatings were measured at temperatures exceeding 600°F. Preliminary analysis of the data indicates that the emissivity at these temperatures is different than the emissivity at room temperature, and that the emissivity is effected by the thermal history of the sample.

Further testing is being carried out in an attempt to determine the basic nature of this breakdown. However, the results to data indicate that the coatings, on fused silica, are satisfactory for the temperature range up to 600°F; below the maximum they would be subjected to in the window configuration.

The electrical properties of the coatings make the coatings useful for several other desirable applications in the window configuration. They can be used as a means for resistive heating. In addition, the electrical continuity which they cause the window to have, provides the appearance of an electrical continuous skin when mounted in the vehicle.

For the case of a vacuum gap between two glazings, the low emissivity coating is used to limit heat transfer by radiation. The relative effectiveness of a coating on either side of the gap can be analyzed. Consider two surfaces, A_1 and A_2, at temperatures T_1 and T_2. The net heat radiation exchange between the two surfaces can be expressed as follows:

Let ϵ_1 and ϵ_2 = emissivity of surface A_1 and A_2 respectively.

W_1 and W_2 = total emissive power of A_1 and A_2 respectively

r_1 and r_2 = reflectivity of A_1 and A_2 respectively.

F_2 = fraction of energy leaving A_1 and falling on A_2

F_1 = fraction of energy leaving A_2 and falling on A_1

The total energy that leaves surface A_1 and falls on surface A_2 is given by[1]:

$$q_{1-2} = \frac{\epsilon_1 W_1 A_1 F_1 + \epsilon_2 W_2 A_2 r_1 F_1 F_2}{1 - r_1 r_2 F_1 F_2}$$

The total energy that leaves surface A_2 and falls on surface A_1 is given by:

$$q_{2-1} = \frac{\epsilon_2 W_2 A_2 F_1 + \epsilon_1 W_1 A_1 r_2 F_1 F_2}{1 - r_1 r_2 F_1 F_2}$$

The net heat-radiation transfer between the two surfaces is, therefore

$$q = q_{1-2} - q_{2-1}$$

If W_1 is replaced by σT_1^4 and W_2 is replaced by σT_2^4, then

$$q = \frac{\sigma A_1 (\epsilon_1 T_1^4 F_2 - \epsilon_2 T_2^4 F_1 \frac{A_2}{A_1} + r_1 \epsilon_2 T_2^4 \frac{A_2}{A_1} F_1 F_2 - r_2 \epsilon_1 T_1^4 F_1 F_2)}{1 - r_1 r_2 F_1 F_2}$$

However for two parallel plates with equal areas, $A_1 = A_2$ and $F_1 = F_2 = 1$. Thus the above relation for the net-radiation heat transfer reduces to

$$q = \frac{\sigma A_1 \epsilon_1 \epsilon_2}{\epsilon_1 + \epsilon_2 - \epsilon_1 \epsilon_2} (T_1^4 - T_2^4)$$

---

[1] A.J. Brown & S.M. Maro, "Introduction to Heat Transfer", Third Edition, McGraw Hill Book Co., Inc., 1958

Therefore, we see that the effectiveness of a coating on one-parallel plate is the same regardless to which parallel plate the coating is applied.

The relative effectiveness of one coating in the first gap; one coating in the second gap; and two coatings, one in each gap was analyzed on the analog computer. Figure G-2 is an example of the results. It is clearly indicated that two coatings are desirable, and that if only one coating can be used it should be located in the outer gap.
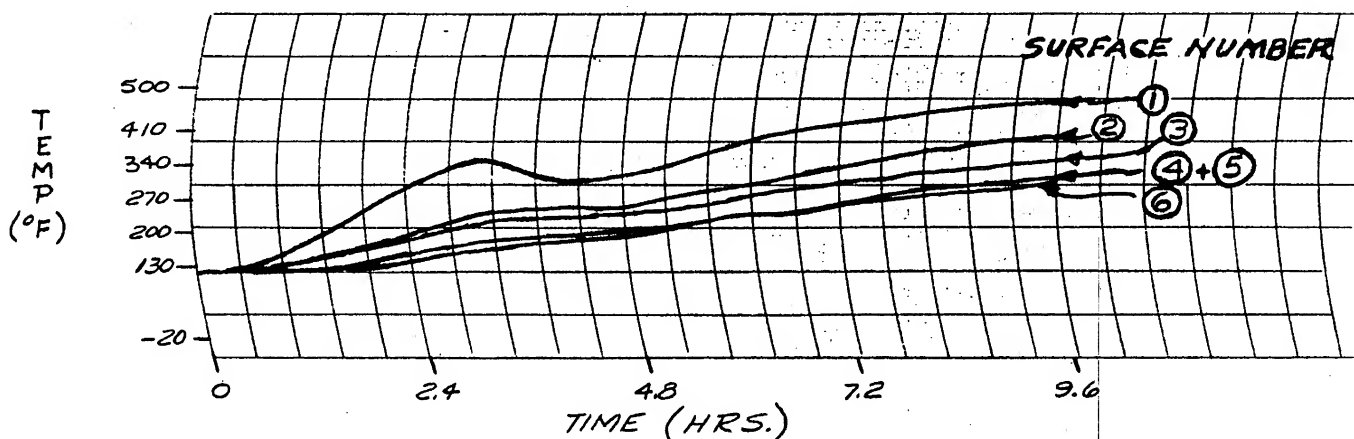
RELATIVE EFFECTIVENESS OF NUMBER OF LOW
EMISSIVITY COATINGS USED, AND COATING LOCATION

DATA OBTAINED BY THERMAL ANALOG
        CONFIGURATION: NO COOLING
                        VACCUM IN BOTH GAPS
                        COATING AS INDICATED

SURFACE NUMBER	CONDITION
1	NO COATING
2	ONE COATING, INNER GAP ONLY
3	ONE COATING, OUTER GAP ONLY
4	TWO COATINGS, INNER GAP ONLY
5	TWO COATINGS, OUTER GAP ONLY
6	ONE COATING, EACH GAP

FIG. G-2

APPENDIX H

MECHANICAL CONSIDERATIONS TO WINDOW CONFIGURATION

Only preliminary investigations have been carried out for determining actual mechanical values, since considerations have been limited to general cases. It has been found that, from a mechanical standpoint, material choice is dictated by thermal shock considerations; and that glazing thickness is dictated primarily by size and pressure.

Mechanical properties of suitable materials is listed in Figure H-1.

THERMAL SHOCK

When a material is subjected to a temperature gradient, adjacent fibers tend to expand in differing amounts. Any constraint prevents the individual expansion of each fiber, thus setting up a system of thermal strains and associated stresses. When the thermal stress is generated by sudden changes in temperature, the action is referred to as thermal shock.

Since glass fails in tension, and usually at the surface, the temporary stresses from sudden cooling are much more severe than those resulting from sudden heating. The most severe thermal shock application in the window appears to be during intermittent cooling in the second gap.

The maximum temperature increment between the cooling air and the glazing surface is a function of the Modulus of Elasticity, the Coefficient of thermal expansion, Poisson's ratio and the allowable working stress of the material. Thus,

$$T = \frac{\sigma_t \ (1-\gamma)}{I \ E \ \alpha}$$

where α = thermal expansion, $\frac{1}{{}^\circ F}$

E = Young's Modulus, psi

γ = Poisson's Ratio

σ_t = Allowable Working stress, psi

Page 82

FIGURE H-1

COMPARISON OF MECHANICAL PROPERTIES [*]

		1723 Aluminosilicate	7900 Vycor	7940 Fused Silica
YOUNG'S MODULUS	psi	12.8×10^6	9.6×10^6	10.5×10^6
POISSON'S RATIO		0.22	0.181	0.17
HARDNESS (KNOOP)		595^{100}	630^{50}	644^{50}
MOD. OF RUPTURE [**]	psi	9.3×10^3	7.13×10^3	8.0×10^3
DENSITY	lb/ft³	164.0	136.1	137.3
EXPANSION	10^{-7}/°F	25.3	4.4	3.0

[*] Data from Corning Glass Works (AF 33(600) 36852) Quarterly Report No. 1

[**] Abraded Annealed.

For a maximum allowable tensile stress of 1000 psi, Corning 7940 fused silica can withstand a ΔT of $263^{\circ}F$. Under the same conditions, Soda Lime (BK-7) can only withstand a ΔT of $17^{\circ}F$. Based on this analysis, BK-7 should not be used as the inside glazing. Table H-2 lists the thermal shock resistance for several glazing materials.

TABLE H-2

THERMAL SHOCK RESISTANEE

Glazing Material	$\Delta T*$
7940 Fused Silica	$263^{\circ}F$
7900 Vycor	$194^{\circ}F$
1723 Aluminosilicate	$24^{\circ}F$
0080 Soda Lime	$17^{\circ}F$

* where $\Delta T = (T_{surface} - T_{air})$

No experiments have been performed to verify the figures in Table H-2. The main factor which would influence these tabulated values is the allowable working stress of 1000 psi. Breaking stress is very dependent upon conditions of the glass, annealing, and surface quality. Allowable ΔT varies directly with increasing working stress.

The analysis upon which the determination of allowable ΔT is based is independent of glazing thickness. Experimental results listed by Corning* indicate a thickness dependence of ΔT, where the ΔT tolerance increases for decreasing thickness. Values calculated in Table H-2 are within expected agreement with the Corning data.

In addition, it should be pointed out that ΔT represents the short term <u>cooling</u> temperature drop of the glazing surface. The factor of a film heat transfer coefficient means that the cooling air introduced may have a temperature difference with respect to the glazing surface greater than ΔT. The magnitude of this coefficient has not yet been investigated.

* Properties of Selected Commercial Glasses; Corning Glass Works; Corning, N.Y.

THICKNESS

The thickness of the glazings were calculated based on the pressure distribution shown in Figure H-3. The glazings were assumed to be simply supported on a rigid frame. Stresses and deflections would be slightly smaller for glazings with fixed edges on a rigid frame.
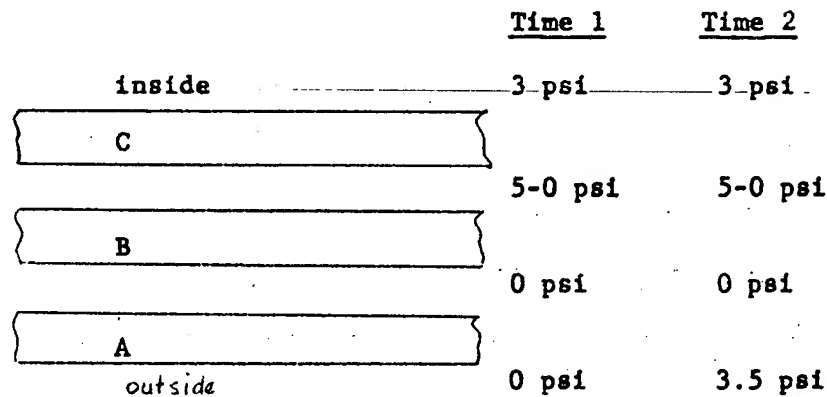
	Time 1	Time 2
inside —————	3 psi	3 psi
C		
	5-0 psi	5-0 psi
B		
	0 psi	0 psi
A		
outside	0 psi	3.5 psi

Figure H-3

Taking 1000 psi as the maximum allowable tensile stress, the minimum thicknesses of glazings A, B & C are about .6", .75" and .6" respectively. Curves of stress vs. thickness, and deflection vs. thickness are presented in Figures H-4 and H-5.

Figure H-6 is a plot of the stresses in glazing A with a pressure differential of 15 psia across the glazing. A pressure differential of this magnitude requires a thickness of 1.25" for glazing A.

The pressure profiles demonstrated in Figure H-3 are realistic of actual pressures if the necessary vacuum between glazings A and B is established after altitude is reached, and bled prior to landing. The condition of 15 psia differential represented in Figure H-6 would be for establishing a hermetically sealed vacuum on the ground.

For the specific case of the 24-inch Schmidt system, the approximate window size necessary is 10.5 x 18.5 inches. The following is the analysis for determining glazing thickness for this case.

FIGURE A-4
MAXIMUM STRESS IN WINDOW
AS FUNCTION OF WINDOW THICKNESS
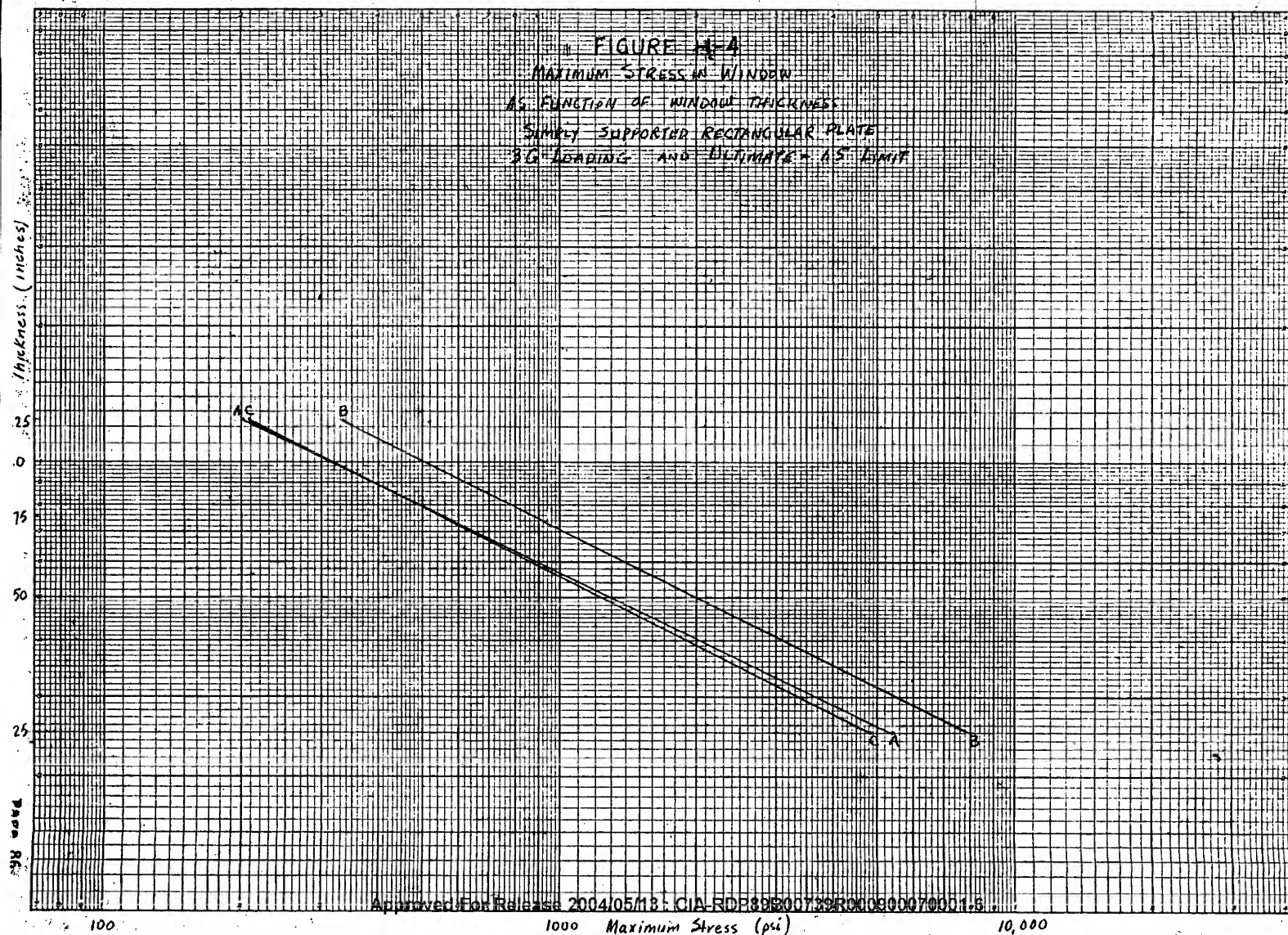SIMPLY SUPPORTED RECTANGULAR PLATE
3G LOADING AND ULTIMATE = 6.5 LIMIT

Thickness (inches)

Maximum Stress (psi)

FIGURE 4-5
MAXIMUM DEFLECTION IN WINDOW
AS FUNCTION OF WINDOW THICKNESS
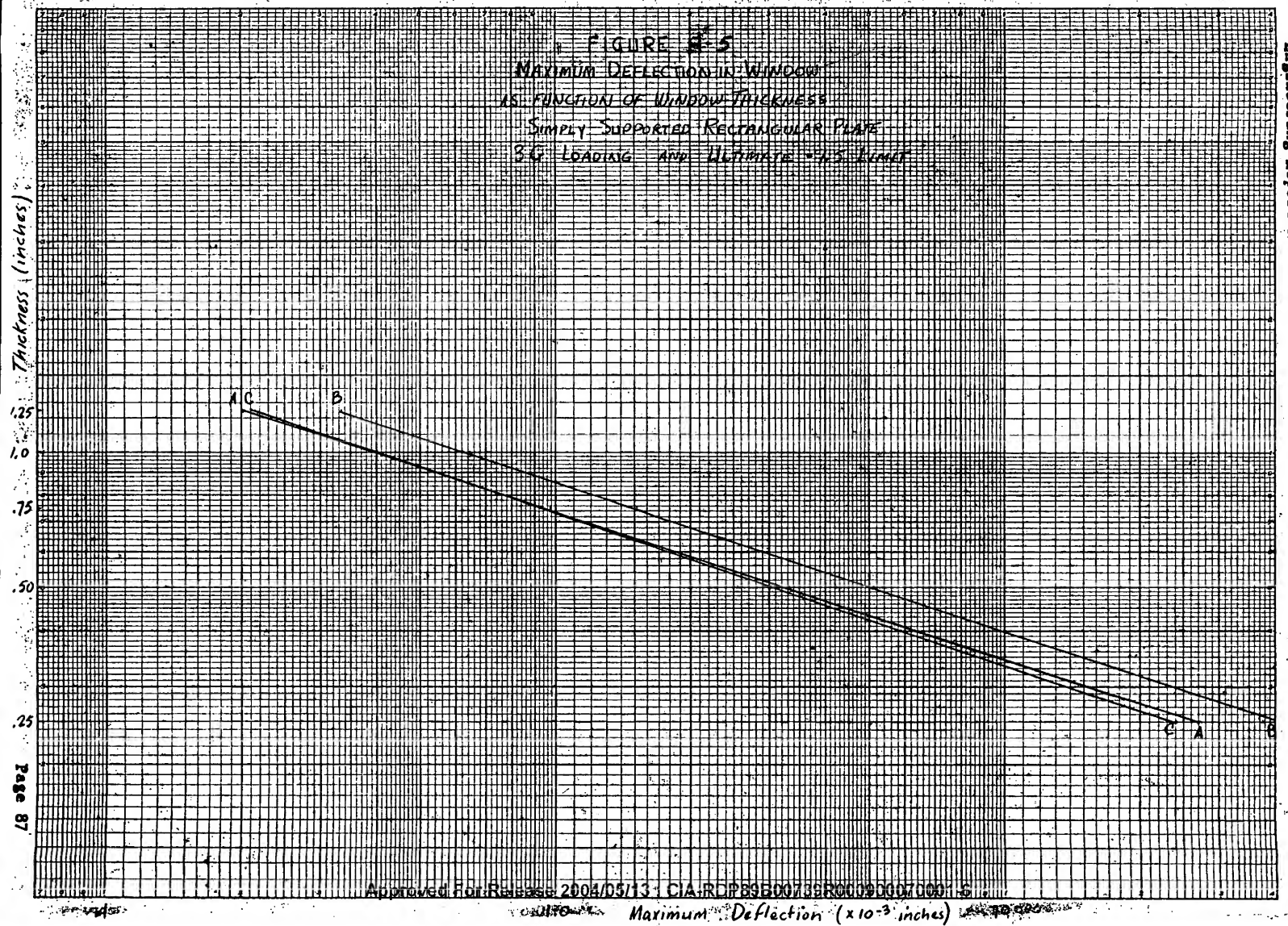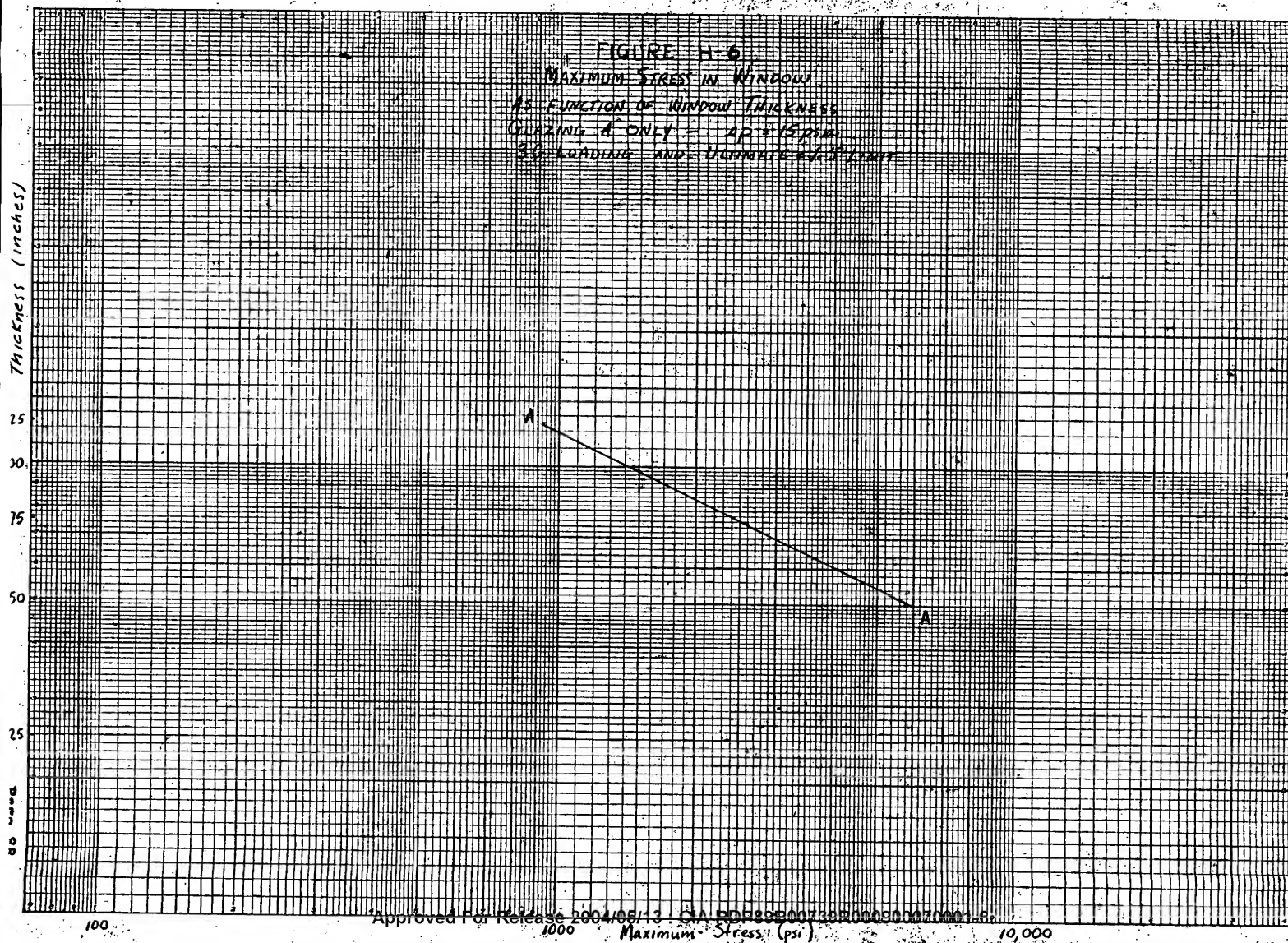SIMPLY SUPPORTED RECTANGULAR PLATE
3 G LOADING AND ULTIMATE 4.5 LIMIT

Thickness (inches)

Maximum Deflection (×10⁻³ inches)

FIGURE H-6
MAXIMUM STRESS IN WINDOW
AS FUNCTION OF WINDOW THICKNESS
GLAZING A ONLY — ΔP ±15 psi
3G LOADING AND ULTIMATE 4.5 LIMIT

ANALYSIS

$$b = 18.5"$$

$$a = 10.5"$$

The maximum tensile stress in a simply supported plate is

$$\sigma_{max} = \frac{6 \beta q a^2}{h^2}$$

where $\beta = .0994$, a dimensionless quantity depending on $\frac{b}{a}$ and ν

h = thickness of plate, in.

q = uniform loadings, psi

a = smaller dimension, in.

$q = \rho h$ psi

$$\therefore \sigma_{max} = \frac{0.596 \left[G \rho h + P \right] (10.5)^2 F}{h^2}$$

where G = "G" loading

P = pressure differential across plate

F = design factor

The maximum deflection in a simply supported plate is

$$\delta_{max} = \frac{\alpha q a^4}{E h^3}$$

where $\alpha = 0.1060$, a dimensionless quantity depending on $\frac{b}{a}$ and

q = uniform loading, psi

h = thickness,

a = smaller dimension,

E = Young's Modulus, psi

$$\therefore \delta_{max} = \frac{0.1060 \left[G \rho h + P \right] (10.5)^4}{10.5 \times 10^6 h^3}$$

where G = "G" loading

P = pressure differential across plate.

APPENDIX I

TECHNICAL SUMMARY - WINDOW CONFIGURATION

The most suitable environment, in order to maintain the desired image quality, minimizes or eliminates index fluctuations in the optical path. This dictates an isothermal equipment bay concept. The equipment, bay walls, and inner-window surface should be kept at the same temperature. If this is accomplished, it will eliminate heat transfer either into the equipment bay, or from one part of the bay to the other; and this will eliminate index fluctations from thermal gradients and resulting pressure changes.

The tolerance on acceptable temperature fluctuations within the equipment bay increases with decreasing equipment bay pressure. Realistically achievable temperature controls are possible at atmospheres no greater than about 75 mm Hg.

It is desirable to maintain minimum temperature drop through the glazing materials themselves, in order to reduce optical wavefront deformation due to index changes. In addition, this will enable thinner glazings to be used, making a more suitable mechanical configuration. The most desirable location for the maximum temperature drop is across the gaps between the window glazings. Since air has a much lower thermal conductivity than the glazing materials, a maximum temperature difference across the gaps is a natural consequence. In order to do this, however, it is necessary to limit or eliminate heat flow from hot to cooler glazings. In order to eliminate heat conduction and convection, vacuum of the order of 5×10^{-3} mm Hg must be maintained (because the thermal conductivity of air is independent of density until the pressures become so low that the mean free path of the air molecules is comparable to the dimension of the gap). In order to limit radiation, a low emissivity coating should be applied to one surface bordering the gap. It is of no consequence to which side of the gap the coating is applied. A

low emissivity coating is most effective in the outermost gap, and two coatings are more effective than one. If only one coating is used, it should be located in the outer gap.

In addition to its low emissivity properties the coating will serve as a conductor across the window, therefore, maintaining the appearance of an electrically continuous skin.

In order to maintain the inner surface of the window glazing at a constant and tolerable temperature, cooling or heat removal from the window glazings must be present. The use of cool air for heat removal is recommended. For the same considerations which dictate the desirability of eliminating air in the equipment bay, it is desirable to eliminate the cooling air from the gaps during a photographic exposure. This can be accomplished by using cooling air only during that portion of the photographic cycle during which no photograph is being taken For the 24" Schmidt-Scanning System, this appears feasible. A cycle of about 3.6 seconds on and 3.6 seconds off is recommended. The use of cyclic cooling requires that cooling air can be introduced, then removed, and a low density atmosphere be reestablished within the allowable cooling cycle time. This seems quite feasible if about 0.3 cubic feet/min. of cooling air can be dumped overboard. Cooling air temperature and rate must still be finalized.

During two portions of the mission profile there is a heat drain to the outside, resulting in a cooling of the inner glazing. Depending on allowable temperature fluctuations of the inner surface, heating may be required in the inner gap. This can be accomplished either by introducing hot air or by resistive heating of the conductive gold coat, if a gold coat is present.

As a maximum tolerance, the net deviation from a linear thermal gradient across the pupil cannot exceed 0.6°F per inch. It would be desirable

to use aluminosilicate for outer glazing due to the fact that its expansion
properties are more nearly similar to those of the vehicle skin than are the
expansion properties of fused silica. However, thermal shock and optical
considerations indicate that the use of fused silica would be desirable.
Further investigation is recommended to finalize material choice. At least
the two inner glazings, subject to large thermal shocks from the cycled cooling
air, should be fused silica.

The approximate window size for the 24-inch Schmidt-System is 10.5 x
18.5 inches with slightly rounded corners and edges. The thickness of the
glazings have been calculated on the basis of establishing a vacuum in the
first gap after altitude has been attained, and bleeding prior to landing,
in order to avoid a 15 psi differential. Calculated thicknesses are 0.6,
0.75, and 0.6 inches from outer to inner glazings.

The dynamic deflection of the window glazings for these thicknesses
is not sufficient to exceed the tolerances established to maintain desired
image quality.

These considerations dictate a basic window configuration concept.
The three glazing configurations shown in Figure I-1 embodies all these
concepts. One side of each gap is coated with a gold coating of 0.2 emissivity.
Regulated cooling air is cycled through the inner gap, to maintain the inner
window surface at $130^{\circ}F$. The bay environment, at a pressure of 0.3 pounds
per square inch, is maintained to provide temperature fluctuations no greater
than $\pm 1^{\circ}F$.

BASIC WINDOW CONFIGURATION
SIZE 10.5 × 18.5 INCHES
(APPROXIMATE FOR 24" SCHMIDT SYSTEM)
BAY PRESSURE 0.3 PSIA

NOMENCLATURE
USED IN THIS REPORT

SURFACE TEMPERATURE MAINTAINED 130°F

SURFACE (6)

FUSED SILICA — 0.6" — INNER GLAZING

SURFACE (5)

GOLD COAT E=.2
CYCLIC COOLING — $\frac{1}{4}$" — INNER GAP

SURFACE (4)

FUSED SILICA — 0.75" — MIDDLE GLAZING

SURFACE (3)

GOLD COAT E=.2
PRESSURE = 5×10^{-3} MM.Hg — $\frac{1}{4}$" — OUTER GAP

SURFACE (2)

FUSED SILICA — 0.6" — OUTER GLAZING

SURFACE (1)

TEMPERATURE MAXIMUM 500°F

FIG I-1

APPENDIX J

FILM TRANSPORT

This area may be divided into two significant aspects. The first
will consist of the arrangement to transport the film at an accurately
programmed velocity; and, the second will consist of arrangements to persuade
the film to conform to a selected geometric-velocity configuration during its
travel past the slit.

Investigations of the accuracies in the velocity of film travel
suggest that a servo control is indicated. Analysis of this problem will
continue.

In the second aspect of the film transport there are unique and
critical design parameters which must be satisfied. Calculations and
empirical investigations have been made in some of these areas. Thin base
film requires special handling because it will damage easily. The film
transport arrangement must facilitate positive film registration without
the advantage of sprocket holes and it must also allow for unavoidable slack
caused by momentary power or component failures, film splices and other
imperfections in the film. In a tentative optical design, the ideal focal
surface would be a 30-inch radius sphere. However, a sphere of this size
is not practical and some compromise in the shape of the focal surface
is indicated. A ten-inch long roller with a 30-inch radius profile in the
axial plane and a maximum radial length of 15/16 inches was fabricated. This
roller (platen roller) is the pressure plate in the film transport bread-
board system constructed to test the behavior of thin base film. The
breadboard will prove a valuable tool as it can be readily modified for
testing of other transport systems. (See Figure J-1).

When the unit was put into operation the following facts were noted:

APERTURE

BARREL   FOCAL   SURFACE

DRIVE ROLLER (RUBBER COATED)

DRIVE MOTOR

FRICTION BRAKE

FILM

FRICTION CLUTCH

SUPPLY SPOOL

TAKE UP SPOOL

TAKE UP MOTOR
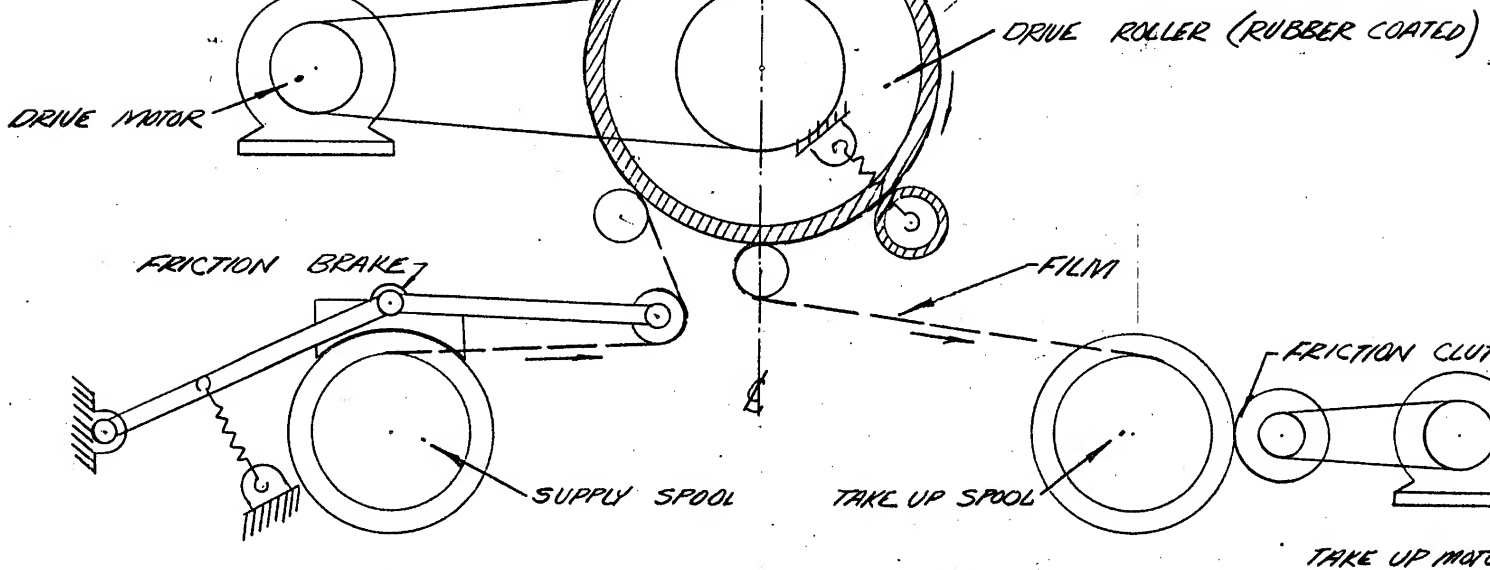
FILM   TRANSPORT   BREADBOARD   FIG J-1

A. The film did not easily stretch over the platen roller. Calculations indicate that approximately 150 pounds tension would be required to achieve the amount of stretch desired. However, from the breadboard it was found that severe stretching produced buckle areas. Pressure and localized heat resulting from the crimping of the film might expose the film.

B. In an effort to stretch the film completely over the barrel-shaped platen roller, concave profiled rollers were substituted for the straight cylindrical rollers which are located adjacent to the platen roller. This arrangement permitted more film to stretch over the barrel with no increase in tension. It was not possible, in any of the tests conducted so far, to obtain intimate contact between the barrel and the entire 9 1/2 inches width of the film.

The most exact method to simulate a spherical focal surface would be to have a fixed, highly polished spherical section and allow the film to slide over it. The detrimental effects of sliding, if any are appreciable, will be established by tests.

Another approach would be to have a plastic belt contoured to the desired shape and permit the film to travel with this belt. The slip between the film and the platen roller present in the other systems would, in such a system, occur between the plastic belt and the guiding roller.

Analysis of the velocities of film transported over contoured rollers shows that the center of the film will travel 3.2% faster than the edges. For the same width film on a 30-inch radius sphere, the percentage variation between the center of the film and the edges would be 1.2%. A compromise condition may be indicated.

The platen roller is barrel-shaped and as such it has different tangential velocities along its axial length. These velocities vary as much

as 60%. Since all elements on the film travel almost at the same velocity
and since the surface of the roller rotates at different velocities, there is
slip between the film and the roller. Total slip over the platen area may
be expressed as follows:

Distance across slit = .25"'

Velocity of film = 10"/sec

Time to pass slit = 25/10 = .025 sec

With 60% slip (V = 10"/sec - 4"/sec) = 6"/sec
D = 6"/sec x .025 sec = .150"

.15 represents 60% of surface and a deformation of film caused by abrasion or
friction of heat would be intolerable.

Assuming a two-pound normal force between the film and the platen,
the heat generated will be approximately .92 watts. Investigation of ambient
conditions and length of operation should indicate if heat can be removed
from the critical roller surface should be this be necessary.

A method of reducing the relative slip is under investigation
and indications are that if a composite roller is fabricated, the slip can
be held to a selected figure. The composite roller would consist of a number
of individual rollers mounted on the same axis and whose integrated surface
profile would duplicate that of the original single roller.

Finally, the tolerance of .0005 inches required in the focal depth is
possible in the static configuration. Dynamic conditions may dictate
unconventional approaches.

APPENDIX K

SKID TURN FILM ROLLER

The system may require that the film path incorporate a compound bend. This is accomplished by passing the film over the roller at an angle other than 90° with the axis of rotation of the roller. This angle relation produces a velocity vector parallel to the axis of rotation. If the roller does not move in the same direction as the resultant vector, slip will occur. This slip is eliminated by moving, parallel to the axis of rotation, that portion of the roller which is in contact with the film an amount equal to the axial vector transmitted by the film to the roller. Therefore this directional roller will consist of a number of axial elements which experience identical angular motion but are independent from each other in their axial confines. Calculations to determine axial length of roller reveal that for a 9-1/2 inch wide film the minimum length required for static accommodation of film is 14.433 inches. The additional length required by the dynamic conditions is a function of angle of wrap, lead angle and number of sliding elements. This figure is 1.309 inches. The total length of roller is 14.433 + 1.309 = 15.742 inches. The axial movement of the elements will be accomplished by cams. This arrangement relieves the film from the burden of moving the sliding elements through friction.

A second method of achieving a compound bend is to have the film pass over a cushion of air emanating from a stationary bar element. Such a device has been used successfully in existing systems.

APPENDIX L

CEMENTED JOINTS

When light-weight structures are considered, normally honeycomb-like structures are conceptually attractive. If these are fabricated by methods which dimple the skin member, such as welding, strength can be substantially reduced. Similarly, fabrication by mechanical joining, as with bolts or rivets, may have the same effect. Consequently, it becomes attractive to consider chemical joining by methods, such as bonding, in which the mechanical shape of the structure is not altered.

Another reason for considering cemented joints results from the difficulty of machining magnesium and beryllium. These two metals have very high strength and rigidity to weight ratios and they also have very high internal damping. As a consequence of this desirable combination of properties, it is attractive to utilize these materials if it can be done practically; and this is partially dependent on the ability to fabricate cemented joints.

APPENDIX M

OPTICAL POWER SPECTRUM ANALYZER

The power spectrum analyzer is a device intended to indicate the amplitude and direction of the frequency components of the image structure of a transparency. If the transparency is a negative or positive photograph, the analyzer will immediately give the resolving power of the photographic system used (the maximum frequency obtained by the analyzer), and the relative content and distribution of the frequency components passed by the photographic system. Different types of scenes will have different distributions, although any given distribution will have a whole class of scenes corresponding to it.

THEORY OF OPERATION:

The operation of the power spectrum analyzer is based on the fact that the Fraunhofer image of a point source produced by a diffracting screen is the Fourier transform of the wave amplitude in the plane of the screen. If $f(x,y)$ represents the wave amplitude in the plane of the diffracting screen and $\psi(k_x, k_y)$ represents the amplitude of the image where (k_x, k_y) is the normalized coordinate of a point in the image plane, then

$$\psi(k_x, k_y) = \frac{1}{2\pi} \int_{-\infty}^{\infty} \int_{-\infty}^{\infty} f(x,y) e^{i(k_x x + k_y y)} dx\, dy \qquad \text{Eq. (1)}$$

In practice $f(x, y)$ is limited to the pupil of an optical system and is zero outside the pupil, and the integral can be restricted to the area of the pupil. It can be seen that k_x and k_y which are position coordinates in the image plane correspond to frequency components in the plane of the diffracting screen.

The value of the normalized coordinate is given by

$$k = \frac{2\pi}{\lambda} \sin \theta \qquad \qquad \text{Eq. (2)}$$

where λ is the wavelength of the light and θ is the angle of diffraction. The actual position (x', y') in the image plane as a function of the actual spatial frequency component (ν_x, ν_y) in the plane of the diffracting screen is given by

$$x' = f \tan \theta_x, \quad y' = f \tan \theta_y, \qquad \text{and} \qquad \text{Eq. (3a)}$$

$$\sin \theta = \lambda \nu. \qquad \qquad \text{Eq. (3b)}$$

The wave amplitude f(x, y) may be complex; that is, it may represent both variations in the magnitude and phase of the wave across the pupil containing the diffracting screen. This phase variation can have a strong effect on the image and is unwanted in the power spectrum analyzer. The manner of its control and the degree to which it can be tolerated will be discussed later. For the present we shall assume that the phase variation is negligible.

Although the phase variation may be negligible in the pupil, phase variations will exist in the image plane depending on the particular geometry of the diffracting screen.

It should be emphasized that the function we are analyzing is the amplitude of the wave in the pupil as modified by the diffracting screen. The transmission of a screen is usually in terms of the intensity of the light transmitted which is the square of the amplitude transmitted if there is no phase variation.

The diffracted image observed is also the intensity of the wave in the image plane rather than the amplitude, and is the product of the amplitude and its complex conjugate.

The amplitude in the image plane is the Fourier transform of the amplitude in the pupil plane. Thus the intensity of the image is the product of this Fourier transform and its complex conjugate. This product is commonly known as

the power spectrum (thus the name of the instrument) and is the Fourier transform of the autocorrelation function of the diffracting screen.

Since the power spectrum has eliminated the phase information (the product of a function and its complex conjugate is the square of the modulus of the function), any given power spectrum corresponds to a whole class of objects which differ from each other only in the manner in which the structural details are distributed, and thus is a statistical measure of the structural content of the object.

The power spectrum analyzer is intended to measure the structural content of the image of a transparency (as measured by its amplitude transmission) by presenting its power spectrum graphically as the variation in intensity of a point image resulting from diffraction by the transparency. The intensity at any point in the image plane is directly proportional to the power spectrum density of that frequency component of the transparency having a frequency proportional to the distance of the point from the center of the image and a direction determined by the direction of the point from the center of the image.

DESCRIPTION OF INSTRUMENT:

Figure M-5 illustrates diagrammatically the layout of the instrument. A monochromatic light source, pinhole, and collimator serve to provide monochromatic plane waves incident on the transparency. An immersion tank is provided to reduce phase variations in transmission to a minimum. A collector lens forms an image of the pinhole after the light has been diffracted by the transparency.

This image is the power spectrum desired, and a sheet of film inserted here would record the image. However, in most cases the center of the image, corresponding to zero frequency, contains an appreciable fraction, frequently more

TRANSPARENCY

MONCROMATIC
SOURCE

PIN HOLE

COLLIMATOR

IMMERSION
TANK

COLLECTOR

MASK FIELD LENS

RELAY
LENS

FILM
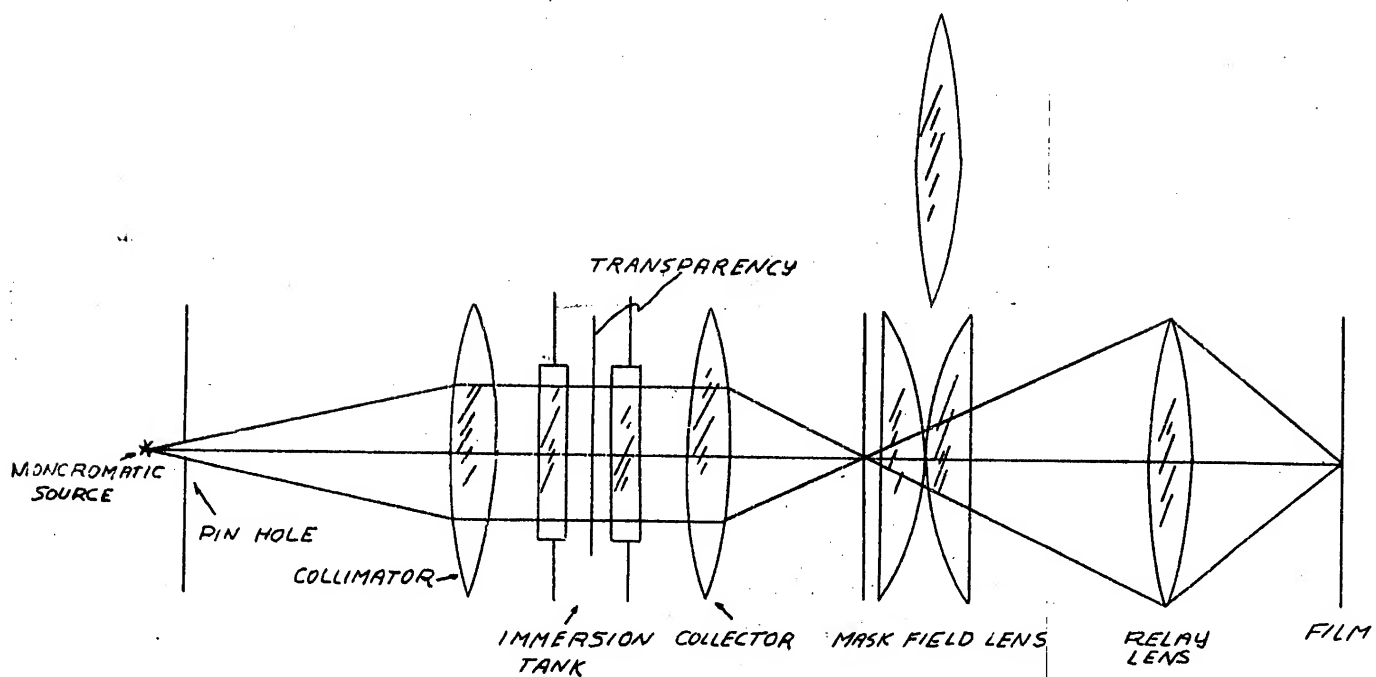
FIG M-5

than half, of the total energy, and the rest is distributed over a large area.
If the exposure is sufficient to record the major part of the power spectrum,
the center will be heavily overexposed and much of the power spectrum will be
spread over by irradiation from the center image.

To reduce this effect to a minimum a mask consisting of an opaque
central spot is inserted in this image plane and the image is relayed to a more
convenient location by a relay lens.

The calibration of the frequency scale is most easily done by inserting
a grating of known frequency, such as a Ronchi grating, in the immersion tank
and recording its image. The fundamental and its harmonics will be recorded,
providing an accurate frequency reference.

A check on the reliability of the system can be made by taking a picture
of the image when the transparency is removed. If the mask is also removed,
the point image obtained will represent the weighting function of the power
spectrum measurement. The intensity at any point in the image plane is not
strictly proportional to the power spectrum density of the corresponding
frequency, but to a weighted average for that frequency and its neighboring
frequencies. The spread of the point image with the transparency removed will
represent the weighting function.

The main effect of enlargement of this image will be a corresponding
change in the weighting function. This includes slow variations in phase, such
as occurs in the presence of aberrations. Such slow variations will have no
high frequency components. However, another effect of the slow phase
variations is a weighting of the areas of the transparency in their contributions
to the power spectrum. If the transparency does not have homogeneous texture,
different aberration distributions will result in slightly different power spectra.

If the power spectrum itself is not expected to have fine structure,
a relatively large weighting function is tolerable. The most efficient use of this

tolerance is the enlargement of the pinhole. The pinhole image is compact so that the weighting does not extend too far out, but the increase in transmitted energy, and consequent reduction in exposure time is considerable.

A picture taken with the transparency removed but the mask in place will show how much light will be spread by the strong zero-frequency component in spite of the central mask. This residual light is a result of the unlimited, although low-level, diffraction spread; scattered light, and out-of-focus ghost images. The diffraction spread is generally very small, the scattered light can be kept at a minimum by having a clean and well-baffled optical system, and the ghost images can be kept to a minimum by means of low-reflection coatings.

EXPERIMENTAL RESULTS:

Figures M-1, M-2, M-3 and M-4 show some power spectra obtained with this instrument along with contact prints of the corresponding transparencies which were used as diffracting screens, and enlargements of selected portions of the transparencies.

The power spectrum of the Ronchi grating shows the fundamental and harmonics of the structure. If the lines and spaces were exactly equal in width, the even harmonics would be absent. Their presence, although they are noticeably weak, indicates that the lines and spaces are not exactly equal. This grating was used to calibrate the frequency scale.

Two of the remaining pictures were taken with a relatively low-resolution system and the third with a high-resolution system. The low-resolution system was limited to about 13 lines per mm. The high resolution system was limited to about 50 lines per mm.

One of the low-resolution pictures is of a river bed with foliage and the other is of a developed area. The river-bed picture has a power spectrum consisting of a broad, generally undifferentiated spread with a diffuse bar across
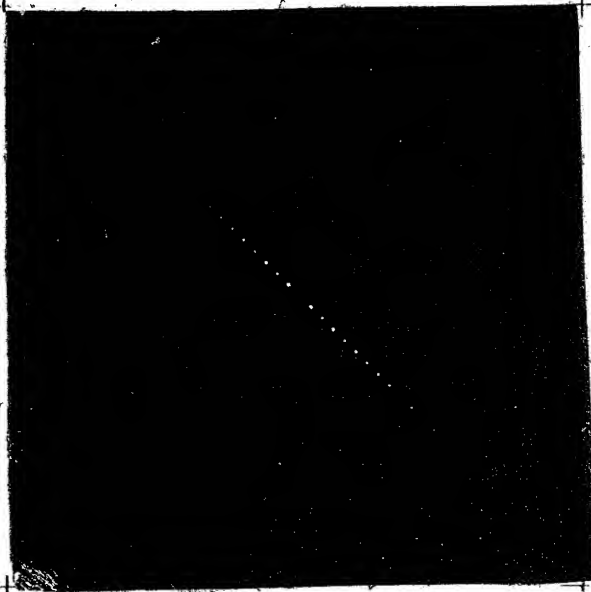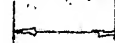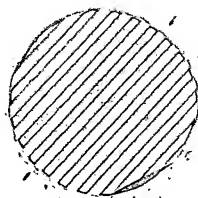
POWER SPECTRA OF SCENE
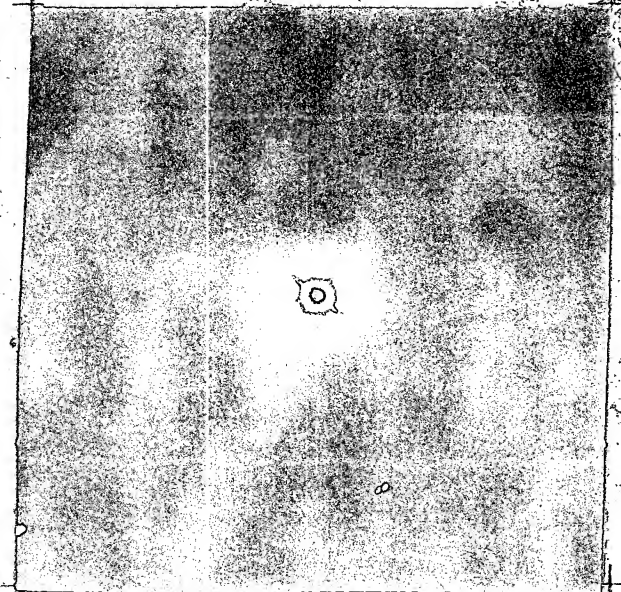
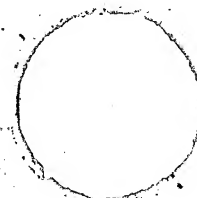POWER SPECTRA OF SCENE
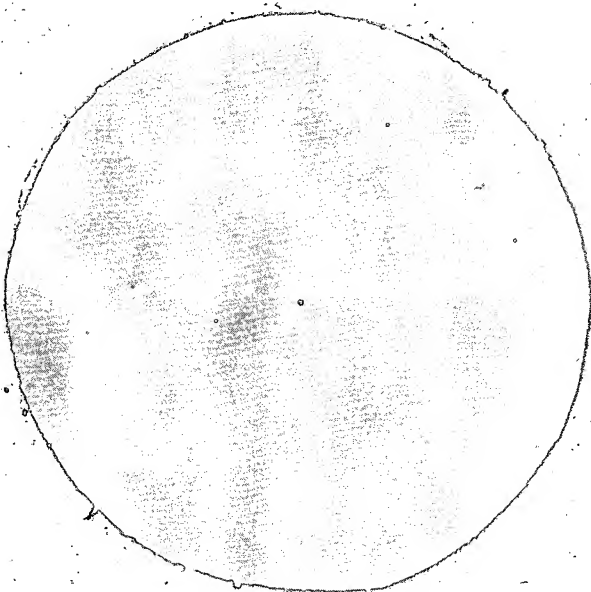
SCENE
RONCHI GRATING - 5.2 lines/mm.
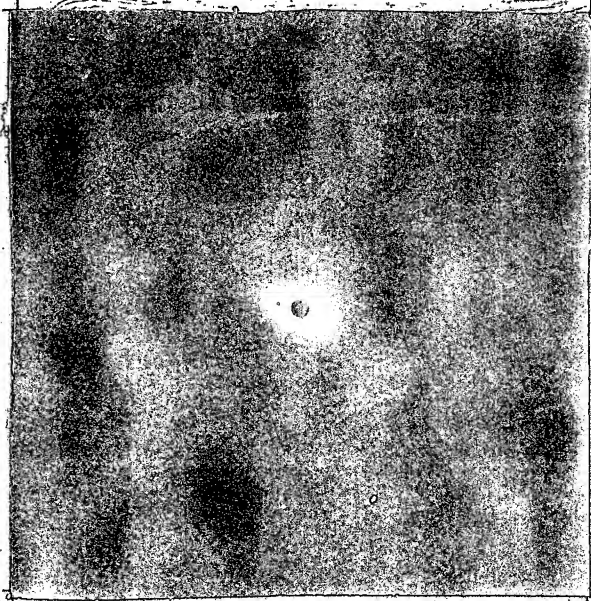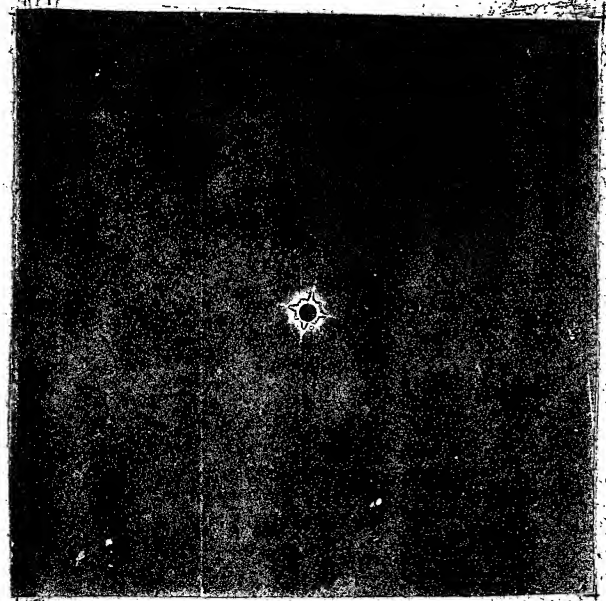
HIGH RESOLUTION SCENE
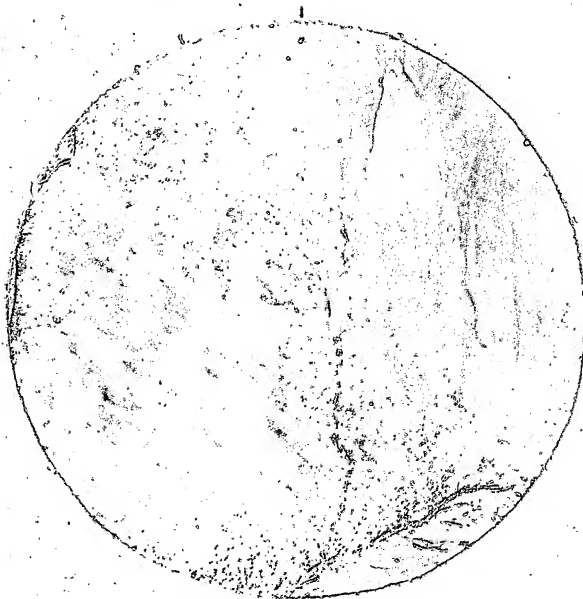POPULATED AREA
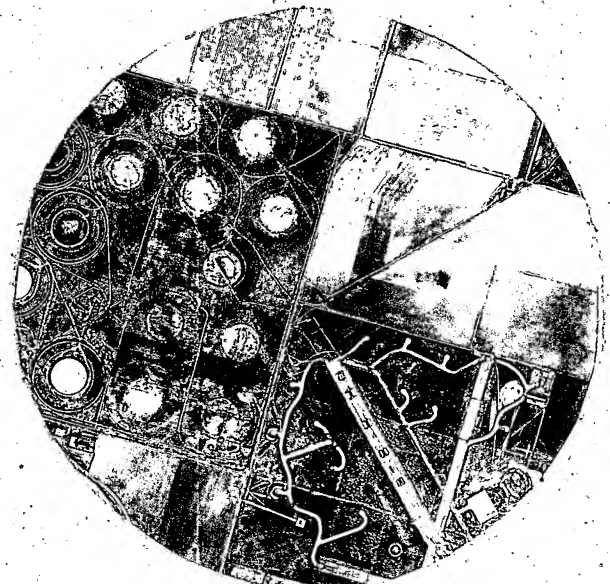
1 mm.

1 mm.

SCENE ENLARGEMENT

Figure M-1

Figure M-2

POWER SPECTRA OF SCENE

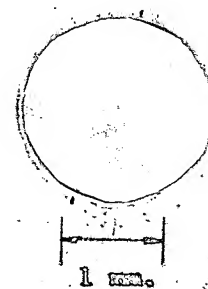POWER SPECTRA OF SCENE

LOW RESOLUTION SCENE
RIVER VALLEY

LOW RESOLUTION SCENE
POPULATED AREA

1 mm.

1 mm.

Figure M-3

Engineering Report No. 5530

Figure M-4

Page 107
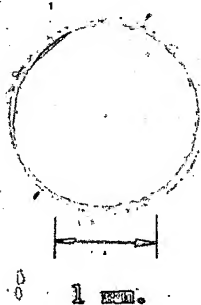
it in one direction. The broad spread indicates a generally random structure. The bar correlates with the direction of illumination of the scene, the shadow being very roughly linear and oriented in the same direction.

The power spectrum of the developed area shows strong spikes oriented along the principal directions of the artifical structure with almost no power associated with the frequencies oriented otherwise. One of these principal spikes shows nodes indicating regular periodic structure covering an appreciable area of the transparency. On examination it can be seen that plowed fields correspond to the nodes.

The high-resolution picture is also of a developed area, and this is again reflected in the strongly spiked structure of the power spectrum. This picture also has a plowed field, but the relative area is small and the nodes are not apparent.

APPENDIX N

IMAGE MOTION COMPENSATION

The present IMC problem is concerned with a slit camera which scans laterally, while the vehicle carrying it moves forward (see Figure N-1). The scan axis is parallel to the line of flight and the optical axis intersects the nadir when the scan angle is zero. In the figure, $\underline{h}$ is the altitude, $\underline{v}$ the forward velocity, $\underline{\beta}$ the scan angle, $\underline{\alpha}$ the field angle and $\underline{f}$ the focal length.

The objective of an IMC technique is to move the film and/or the image in such a way that the relative velocity between the two is negligibly small. The most direct way of approaching the problem is to refer the coordinate system to the surface defined by the slit and to develop the equations of motion of the image relative to the slit as a function of $\underline{v}$, $\underline{h}$, $\underline{f}$, $\underline{\alpha}$, and $\underline{\beta}$. Two types of focal surface will be considered--the sphere and the plane.

INSTANTANEOUS IMAGE VELOCITIES

Figure N-2 illustrates the derivation of the image velocity in the plane of the slit. Table N-3 shows the image velocity relationships.

An interesting fact is that the image velocity in the plane focal surface is independent of the field angle x whereas the spherical focal surface is not.

IMC TECHNIQUES

The simplest scan rate is a constant rate. In order to achieve a required overlap $\underline{p}$ with a given maximum field angle α_m, the scan rate is given by

$$\left.\frac{d\beta}{dt}\right|_o = \frac{\pi}{4} \cdot \frac{v}{h} \cdot \frac{\cot \alpha_m}{(1 - p)} \tag{1}$$
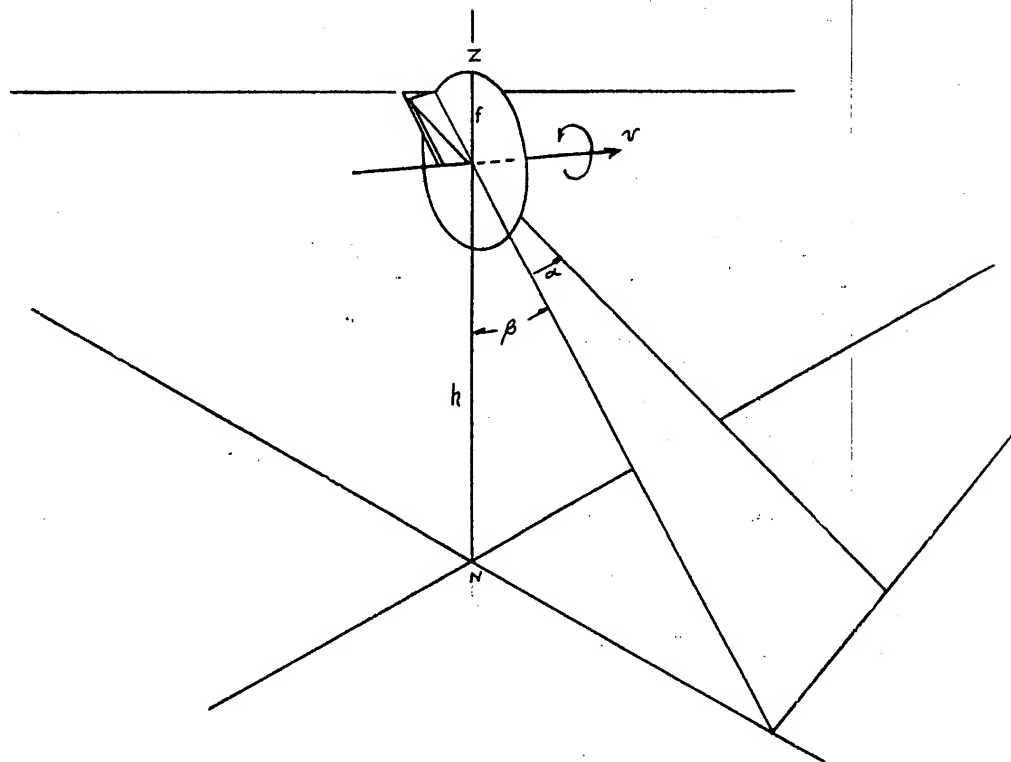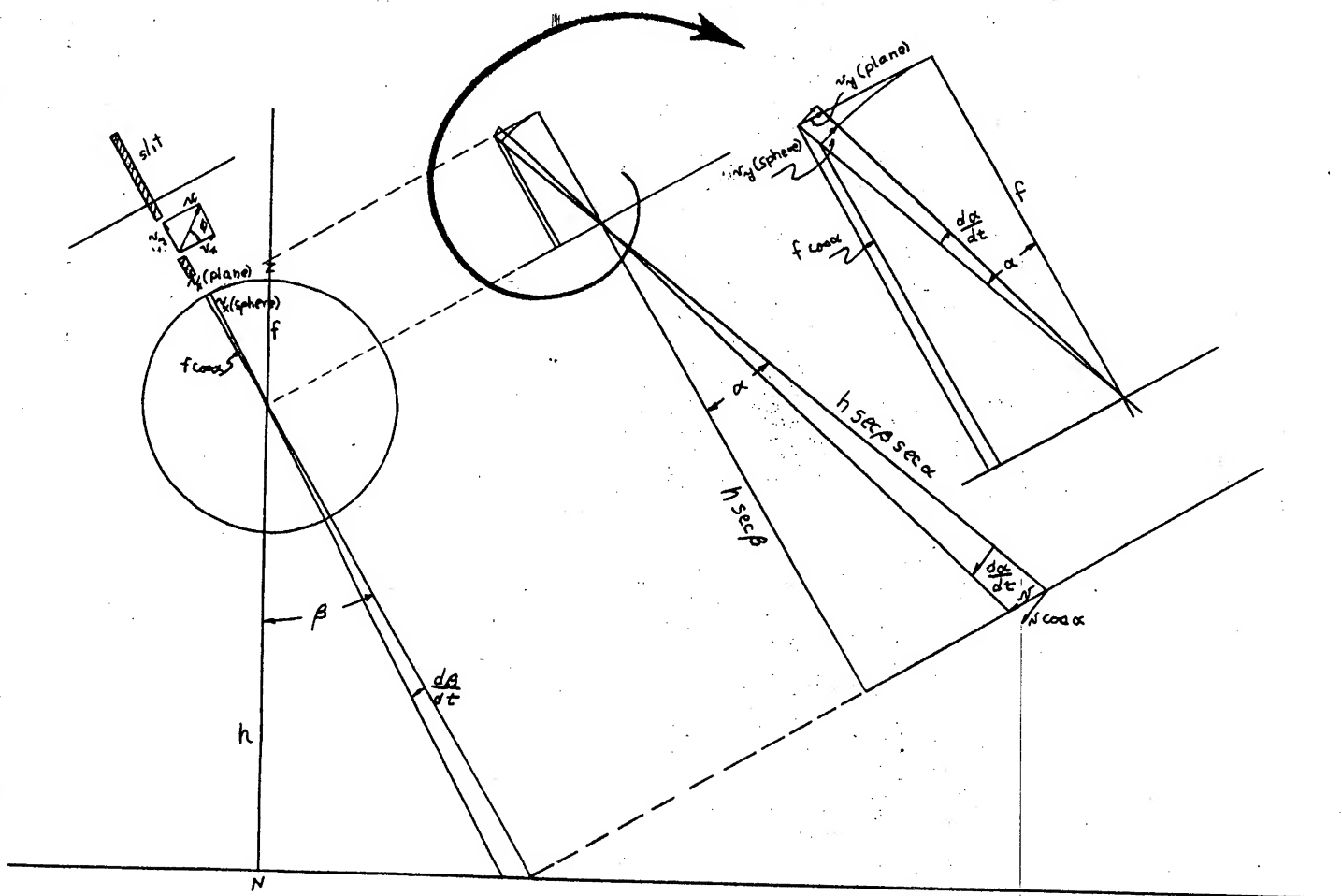
FIG N-1

FIG N-2

TABLE N-3   IMAGE VELOCITY RELATIONSHIPS

SPHERICAL FOCAL SURFACE

$$\frac{d\alpha}{dt} = \frac{V}{h} \cos^2 \alpha \cos \beta$$

$$V_y = f \frac{d\alpha}{dt} = f \cdot \frac{V}{h} \cdot \cos^2 \alpha \cos \beta$$

$$V_x = f \cos \alpha \frac{d\beta}{dt}$$

$$\tan \phi = \frac{\frac{V}{h} \cos \alpha \cos \beta}{\frac{d\beta}{dt}}$$

$$V_r = V_x \sec d = f \cdot \cos \alpha \sec \phi \cdot \frac{d\beta}{dt}$$

$$= V_y \csc \phi = f \cdot \frac{V}{h} \cdot \cos^2 \alpha \cos \beta \csc \phi$$

PLANE FOCAL SURFACE

$$\frac{d\alpha}{dt} = \frac{V}{h} \cos^2 \alpha \cos \beta$$

$$V_y = f \sec^2 \alpha \frac{d\alpha}{dt} = f \cdot \frac{V}{h} \cdot \cos \beta$$

$$V_x = f \frac{d\beta}{dt}$$

$$\tan \phi = \frac{\frac{V}{h} \cos \beta}{\frac{d\beta}{dt}}$$

$$V_r = V_x \sec d = f \cdot \sec \phi \cdot \frac{d\beta}{dt}$$

$$= V_y \csc \phi = f \cdot \frac{V}{h} \cdot \cos \beta \csc \phi$$

in radians per second, assuming that successive scans are 90° ($\pi/2$ radians) apart.

The components of image velocity when scan rate is constant are as follows: the lateral velocity component v_x is constant; the longitudinal component v_y varies directly as $\cos \beta$; and $\beta = \left.\frac{d\beta}{dt}\right|_{o} t$. Thus, neglecting the field angle factor for the spherical focal surface, perfect compensation may be achieved by using a constant scan rate, a constant film velocity in the lateral direction and film motion varying as $\cos \beta$ in the longitudinal direction.

It may be that moving the film accurately in the longitudinal direction may be more difficult to achieve than accurately varying the scan rate and film velocity. In this case it would be preferable to keep ϕ constant by varying $\frac{d\beta}{dt}$ so that it is proportional to $\cos \beta$. The film velocity will then be directly proportional to $\frac{d\beta}{dt}$ and unchanging in its direction ϕ, which is no longer perpendicular to the scan axis. Then the differential equation

$$\frac{d\beta}{dt} = A \cos \beta \tag{2}$$

must be satisfied, where $A = \frac{v}{h} \cos \alpha \cot \phi$ for the spherical focal surface and $\frac{v}{h} \cot \phi$ for the plane focal surface. The solution is

$$\tan (\beta/2 + \frac{\pi}{4}) = e^{At.} \tag{3}$$

β and $\frac{d\beta}{dt}$ as a function of time are shown in Figure N-4.

Clearly, this mode of IMC is efficient only if relatively small scan angles are involved, whereas the previous method is unrestricted.

Four pictures are to be taken in one complete cycle but only 60° are used for each picture. Figure N-5 shows as a solid line those portions of the scan which must be matched accurately, the plot being one of scan rate versus time.
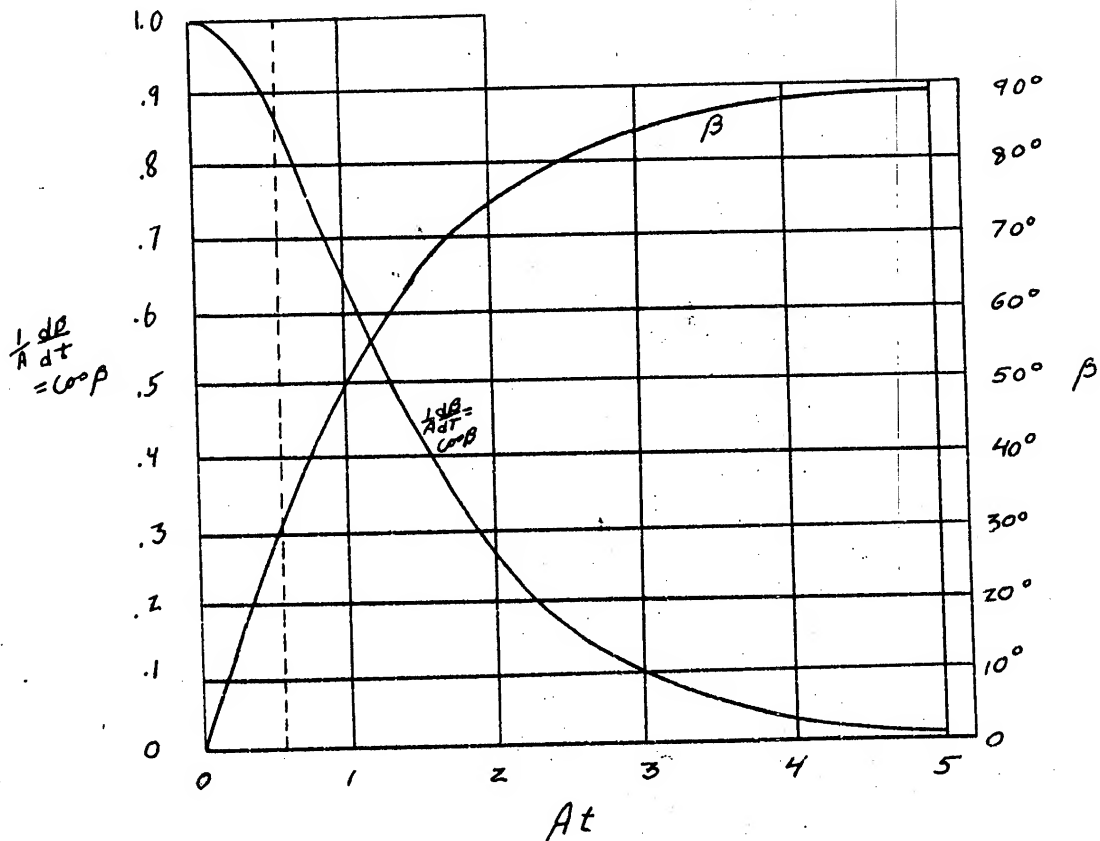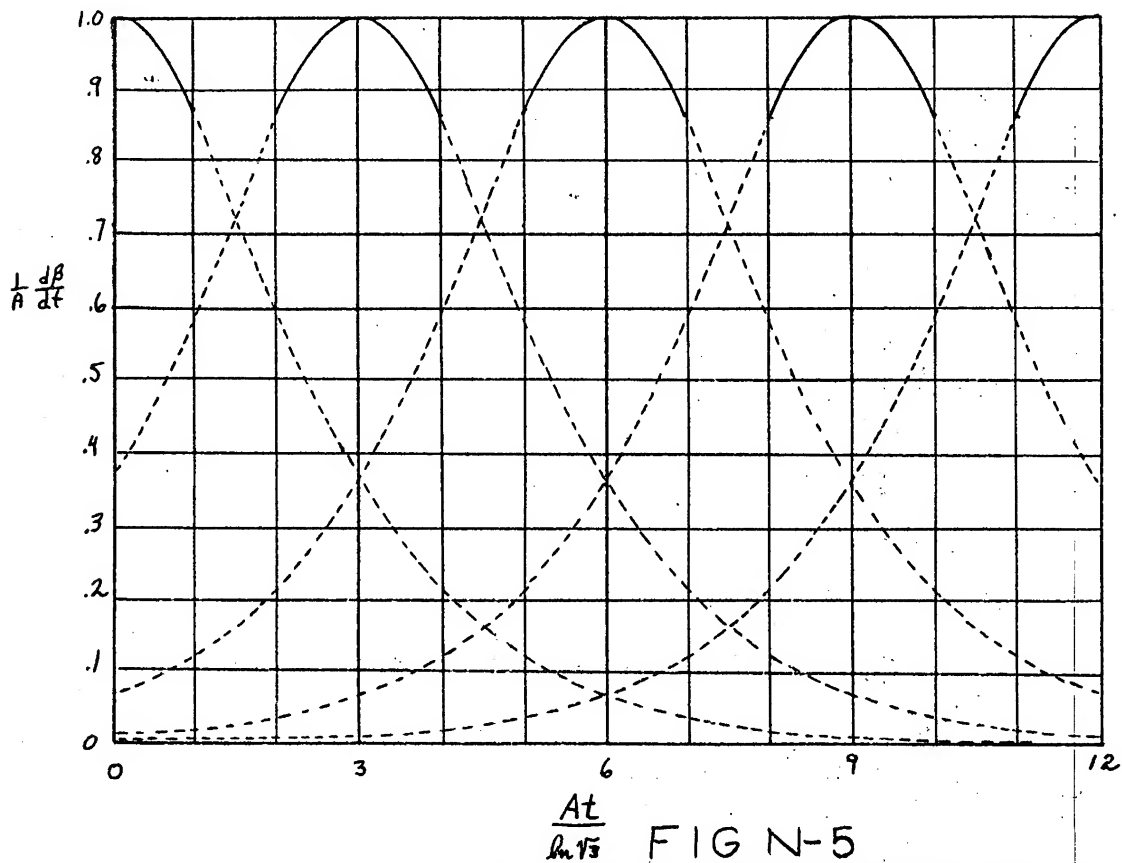
FIG N-4

$$\frac{1}{A}\frac{d\beta}{dt}$$

$$\frac{At}{\ln\sqrt{3}}$$ FIG N-5

Figure N-6 shows the result of trying to match the required variation by a simple sinusoidal variation of the rate given by

$$\frac{1}{A} \frac{dB}{dt}\bigg|^* = 1 - a(1 - \cos \psi) \tag{4}$$

where

$$\psi = \frac{2\pi A}{3 \ln \sqrt{3}} t \tag{5}$$

and a is determined to minimize the error.

Figure N-7 shows the error as a function of the scan angle β for two values of a. The upper curve equalizes the positive and negative errors whereas the lower curve attempts to get the maximum scan range with the least error. It is apparent that this approximation would be adequate only over a range of about 15°.

A possibility for achieving a good approximation to the scan rate variation for the scanning prisms is that each of the prisms is used only in every other scan. This is done by varying each of the prisms at only half the frequency given above and 180° out of phase with each other. This situation is desirable mechanically because of the automatic balancing of moments. Figure N-8 illustrates this method and Figure N-9 shows the error resulting. This approximation is adequate over the full 30° range.

However, the magnitude of the variation has gone from about 9% to 37% of the average rate. In addition, the film velocity variation must be obtained from a separate mechanism which will operate roughly as in Figure 5, but with a better fit.
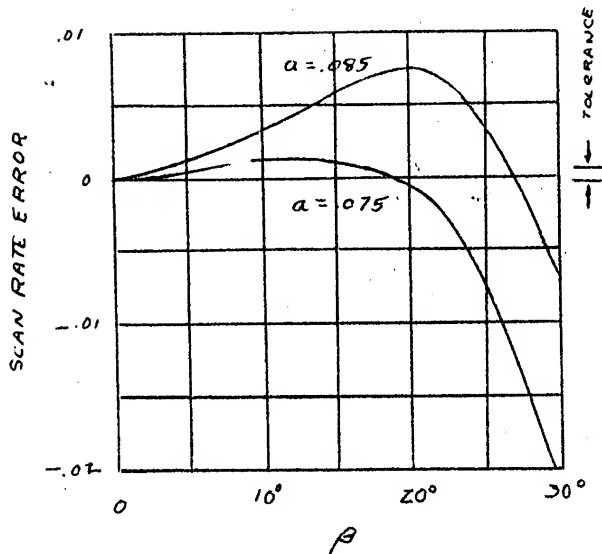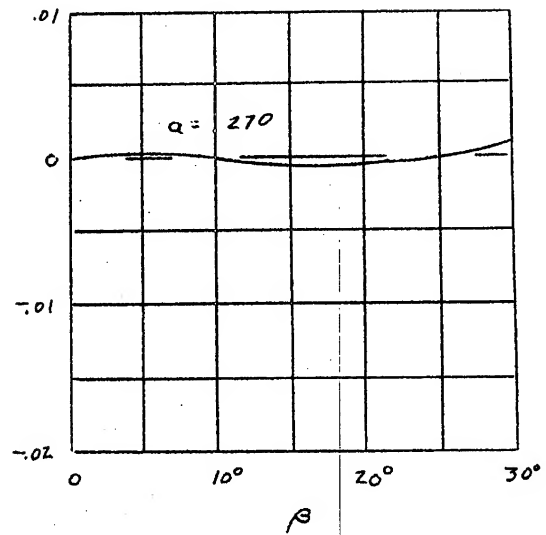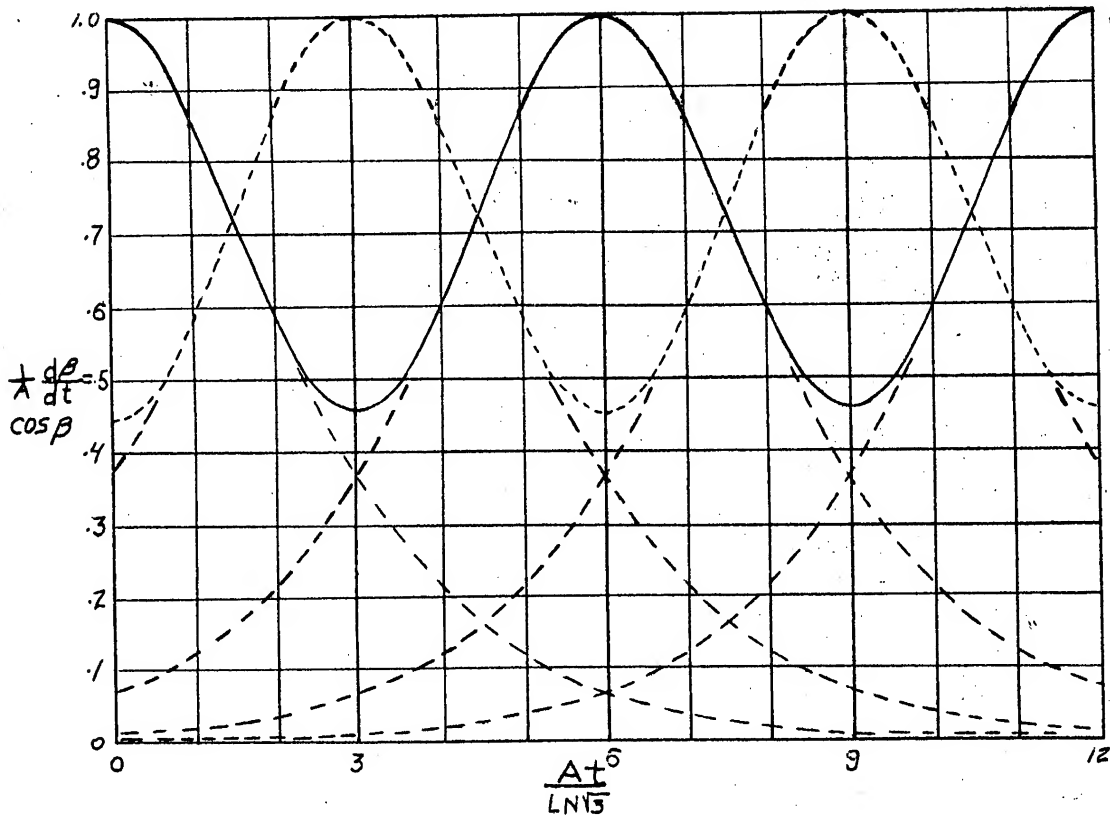
FIGN-6
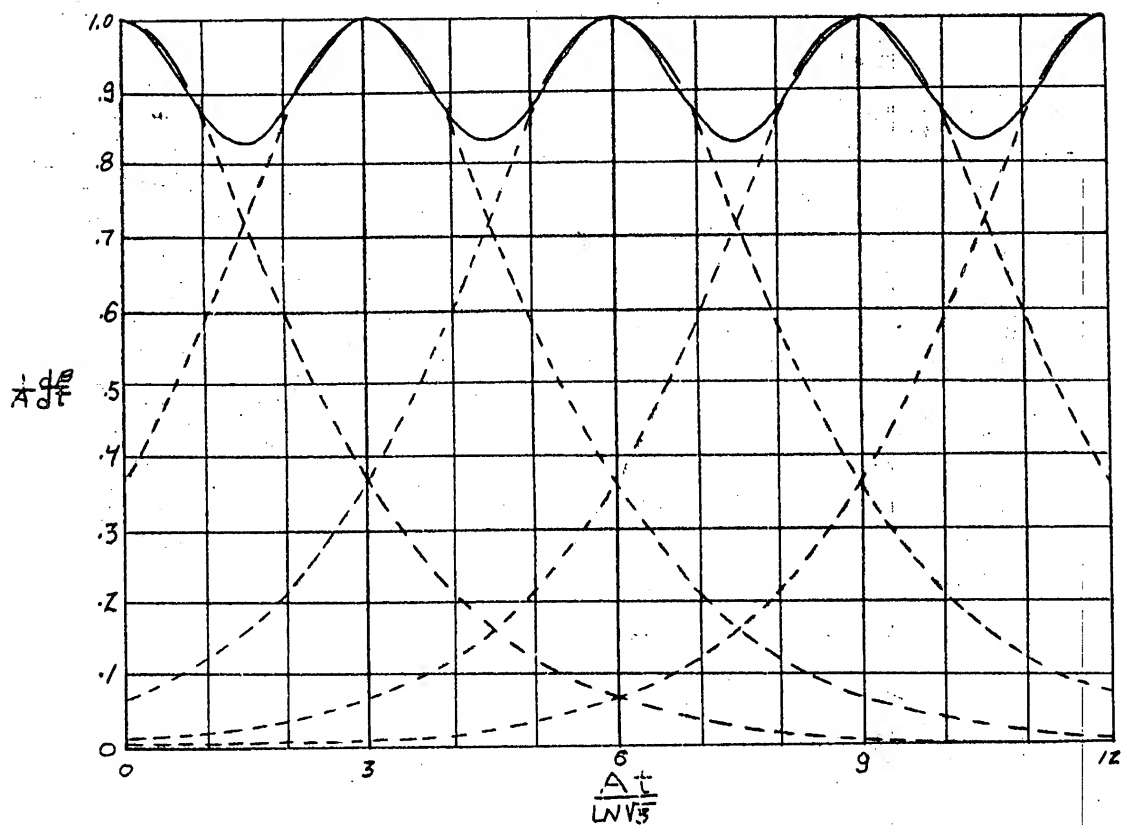
FIG N-7

FIG N-9

FIG N-8

APPENDIX O

FILM EVALUATION EQUIPMENT

Several pieces of equipment, specifically designed for film evaluation, have been constructed. An arrangement consisting of a light source and two cameras is used for the production of targets and for the photography of those targets onto the film being evaluated. One camera photographs ronchi rulings onto Kodak High Resolution Plates to produce targets having a frequency range of 4 to 15 lines per millimeter.

The second camera photographs targets at a 20X reduction onto the films being studied, offering a frequency range of 80 to 300 lines per mm. The camera employs a microscope apochromatic objective mounted in a precision focussing mount; a beam splitting plane and external light source in the optical path give the capability of introducing controlled non-image forming light which in effect reduces the contrast of the target image.

A plate processing rack and a film agitator were built for the precision processing of plates and films. The design emphasis was on even development over the emulsion surface and processing repeatability.

A Leeds and Northrup microphotometer is in the process of being modified. A ribbon filament lamp and an adjustable mechanical slit comprise the light source, and a photomultiplier as the output source activates a recorder. The size of the scanning slit is limited only by the sensitivity of the photomultiplier and associated amplifier.
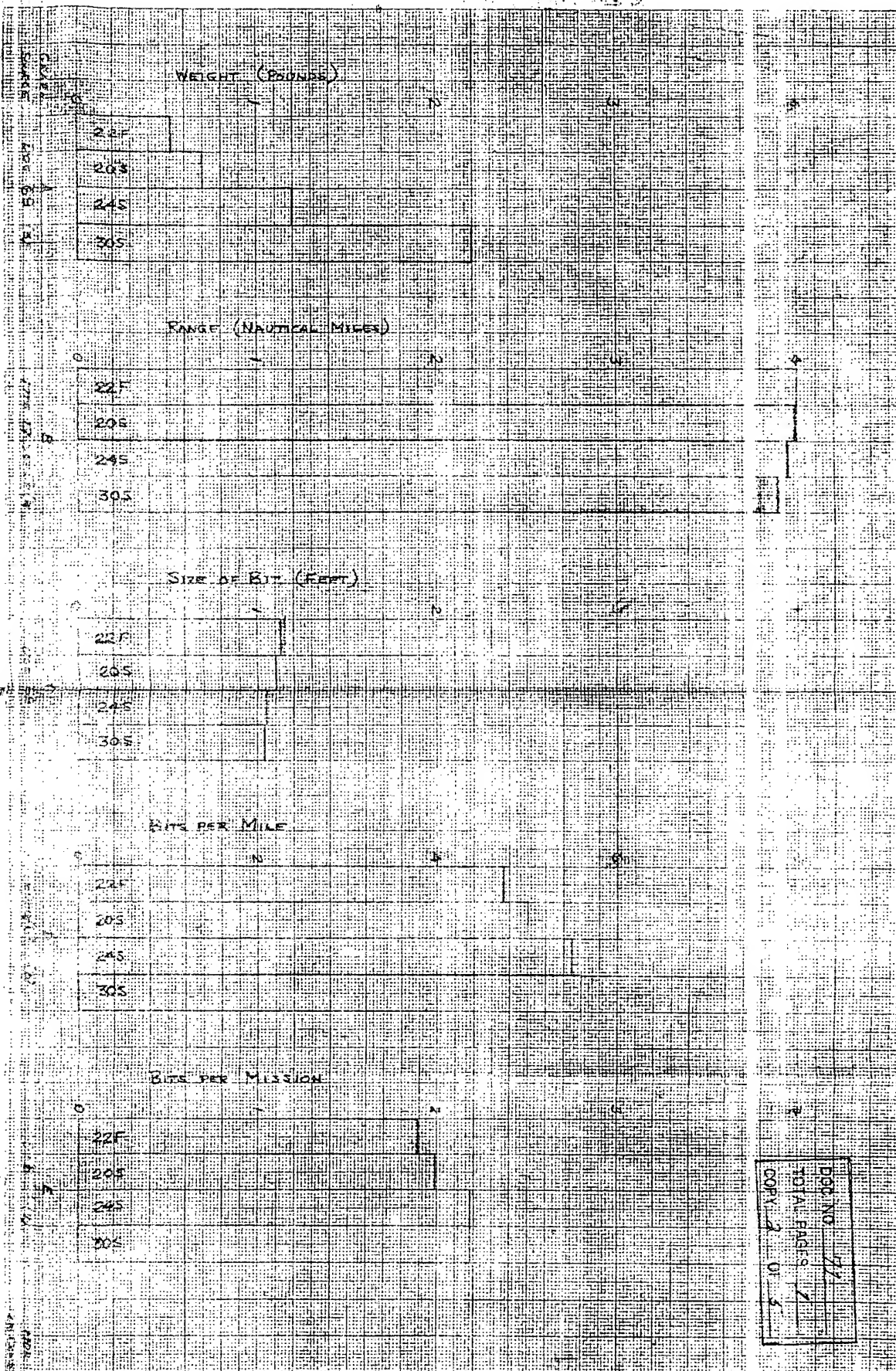
APPENDIX P

PERTINENT DOCUMENTS LIST

The following is a list of pertinent documents concerning this program:

	DATE	DOC. NO.	ER NUMBER	TITLE
1.	1 February 1959	-	----	Aerial Reconnaissance System Progress Report No. 1
2.	2 March 1959	1	5394	High Acuity Reconnaissance Systems for A High Performance Aircraft
3.	30 March 1959	5	----	Letter from JGB to Mr. B.
4.	13 April 1959	4	5414	Project Plan 13 April - 30 June 1959
5.	1 May 1959	15	5424	Progress Report No. 1 14 - 30 April 1959
6.	7 May 1959	17	----	Letter from MDR to LEW Evaluation plans
7.	28 May 1959	22	5442	Progress Report No. 2 1 - 28 May 1959
8.	28 May 1959	23	5443	Preliminary Considerations of Special Equipment for an Alternate Carrier
9.	22 June 1959	27	----	Letter from MDR to DRK Window
10.	26 June 1959	32	5465	Progress Report No. 3 29 May 1959 - 26 June 1959
11.	2 July 1959	37	----	Quality Evaluation
12.	10 July 1959	39	----	Letter from MDR to LEW 5A & 5B n.g.
13.	20 July	--	----	Letter from RMS to LEW Catad. Systs.
14.	27 July 1959	40	5485	Progress Report No. 4 27 June 1959 - 24 July 1959
15.	31 July 1959	43	----	Revised Side Views for Append. C - ER 5485
16.	24 August 1959	50	----	Information from August 19-20 Meeting re Payload Cooling
17.	1 September 1959	53	----	Letter from MDR to RSQ Trip Reports

	DATE	DOC. NO.	ER NUMBER	TITLE
18.	4 September 1959	54	----	Letter from MDR to RSQ Sketches 5C and 6A
19.	10 September 1959	57	5506	Progress Report No. 5 25 July - 9 September 1959
20.	15 September 1959	59	----	Configurations E, F, G, H
21.	12 October 1959	62	----	Selection of System
22.	13 October 1959	63	----	Drawings 546-0900 thru 546-0903
23.	20 October 1959	68	----	Project Plan and Budget Cost Estimate for Project
24.	20 October 1959	69	----	Potential Systems

Engineering Report No. 5530

WEIGHT (POUNDS)

RANGE (NAUTICAL MILES)

SIZE OF BIT (FEET)

BITS PER MILE

BITS PER MISSION